NASA TECHNICAL NOTE

NASA TN D-5633

SHEAR LAYER AND JET INSTABILITY IN STRATIFIED MEDIA

by George H. Fichtl

George C. Marshall Space Flight Center
Marshall, Ala.

NATIONAL AERONAUTICS AND SPACE ADMINISTRATION • WASHINGTON, D. C. • FEBRUARY 1970

1. Report No.	2. Government Accession No.	3. Recipient's Catalog No.
NASA TN D-5633		

4. Title and Subtitle	5. Report Date
Shear Layer and Jet Instability in Stratified Media	February 1970
	6. Performing Organization Code
7. Author(s) George H. Fichtl	8. Performing Organization Report No. M147
9. Performing Organization Name and Address Aerospace Environment Division Aero-Astrodynamics Laboratory Marshall Space Flight Center, Alabama 35812	10. Work Unit No. 933-50-02-00-62 11. Contract or Grant No.
12. Sponsoring Agency Name and Address National Aeronautics and Space Administration Washington, D.C. 20546	13. Type of Report and Period Covered Technical Note 14. Sponsoring Agency Code

15. Supplementary Notes This report was submitted in partial fulfillment of the requirements for the Degree of Doctor of Philosophy to the Pennsylvania State University, June 1969.

16. Abstract

The stability to small perturbations of shear layer and jet flows $\bar{u}(z)$ in atmospheres with potential temperature $\bar{\theta}(z)$ is investigated. The problem is reduced to a characteristic value problem for the dimensionless wave frequency ν which appears in a second-order differential equation with the dependent variable being the horizontal and temporal Fourier transform amplitude of the vertical component of the perturbation momentum vector. Broken-line profiles of $\bar{u}(z)$ and $\bar{\theta}(z)$ are used in the analysis of this problem.

Integral equations, over the domain of the fluid, which contain both quadratic forms and interfacial contributions, are derived. The interfacial terms vanish for continuous flows, and the theorems of Synge, Howard, and Miles follow. A necessary and sufficient condition for instability is also obtained for continuous flows; however, its usefulness is compromised by integrands which depend on both the basic state flow and the dependent variable of the governing differential equation. The theorems just cited are

17. Key Words	18. Distribution Statement
Clear Air Turbulence, Kelvin Helmholtz instability, Orr-Sommerfeld equation, Discontinuous profiles, Broken line profiles	Unclassified - Unlimited

19. Security Classif. (of this report)	20. Security Classif. (of this page)	21. No. of Pages	22. Price
Unclassified	Unclassified	176	$3.00

*For sale by the Clearinghouse for Federal Scientific and Technical Information Springfield, Virginia 22151

examined in the context of broken-line flows and it appears that they can be derived only for special cases. The difficulty is traced to the interfacial contributions.

A three-layer model in which $\bar{u}(z)$ and $\bar{\theta}(z)$ have piecewise constant values and which is disturbed by longitudinal perturbations with dimensionless wave number k is examined in detail. The characteristic values are given by a quartic equation in ν in which the basic state flow appears via four dimensionless parameters and are measures of the "jumps" in $\bar{\theta}(z)$ and $\bar{u}(z)$ across the interfacial surfaces. For sufficiently large k, the motions at the upper and lower interfaces behave as unstable two-layer Kelvin-Helmholtz flows. As k approaches zero, the coupling between the motions at the two interfaces is enhanced, and for sufficiently small values of k, the motions are neutral provided the "jumps" in $\bar{\theta}(z)$ across the interfacial surfaces do not vanish; otherwise, all perturbations are unstable. Numerical calculations show that the critical wave number can be both single- and triple-valued functions of the basic state flow parameters with the curious result that a decrease in shear or an increase in static stability could result in destabilization. The three-layer model is applied to synoptic scale jet stream flows, and explicit results are obtained for the Endlich and McLean jet stream model.

TABLE OF CONTENTS

TABLE OF CONTENTS (Concluded)

LIST OF ILLUSTRATIONS

LIST OF ILLUSTRATIONS (Concluded)

LIST OF SYMBOLS

Symbol	Definition
English Symbols	
C_v	specific heat at constant volume
C_p	specific heat at constant pressure
c_p	phase velocity
c_g	group velocity
E	energy spectrum of turbulence
F	$\Omega^{-1}\psi$
g	acceleration of gravity
H	$\Omega^{-1/2}\psi$
H	distance from earth's surface to a broken-line discontinuity or thickness of fluid in constant S model
h	half-width of three-layer shear or jet flow
$\vec{i}$, $\vec{j}$, $\vec{k}$	unit vectors directed along x, y, and z axes
i	$\sqrt{-1}$
J	Richardson number in Miles and Goldstein-Taylor models
k	dimensionless wave number
k_1^*, k_2^*	critical dimensionless wave numbers in three-layer model
L_1, L_2, L_3	x, y, and z perturbation pressure length scales
p	pressure
p_1	1000 mb
$\vec{r}$	position vector
R	specific gas constant for dry air, Richardson number of odd shear layers

LIST OF SYMBOLS (Continued)

Symbol	Definition
English Symbols (Cont'd)	
R_1, R_2	Richardson numbers of three-layer model
$R_{K.H.}$	Richardson number of Kelvin-Helmholtz model
S	static stability of basic state flow
t	time
T	Kelvin temperature
$T(\omega)$	aircraft response function
u, v, w	x, y, and z velocity components
x, y	horizontal space coordinates
z	vertical space coordinate
Greek Symbols	
β	ratio of basic state potential temperatures
δ	length scale of basic state wind profile in Miles and Drazin and Howard models
ϵ	perturbation expansion parameter
η	dimensionless vertical space coordinate
η^*	$\eta + \frac{1}{2}$
θ	potential temperature
$\vec{\kappa}$	wave number vector

LIST OF SYMBOLS (Continued)

Symbol	Definition
Greek Symbols (Cont'd)	
κ	magnitude of wave number vector
κ_1, κ_2	x and y wave number components
Λ	vertical shear of basic state flow
Λ^*	wave number of critical state perturbation
λ	ratio of basic state velocities across interface
ν	dimensionless eigenfrequency
ξ	Lagrangian displacement
ρ	density of dry air
ρ_o	density profile parameter in Goldstein-Taylor model
σ	standard deviation of gust loads, or density profile parameter in Goldstein-Taylor model
ϕ	dependent variable
ψ	vertical component of perturbation momentum vector
ω	eigenfrequency
Ω	$\omega + \kappa_1 \bar{u}$
Ω_x, Ω_y, Ω_z	x, y, and z components of the earth's angular velocity vector at latitude ϕ

LIST OF SYMBOLS (Concluded)

Symbol	Definition
Mathematical Operators and Miscellaneous Notation	
$\frac{\partial}{\partial x}, \frac{\partial}{\partial y}, \frac{\partial}{\partial z}$	partial differentiation operators with respect to space coordinates
$\frac{\partial}{\partial t}$	partial differentiation with respect to t
$D = \frac{d}{dz}$	total differentiation with respect to z
L	$\frac{\partial}{\partial t} + \bar{u}\frac{\partial}{\partial x}$
$\Delta_s(f)$	"jump" in f across a fluid interface
$( )'$	perturbation quantity
$\overline{( )}$	basic state quantity
$\hat{( )}$	Fourier transform
$( )^*$	complex conjugation

SHEAR LAYER AND JET INSTABILITY IN STRATIFIED MEDIA

SUMMARY

The stability to small perturbations of shear layer and jet flows $\bar{u}(z)$ in atmospheres with potential temperature $\bar{\theta}(z)$ is investigated. The problem is reduced to a characteristic value problem for the dimensionless wave frequency ν which appears in a second-order differential equation with the dependent variable being the horizontal and temporal Fourier transform amplitude of the vertical component of the perturbation momentum vector. Broken-line profiles of $\bar{u}(z)$ and $\bar{\theta}(z)$ are used in the analysis of this equation.

Integral equations, over the domain of the fluid, which contain both quadratic forms and interfacial contributions, are derived. The interfacial terms vanish for continuous flows, and the theorems of Synge, Howard, and Miles follow. A necessary and sufficient condition for instability is also obtained for continuous flows; however, its usefulness is compromised by integrands which depend on both the basic state flow and the dependent variable of the governing differential equation. The theorems just cited are examined in the context of broken-line flows, and it appears that they can be derived only for special cases. The difficulty is traced to the interfacial contributions.

A three-layer model in which $\bar{u}(z)$ and $\bar{\theta}(z)$ have piecewise constant values and which is disturbed by longitudinal perturbations with dimensionless wave number k is examined in detail. The characteristic values are given by a quartic equation in ν in which the basic state flow appears via four dimensionless parameters and are measures of the "jumps" in $\bar{\theta}(z)$ and $\bar{u}(z)$ across the interfacial surfaces. For sufficiently large k, the motions at the upper and lower interfaces behave as unstable two-layer Kelvin-Helmholtz flows. As k approaches zero, the coupling between the motions at the two interfaces is enhanced, and for sufficiently small values of k, the motions are neutral provided the "jumps" in $\bar{\theta}(z)$ across the interfacial surfaces do not vanish, otherwise all perturbations are unstable. Numerical calculations show that the critical wave number can be both single- and triple-valued functions of the basic state flow parameters with the curious result that a decrease in shear or an increase in static stability could result in destabilization. The three-layer model is applied to synoptic scale jet stream flows and explicit results are obtained for the Endlich and McLean jet stream model.

INTRODUCTION

Typical vertical wind profiles in the first 20 km of the atmosphere show that jet and shear layer flows occur frequently. The vertical length scales of these flows range between 0.1 and 10 km. The flows that possess the vertical length scales on the order of 10 km correspond to the synoptic scale baroclinic jets, while those flows characterized by length scales on the order of 0.1 km correspond to small meso- and micro-scale jets and shear layers. In many of these flows, the growth of perturbations through hydrodynamic instability is made possible by certain configurations of thermodynamic (entropy, temperature, etc.) and dynamic (vorticity, momentum, etc.) variables. The horizontal length scales of these perturbations or eddies range between 0.1 and 10^3 km, while the associated vertical length scales are on the order of the vertical scales of the configurations responsible for the generation of these instabilities.

The generation in statically stable atmospheres of shear layer and jet instabilities with typical horizontal length scales less than 50 km is now an important subject for investigation in both the meteorology and engineering communities. The main source of the instability is the presence of sufficient shear of the wind to overcome stabilizing forces. In order for the perturbations to grow, in an inviscid context, the production rate of eddy kinetic energy must be greater than the rate at which energy is expended by the eddies in performing work to overcome the stabilizing character of the statically stable distribution of potential temperature associated with the vertical profile of the wind.

The motivation for the interest in the subject is by no means academic. It has been suggested that this type of instability is responsible for the generation of clear air turbulence in the vicinity of the synoptic scale jet streams [1]. It is also possible to envision the generation of clear air turbulence via this instability mechanism in mesoscale jet and shear layer flows. For synoptic scale flows, the generation of shear layer and jet instabilities is a process whereby kinetic energy is directly converted from the synoptic scale to the small meso- and micro-scale motions. This report will be devoted to the examination of shear layer and jet instability phenomena characterized by horizontal length scales less than 50 km.

Problem

To understand how shear layer and jet instabilities occur in the atmosphere, it is necessary to relate the shear layer or jet flow in either case to the instability. This can be accomplished by taking the shear layer or jet flow to be a steady-state solution of the hydrodynamic equations and superimposing a disturbance. The sums of the steady-state and disturbance dependent variables are assumed to satisfy the hydrodynamic equations. This representation of the instability or disturbance in relation to the steady-state flow will result in a set of nonlinear, homogeneous, partial differential "disturbance" or "perturbation" equations. These equations are explicitly dependent on the steady-state flow which forces the disturbance. It is also possible to force the disturbance through the boundary or initial conditions. The solution of the disturbance equations for specified boundary and initial conditions will yield the stability properties of the steady-state flow configuration and, if instability is possible, will also yield the relationship between the steady-state flow and the instability. If the solution shows that all disturbances decay in time, then the steady-state flow is said to be stable. However, if a nondecaying solution exists, then the steady-state flow is said to be unstable [2]. Finally, if the disturbance amplitudes neither decay nor grow in time, then the steady-state flow is said to possess neutral stability.

A variety of techniques exist for obtaining solutions to the nonlinear disturbance equations. One of the most elegant schemes is the method of linear perturbation expansions in which one systematically linearizes these equations. In this procedure, the dependent disturbance variables, ϕ, are expanded in terms of a small scaling parameter ϵ, so that

$$\phi = \sum_{n=1}^{\infty} \epsilon^n \phi_n \quad , \tag{1}$$

where ϕ_n is the n^{th} order contribution to ϕ. The selection of the scaling parameter is dictated by the problem. Upon substituting these expansions into the disturbance equations, collecting terms in ascending powers of ϵ, and requiring the equation to be satisfied for arbitrary ϵ, one obtains an infinite system of linear differential equations that govern the behavior of ϕ_n ($n = 1, 2, 3, \ldots$). The equations associated with ϵ (first order) govern the first-order disturbances ϕ_1 and could have been derived from the nonlinear disturbance equations by neglecting all terms that are nonlinear in the

disturbance quantities ab initio. The solution of the first-order equations yields the conditions for the initial onset of instability when the disturbances are infinitesimally small. The first-order instabilities are forced by the steady-state shear layer or jet flow (zero-order flow). This forcing does not occur explicitly through a forcing function, but it occurs implicitly through the coefficients in the first-order disturbance equations and through the associated boundary conditions. The disturbance or perturbation equations associated with ϵ^2 (second order) govern the second-order contributions to the disturbances. These equations are nonhomogeneous and they are linear in the second-order dependent variables ϕ_2. The second-order instabilities are forced explicitly by the zero- and first-order flows through forcing functions that make the second-order equations nonhomogeneous. The origin of this explicit forcing can be traced to the nonlinear terms in the original disturbance equations. This iterative procedure can be carried out ad infinitum — the only limitation of the procedure is the mathematical prowess of the theoretician.

It is unusually difficult to solve the linearized disturbance equations for the second- and higher-order instabilities for all but the most simple zero-order flows. An example of the type of flow that has been analyzed with this technique is finite amplitude cellular convection [3,4] in a hydrostatic layer of fluid. Even in this case, the fifth- and higher-order instabilities are difficult to analyze. Shear layer and jet flows in stratified media are a class of flows that have been extremely difficult to analyze with regard to the second- and higher-order instabilities. In fact, our knowledge concerning the first-order instabilities is meager, especially in the case of jet flows. A thorough understanding of the generation of the first-order instabilities would aid theoreticians in developing a comprehensive approach to the problem of analyzing the second- and higher-order flow states. In addition, the first-order solutions could also enable one to obtain a clearer picture of the generation of clear air turbulence in jets and shear layers, which is of manifest importance in developing clear air turbulence forecasting procedures.

The perturbation equations which govern the first-order instabilities to be considered here permit consideration of disturbances ϕ_1 of the form

$$\phi_1 = \hat{\phi}_1(\vec{r})\, e^{i\omega t} \tag{2}$$

where t is the time, $\hat{\phi}_1(\vec{r})$ is a function of the position vector $\vec{r}$, and and $i = \sqrt{-1}$. Upon substituting this form of the disturbance into the

first-order equations, a set of partial differential equations are obtained relating $\hat{\phi}_1(\vec{r})$ and ω. These equations and the associated boundary conditions constitute an eigenvalue problem for ω. The stability properties of the zero-order flow are specified by determining the ensemble of eigenvalues or characteristic values of ω. If we denote the real and imaginary parts of ω by $\mathrm{Re}(\omega)$ and $\mathrm{Im}(\omega)$, respectively, then it follows from equation (2) that the disturbances will decay in time if $\mathrm{Im}(\omega) > 0$. In this case, the zero-order flow is said to be stable. However, if $\mathrm{Im}(\omega) < 0$, then the disturbance will increase in time without bound and the zero-order flow is said to be unstable. Finally, if $\mathrm{Im}(\omega) = 0$, then the disturbance will be steady if $\mathrm{Re}(\omega) = 0$, or oscillatory in time if $\mathrm{Re}(\omega) \neq 0$; in either case, the flow is said to be neutral.

The appropriate disturbance equations for studying the first-order shear layer and jet instabilities are the linearized, Boussinesq-approximated, hydrodynamic equations. These equations are valid for vertical length scales less than the local zero-order scale height and frequencies less than a typical zero-order Brunt-Vaisala frequency. The zero-order flow is taken to be a steady-state jet or shear layer flow characterized by a velocity distribution $\bar{u}(z)\vec{i}$ and a potential temperature distribution $\bar{\theta}(z)$, where z is the zenith-directed coordinate and $\vec{i}$ is a horizontal unit vector. Although the zero-order flows depend on z, the horizontal space coordinates, x and y, and the time t, in the stability calculations, the horizontal and temporal variations will be neglected. In order for this approximation to be valid, the horizontal length scales and the time scales of the zero-order flow must be very large in comparison to the corresponding scales of the perturbations. The first-order perturbation equations consist of three linearized momentum conservation equations, a linearized mass conservation equation, and a linear form of the first law of thermodynamics. Upon combining these equations into one equation with one unknown, and assuming normal mode solutions, one finds that

$$(\omega + \kappa_1\bar{u})^2 \frac{d^2\psi}{dz^2} - \left\{ \kappa_1(\omega + \kappa_1\bar{u}) \frac{d^2\bar{u}}{dz^2} - (\kappa_1^2 + \kappa_2^2) \left[\frac{g}{\bar{\theta}} \frac{d\bar{\theta}}{dz} - (\omega + k_1\bar{u})^2 \right] \right\} \psi = 0 \quad . \tag{3}$$

In this equation, κ_1 and κ_2 are the horizontal components of the wave number vector of the first-order disturbances parallel and normal to $u(z)\vec{i}$, and ψ is the normal mode amplitude of the vertical component of the first-order momentum density vector. The quantities $\bar{u}$ and $\bar{\theta}$ are known functions of z. The boundary conditions for this equation are given by

$$\psi = 0 \qquad \text{(at a rigid surface)} \tag{4}$$

and

$$\lim_{z \to \infty} \left[(\omega + \kappa_1 \bar{u}) \frac{d\psi}{dz} - \kappa_1 \psi \frac{d\bar{u}}{dz} \right] = 0 \quad . \tag{5}$$

Equation (4) is a statement that the vertical velocity must vanish on a horizontal rigid surface and equation (5) requires the perturbation pressure to vanish as z approaches infinity.

Equations (3), (4), and (5) represent a characteristic value problem for ω. Thus, upon determining the solution, ω will automatically be determined and the stability properties of the zero-order of basic state flow will be known within the context of the first-order theory. However, only very special forms of $\bar{u}$ and $\bar{\theta}$ permit one to obtain analytical solutions for the system given by equations (3) through (5). In the case of such closed-form solutions, one has an eigenvalue equation or dispersion relation available to perform the stability analysis. This equation relates the eigenfrequencies of the system to the disturbance wave numbers and the adjustable parameters of the basic state flow. The important point is that closed-form solutions permit one to analyze the eigenvalues of the system directly through the dispersion relation.

When $\bar{u}$ and $\bar{\theta}$ do not permit analytical integration of equation (3), one must use numerical methods; but then, many solutions are needed to determine how the stability of the basic state depends upon the features of the basic state profiles. Moreover, an explicit characteristic equation is no longer available to relate the system parameters to the eigenvalues; therefore, a succession of numerical experiments is necessary to determine the dependence of the eigenvalues upon the system parameters. The numerical results tend to become voluminous, so that one must usually restrict the analysis to a few special cases. These difficulties can be circumvented by adopting an approximate model of the basic state which yields closed-form solutions and dispersion relations. The method of broken-line analysis is an often-used procedure which has played a major role in the development of meteorology and fluid mechanics. In the broken-line model, the basic state flow is partitioned into a series of layers in which the variables $\bar{u}$ and $\bar{\theta}$ take on constant but different values. From a mathematical point of view, these discontinuous, or broken-line, profiles allow closed-form solutions to equations (3) through (5). Variation of the magnitudes of $\bar{u}$ and $\bar{\theta}$ simulates a host of basic state

flows. Admittedly, discontinuous profiles of $\bar{u}$ and $\bar{\theta}$ do not occur in nature; nevertheless, they permit solutions to equations (3) through (5) which resemble those associated with the continuous counterparts for disturbances with sufficiently long wavelengths. The main purpose of this report is to exploit this method to analyze the stability properties of shear layer and jet flows in the context of equations (3) through (5).

Literature Review

The subject of jet and shear layer instability in heterogeneous (or stratified) fluids has received extensive investigation during the last 100 years. The well-known and powerful tool of linear perturbation analysis has been one of the primary means for investigation of this subject. The first reference to shear layer instability is due to Von Helmholtz [5] who treated the topic qualitatively. Lord Kelvin [6] in 1871 investigated the subject quantitatively by examining the stability properties of a simple unbounded two-layer model, in which each layer had constant but different values for the unperturbed density and velocity and the mean velocity vectors in each layer were parallel. The primary conclusion of his analysis was that spatially and temporally sinusoidal perturbations will be unstable and will thus grow exponentially in time if the quantity

$$R_{K.H.} = g \frac{\left(\kappa_x^2 + \kappa_y^2\right)^{1/2}}{\kappa_x^2} \frac{(\bar{\rho}_1 - \bar{\rho}_2)(\bar{\rho}_1 + \bar{\rho}_2)}{\bar{\rho}_1\bar{\rho}_2(\bar{u}_1 - \bar{u}_2)^2} \tag{6}$$

is less than unity. The perturbations will be neutral oscillations if $R_{K.H.} \geqq 1$. In equation (6), $\bar{\rho}$ and $\bar{u}$ denote the unperturbed density and velocity, and the subscripts 1 and 2 denote conditions in the lower and upper layers. According to equation (6), if a disturbance with energy in a wave number band containing a wave number vector $\vec{\kappa}$ such that $|\vec{\kappa}| > \kappa^*$, then instability will occur and the perturbations will grow exponentially in time. The critical wave number κ^* is defined as

$$\kappa^* = g \frac{(\bar{\rho}_1 - \bar{\rho}_2)(\bar{\rho}_1 + \bar{\rho}_2)}{\bar{\rho}_1\bar{\rho}_2(\bar{u}_1 - \bar{u}_2)^2 \cos^2\varphi} , \tag{7}$$

φ being the angle between the mean flow direction and the direction of propagation of the disturbance. This type of instability has come to be known as the Kelvin-Helmholtz instability in honor of the first contributors, and subsequent analyses have been extensions of their pioneering work. Many authors refer to all shear layer and jet instabilities as Kelvin-Helmholtz instabilities. However, in this report there will be occasions in which we will relate the results of the analyses to those of Kelvin and Helmholtz, as well as to the results of other investigators. Thus, to avoid ambiguity we will use "Kelvin-Helmholtz instability" to refer exclusively to the original model of Kelvin and Helmholtz.

The first application of shear layer instability theory to meteorological problems was in the field of cloud physics where it was used to explain the formation of transverse cloud rows which are normal to the direction of the shear vector. The major contributors were Von Helmholtz [7], Wegener [8, 9], Haurwitz [10], and Sekera [11]. More recently, Lundlum [12] has analyzed billow cloud formation in relation to clear air turbulence in the context of shear layer instability theory.

Many investigators have used discontinuous flow models to analyze various types of hydrodynamic instabilities. The monumental volumes Physikalische Hydrodynamik by V. Bjerknes et al. [13] and Dynamic Meteorology and Weather Forecasting by Godske et al. [14] give accurate accounts of the major contributions during this period. In most of these analyses the investigators used two-layer models characterized by four basic state parameters, a dynamic or kinematic quantity (wind speed, wind shear, etc.) and a thermodynamic quantity (density, temperature, lapse rate, etc.) for each layer and were usually specified as constants. Multilayered flows were usually modeled in a similar manner, but as the number of layers increased the complexity of the associated characteristic equations increased. The dispersion equations of these layered systems were either polynomials in ω of degree 2N, where N is the number of interfaces in the system, or transcendental equations in ω. In the absence of modern digital computers, these investigators had to restrict their analyses to special cases for which they could extract the roots of the characteristic equation.

The efforts of Taylor [15] and Goldstein [16] are good examples of the type of multilayered calculations that were made during this period. Taylor and Goldstein elaborated upon Kelvin's work by introducing more layers, as well as single-valued piecewise continuous velocity profiles. However, in no case was a jet-like profile examined. The work of Goldstein and Taylor appears to yield results that contradict Kelvin's work. For example, Taylor

examined a three-layer model in which the density assumed constant but different values in each layer, and the velocity in the upper and lower semi-infinite layers also had constant but different values in each layer. However, the velocity distribution in the middle layer was assumed to have a linear variation such that the complete profile was single-valued at the density discontinuities. In this case, Taylor found that, for a given velocity and density distribution, the range of the unstable wave numbers is bounded from above and below and is rather narrow. This result is to be compared with Kelvin's which states that all disturbances with wave numbers greater than a lower cutoff value are unstable. Taylor argued that his result could be explained by a backward-moving free wave on the upper interface moving with the same speed as a forward-moving free wave at the lower interface, so that the instability might be regarded as due to a sort of resonance between two waves with the same wavelength moving in opposite directions with the same wavelength and speed.

Rosenhead [17] replaced Kelvin's interfacial vortex sheet with finite two-dimensional vortices, arranged at equal distances along a straight line. Disturbing this system sinusoidally, Rosenhead found that the mutual action of the vortices will accelerate the disturbance and render the initial motions unstable. As the instability grows, the interface between the two fluids will roll up, and the motions which are thus eventually produced will resemble vortex motions rather than wave motions. This rolling up of the unstable interface causes the wave to break. This type of wave breaking has been observed by Thorpe [18] in laboratory experiments. According to Woods in 1968, it is believed that a similar wave-breaking phenomenon occurs in the atmosphere and is one of the sources of clear air turbulence. The linear first-order perturbation theory cannot be applied to this breaking phenomenon, because it is only applicable at the initial stages of the instability when the amplitudes of the disturbance are small. However, the linear first-order theory can predict the wavelengths of the perturbations that could ultimately break in the subsequent growth of the instability.

The renewed interest in the subject of shear layer and jet instability during the last 10 years has been motivated by both engineering and scientific considerations. In the last decade, it became obvious that aircraft designers would have to account for the phenomenon of clear air turbulence in the design of high performance military and commercial aircraft. To supply the design engineer with design criteria, many investigators in the meteorological community intensified their efforts in the study of meso- and micro-scale flows in the free atmosphere. Most of these investigations have been empirical in nature, while a few investigators have attempted to study these flows from a theoretical point of view.

A great deal of effort has been spent in empirical determination of the spectral nature of meso- and micro-scale motions in the free atmosphere. Data on meso- and micro-scale flows have been obtained with accelerometers, gust recorders, and doppler radars over various portions of the globe. Thus, energy spectra of meso- and micro-scale flows have been obtained for conditions over the United States [19,20], over Australia [21], and over the USSR [22,23,24,25,26,27]. Pinus, Reiter, Shur, and Vinnichenko [1] have summarized these spectra, most of which appear to show a dependence on wave number κ like $\kappa^{-5/3}$ up to scales on the order of 10 km. However, some had slopes greater than "-5/3" for scales greater than 600 m. Various authors have attempted to explain this behavior of the spectrum with the concept of the buoyant subrange in which the energy dissipating effects of the Archimedian forces resulting from the stable stratification are taken into account. Pinus et al. [1] point out that the buoyant subrange may exist under conditions of stable stratification and may be seen from scales of about 30 to 100 m up to scales where the energy sources (of unspecified nature) balance the buoyant forces. Based upon dimensional analysis and an assumption about the relation between the rate of energy transfer through the spectrum and the Archimedian forces, various slopes can be derived. Bolgiano [28] suggests a slope equal to "-11/5," while Lumley [29] finds the slope to be "-3." Pinus et al. [1] also point out that the buoyant subrange may also exist under conditions of stable stratification at scales greater than 600 m with a slope of the spectral curve approaching "-3" [25]. The data in their paper seem to corroborate this result. However, these authors point out that the buoyant subrange does not exist as a "pure" phenomenon. They note that similarity considerations in the theoretical derivation of the spectrum in the buoyant subrange take into account only the turbulence-alleviating Archimedian forces under thermally stable conditions, but not the generating forces of vertical wind shear. In the atmosphere mechanical shear production of eddy energy may closely balance buoyant eddy energy dissipation, thus leaving no room for the development of a buoyant subrange. These authors point out that mathematical theory, taking into account the effects of vertical shear on turbulence spectra, has yet to be formulated.

Based upon an analysis of the power spectra depicted in their paper, Pinus et al. [1] suggest five regions in the spectrum in which energy may be supplied for the production of clear air turbulence. At scales on the order of 1000 km energy may be input by planetary inertial waves in the general circulation. At wavelengths somewhat longer than 100 km, energy may be supplied by gravity-inertial waves and the "striated" flow patterns that occur in the synoptic scale jet streams. At wavelengths somewhat shorter than 60 km, energy may be supplied by mesoscale phenomena associated with long

gravity and lee waves. At horizontal length scales on the order of 1 km energy may be supplied by short shear-gravity waves in a stably stratified environment. Finally, energy may be input at scales that correspond to convection cells in statically unstable layers.

Investigators are also devoting their efforts to determining those conditions in fluids which can produce clear air turbulence. Based on either perturbation theory or energy considerations, the conclusion is usually reached that there exists a "critical" value of the Richardson number, defined by

$$\mathrm{Ri} = \frac{\frac{g}{\theta}\frac{\partial \theta}{\partial z}}{\left|\frac{\partial \vec{u}}{\partial z}\right|^2} \quad , \tag{8}$$

which may characterize the critical condition for the onset of clear air turbulence. If Ri is less than a "critical" value R_c, perturbations can grow and turbulence will be produced. The question of what the critical Richardson number is for clear air turbulence is by no means a closed subject. In fact, one of the main goals of the first-order perturbation theory is the determination of critical values of the Richardson number. Investigators have approached the problem of determining R_c by both experimental and theoretical methods.

The work of Panofsky et al. [30] is one of the most recent examples of the work that has been done to determine R_c from an experimental point of view. They analyzed two separate cases of clear air turbulence, one in the stratsophere over the Rocky Mountains, the other in the upper troposphere over the midwestern Great Plains. They explain that the mechanism in both situations appeared to be similar; namely, strong baroclinic zones with strong vertical wind shears. They discovered that there is a tendency for the most severe clear air turbulence to be located at the edges of baroclinic zones, and calculated Richardson numbers for these zones from finite differences of wind speed and potential temperature over a constant increment of height, $\Delta z = 500$ m. They discovered values of Ri that ranged between 0.23 and 0.71 and the turbulence intensities ranged between moderate and severe. Based upon these results, they conclude that the "critical" Richardson number for the generation of clear air turbulence in strong baroclinic zones is in the

neighborhood of 0.50; however, they note that the actual value may be lower because of data processing and reliability problems or because the data density was not sufficient to resolve the fine structure in the spatial distributions of potential temperature and wind speed.

From a theoretical point of view, significant progress has been made with the first-order perturbation theory in determining the critical conditions for the onset of shear layer and jet instabilities. The theory has also improved our understanding of the essential mechanics of the initial stages of these instabilities. The major contributors to the subject, Miles [31,32], Howard [33,34], and Drazin [35,36], have analyzed the stability properties of both continuous and discontinuous flows. For continuous flows, they have derived some general theorems concerning these instabilities. The theorems, which are discussed later in this report, do not specify the total relationship between the basic state flow and the instability; thus, to understand the details one must make calculations with specific basic state flows. It appears that these investigators, as well as others, have restricted their calculations with specific basic state flows to those in which the velocity distributions are either odd or even and the associated static stability is even. Thus, one of the objectives of this report is to determine the dependence of shear layer and jet instability upon the asymmetry and symmetry properties of the basic state flow.

Of Things to Come

Later in this report, we derive the first-order perturbation equations appropriate for analyzing shear layer and jet instabilities from the hydrodynamic equations for isentropic flow. The basic state is assumed to be a horizontal parallel isentropic flow. It is shown, by restricting the analysis to perturbations with horizontal length scales less than 50 km, that Coriolis forces and horizontal variations in the basic state flow can be neglected in the first-order perturbation equations. Acoustic modes are filtered from the equations with the Boussinesq approximation. In a stable stratification, the maximum permissible frequency of the perturbations is on the order of the Brunt-Vaisala frequency. The perturbations are represented by Fourier integrals and the resulting Fourier transformed first-order equations are combined into one second-order differential equation in the Fourier amplitude of the vertical component of the perturbation momentum density vector. Finally, boundary and interfacial conditions for continuous and broken-line flows are derived.

Next, we consider the general properties of the governing differential equation and the associated boundary and interfacial conditions. The subject begins with a general discussion of the solutions for three classes of broken-line flows, namely, (1) continuous layers in which $\bar{u}$ and $\bar{\theta}$ are constants, (2) contiguous layers in which u and $\frac{1}{\bar{\theta}} \frac{d\bar{\theta}}{dz}$ are constants, and (3) continuous layers in which u is a linear function of z and θ is constant. A theorem concerning the permissible number of modes these systems can possess is derived. We then examine the consequence of two transformations of the dependent variable. The utilization of these transformations will yield three theorems that were first derived by Miles [31], Howard [33], and Synge [37] for continuous $\bar{\theta}$ and $\bar{u}$ profiles. In addition, a necessary and sufficient condition for the existence of unstable solutions for atmospheres characterized by $\frac{1}{\bar{\theta}} \frac{d\bar{\theta}}{dz} \neq 0$ is derived. It is shown that this condition leads to the result that all continuous flows which are statically unstable everywhere are dynamically unstable to small perturbations. These theorems are also discussed in the context of broken-line flows.

Finally, we examine in detail the dynamic stability properties of three-layer flows of type 1 (contiguous layers in which u and θ are constants). The dispersion relation for this model is a quartic in ω, and the coefficients in this equation are functions of the basic state parameters and the wave number of the perturbations. By varying the basic state flow parameters we are able to examine jets and shear layers which possess a wide range of symmetry and asymmetry properties. The stability properties of these three-layer flows are compared with the results of other investigators. The theory is applied to the problem of the generation of instabilities in the vicinity of the synoptic scale jet streams.

DEVELOPMENT OF BASIC EQUATIONS AND BOUNDARY AND INTERFACIAL CONDITIONS

The fundamental equations and boundary and interfacial conditions appropriate for the analysis of shear layer and jet instabilities are derived in this part of this report. The hydrodynamic equations for isentropic flows will be linearized by employing the theory of linear perturbations. It is assumed that the atmosphere is infinite in horizontal extent, so that the

perturbation dependent variables can be expressed as normal modes with respect to the horizontal and time coordinates. The Fourier amplitudes of these normal mode representations are functions of the vertical coordinate, z. A set of five homogeneous, ordinary, linear differential equations with nonconstant coefficients that govern the normal mode amplitudes will be obtained upon substituting the normal mode representations of the dependent variables into the linear perturbation equations. These equations will be combined to yield a second-order homogeneous differential equation in the Fourier amplitude of the vertical component of the perturbation momentum vector. In the later portion of this report, the stability properties of shear layer and jet flows are obtained by solving this equation with respect to certain boundary and interfacial conditions. As the first step, the appropriate boundary and interfacial conditions for continuous and broken-line jet and shear layer flows will be presented here.

Isentropic Hydrodynamic Equations

We choose as our coordinate system a right-hand orthogonal frame of reference, defined by the x, y, and z axes. The x and y axes define a plane that is tangent to the earth at latitude ϕ. The point of tangency is the intersection of the x and y axes. The z axis is directed toward the local zenith. In this coordinate system the atmospheric hydrodynamic equations valid for isentropic flows are given by

$$\frac{\partial u}{\partial t} + u\frac{\partial u}{\partial x} + v\frac{\partial u}{\partial y} + w\frac{\partial u}{\partial z} = -\frac{1}{\rho}\frac{\partial p}{\partial x} - 2\Omega_y w + 2\Omega_z v \quad , \tag{9}$$

$$\frac{\partial v}{\partial t} + u\frac{\partial v}{\partial x} + v\frac{\partial v}{\partial y} + w\frac{\partial v}{\partial z} = -\frac{1}{\rho}\frac{\partial p}{\partial y} - 2\Omega_z u + 2\Omega_x w \quad , \tag{10}$$

$$\frac{\partial w}{\partial t} + u\frac{\partial w}{\partial x} + v\frac{\partial w}{\partial y} + w\frac{\partial w}{\partial z} = -\frac{1}{\rho}\frac{\partial p}{\partial z} - 2\Omega_x v + 2\Omega_z u - g \quad , \tag{11}$$

$$\frac{\partial(\rho u)}{\partial x} + \frac{\partial(\rho u)}{\partial y} + \frac{\partial(\rho w)}{\partial z} = -\frac{\partial \rho}{\partial t} \quad , \tag{12}$$

and

$$\frac{\partial \theta}{\partial t} + u\frac{\partial \theta}{\partial x} + v\frac{\partial \theta}{\partial y} + w\frac{\partial \theta}{\partial z} = 0 \quad . \tag{13}$$

In this system of equations, u, v, and w denote the x, y, and z components of the velocity vector; p, ρ, and θ represent the pressure, density, and potential temperature; and Ω_x, Ω_y, and Ω_z are the x, y, and z directed components of the earth's angular velocity vector at latitude ϕ. Since these equations govern inviscid, non-heat-conducting flows and phase changes are forbidden, the results of this report must be viewed in that light. The variables p, ρ, and θ are connected through the equation of state for an ideal gas,

$$p = R\rho T \quad , \tag{14}$$

and Poisson's equation,

$$\theta = T\,(p_1/p)^{R/C_p} \quad , \tag{15}$$

where T is the Kelvin temperature. R and C_p denote the specific gas constant and specific heat at constant pressure for dry air and $p_1 = 1000$ mb.

Linearized Perturbation Equations

In this section we will linearize equations (9) through (15) to isolate the essential physics of shear layer and jet instabilities. The equations will be valid for analyzing perturbations characterized by ratios of the horizontal to vertical length scales much less than 10^2 and frequencies less than the local Brunt-Vaisala frequency.

Linearization. The known dependent variables associated with the basic state flows are indicated by an overbar. The combined motion of the jet or shear layer basic flow and the superimposed perturbation may be represented by

$$\left.\begin{aligned} u &= \bar{u} + u' \\ v &= \bar{v} + v' \\ w &= \bar{w} + w' \end{aligned}\right\} \quad , \tag{16}$$

where prime indicates a perturbation quantity. Similarly, the thermodynamic variables can be represented as

$$\left.\begin{aligned} p &= \bar{p} + p' \\ \theta &= \bar{\theta} + \theta' \\ \rho &= \bar{\rho} + \rho' \\ T &= \bar{T} + T' \end{aligned}\right\} \quad . \tag{17}$$

It is assumed that the unprimed quantities satisfy equations (9) through (15) and that the perturbation quantities are small enough that products of perturbation quantities appearing in the equations can be neglected in comparison with the first-order terms. Therefore, upon substituting equations (16) and (17) into equations (9) through (15) and noting that the meso- and synoptic-scale dependent variables (overbarred quantities) satisfy equations (9) through (15), it follows that

$$\begin{aligned} &\frac{\partial u'}{\partial t} + \bar{u}\frac{\partial u'}{\partial x} + \bar{v}\frac{\partial u'}{\partial y} + \bar{w}\frac{\partial u'}{\partial z} + u'\frac{\partial \bar{u}}{\partial x} + u'\frac{\partial \bar{u}}{\partial y} + w'\frac{\partial \bar{u}}{\partial z} \\ &= -\frac{1}{\bar{\rho}}\frac{\partial p'}{\partial x} + \frac{\rho'}{\bar{\rho}^2}\frac{\partial \bar{p}}{\partial x} - 2\Omega_y w' + 2\Omega_z v' \quad , \end{aligned} \tag{18}$$

$$\begin{aligned} &\frac{\partial v'}{\partial t} + \bar{u}\frac{\partial v'}{\partial x} + \bar{v}\frac{\partial v'}{\partial y} + \bar{w}\frac{\partial v'}{\partial z} + u'\frac{\partial \bar{v}}{\partial x} + v'\frac{\partial \bar{v}}{\partial y} + w'\frac{\partial \bar{v}}{\partial z} \\ &= -\frac{1}{\bar{\rho}}\frac{\partial p'}{\partial y} + \frac{\rho'}{\bar{\rho}^2}\frac{\partial \bar{p}}{\partial y} - 2\Omega_y u' + 2\Omega_x w' \quad , \end{aligned} \tag{19}$$

$$\frac{\partial w'}{\partial t} + \bar{u}\frac{\partial w'}{\partial x} + \bar{v}\frac{\partial w'}{\partial y} + \bar{w}\frac{\partial w'}{\partial z} + u'\frac{\partial \bar{w}}{\partial x} + v'\frac{\partial \bar{w}}{\partial y} + w'\frac{\partial \bar{w}}{\partial z}$$

$$= -\frac{1}{\bar{\rho}}\frac{\partial p'}{\partial z} + \frac{\rho'}{\bar{\rho}^2}\frac{\partial \bar{p}}{\partial z} - 2\Omega_x v' + 2\Omega_z u' - g \quad , \tag{20}$$

$$\frac{\partial(\bar{\rho}u')}{\partial x} + \frac{\partial(\bar{\rho}v')}{\partial y} + \frac{\partial(\bar{\rho}w')}{\partial z} + \frac{\partial(\rho'\bar{u})}{\partial x} + \frac{\partial(\rho'\bar{v})}{\partial y} + \frac{\partial(\rho'\bar{w})}{\partial z} = -\frac{\partial \rho'}{\partial t} \quad , \tag{21}$$

$$\frac{\partial \theta}{\partial t} + \bar{u}\frac{\partial \theta'}{\partial x} + \bar{v}\frac{\partial \theta'}{\partial y} + \bar{w}\frac{\partial \theta'}{\partial z} + u'\frac{\partial \bar{\theta}}{\partial x} + v'\frac{\partial \bar{\theta}}{\partial y} + w'\frac{\partial \bar{\theta}}{\partial z} = 0 \quad , \tag{22}$$

$$\frac{p'}{\bar{p}} = \frac{\rho'}{\bar{\rho}} + \frac{T'}{\bar{T}} \quad , \tag{23}$$

and

$$\frac{\theta'}{\bar{\theta}} = \frac{T'}{\bar{T}} - \frac{R}{C_p}\frac{p'}{\bar{p}} \quad . \tag{24}$$

This system of equations governs the perturbation-dependent variables. The perturbations are "forced" by the jet or shear layer flow through the coefficients in the equations. This "forcing" process is a conversion of kinetic and potential energies from the synoptic- and meso-scale flows to the small-scale disturbances.

Approximations. We intend to examine small-scale instabilities with typical horizontal length scales which are less than 50 km and time scales on the order of 5 to 10 minutes. The instabilities are primarily generated by a vertical shear of the synoptic- and meso-scale basic flows. The horizontal length scales of these basic state flows are of the order of $5 \cdot 10^2$ to $5 \cdot 10^3$ km, while the associated time scales are of the order of 1/2 to 5 days. In view of the magnitude of these scales in comparison to the length and time scales of the perturbations, it is assumed that the horizontal and temporal variations of the basic shear layer or jet flow can be neglected in the perturbation equations.

Further simplifications can be introduced by noting that synoptic and large meso-scale systems are quasi-horizontal hydrostatic flows, so that

$$\bar{w} \simeq 0 \tag{25}$$

and

$$\frac{\partial \bar{p}}{\partial z} \simeq -\bar{\rho} g \quad . \tag{26}$$

In addition, it is often true that these flows exhibit quasi-parallel motion over large distances in the horizontal ($\sim$ 500 km) and vertical ($\sim$ 5 km). Accordingly, if we orient the x-axis of the coordinate system parallel to the direction of the shear layer or jet flow, then

$$\bar{v} \simeq 0 \quad . \tag{27}$$

Introducing these approximations into equations (18) through (22) yields

$$L(\bar{\rho}u') + \bar{\rho}w' \frac{d\bar{u}}{dz} = -\frac{\partial p'}{\partial x} - 2\Omega_y \bar{\rho}w' + 2\Omega_z \bar{\rho}v' \quad , \tag{28}$$

$$L(\bar{\rho}v') = -\frac{\partial p'}{\partial y} - 2\Omega_z \bar{\rho}u' + 2\Omega_x \bar{\rho}w' \quad , \tag{29}$$

$$L(\bar{\rho}w') = -\frac{\partial p'}{\partial z} - g\rho' - 2\Omega_x \bar{\rho}v' + 2\Omega_z \bar{\rho}u' \quad , \tag{30}$$

$$-L\rho' = \frac{\partial (\bar{\rho}u')}{\partial x} + \frac{\partial (\bar{\rho}v')}{\partial y} + \frac{\partial (\bar{\rho}w')}{\partial z} \quad , \tag{31}$$

and

$$L\theta' + w' \frac{d\bar{\theta}}{dz} = 0 \quad , \tag{32}$$

where

$$L = \frac{\partial}{\partial t} + \bar{u}\frac{\partial}{\partial x} \quad . \tag{33}$$

Further simplifications can be introduced with regard to the Coriolis terms in equations (28) through (30). We may neglect the Coriolis terms if

$$\frac{2\left\{\Omega_y w'\right\}_M}{\left\{\frac{1}{\bar{\rho}}\frac{\partial p'}{\partial x}\right\}_M} \sim \frac{2\left\{\Omega_z v'\right\}_M}{\left\{\frac{1}{\bar{\rho}}\frac{\partial p'}{\partial x}\right\}_M} \ll 1 \quad , \tag{34}$$

$$\frac{2\left\{\Omega_x w'\right\}_M}{\left\{\frac{1}{\bar{\rho}}\frac{\partial p'}{\partial y}\right\}_M} \sim \frac{2\left\{\Omega_z u'\right\}_M}{\left\{\frac{1}{\bar{\rho}}\frac{\partial p'}{\partial y}\right\}_M} \ll 1 \quad , \tag{35}$$

$$\frac{2\left\{\Omega_x v'\right\}_M}{\left\{g\frac{\rho'}{\bar{\rho}}\right\}_M} \ll 1 \quad , \tag{36}$$

and

$$\frac{2\left\{\Omega_z u'\right\}_M}{\left\{g\frac{\rho'}{\bar{\rho}}\right\}_M} \ll 1 \tag{37}$$

where $\{\ \}_M$ denotes that we select the order of magnitude of the quantity within the braces. We may assume for atmospheric problems that $\rho'/\bar{\rho} \sim 0.01$, $\Omega_z = 0.504 \cdot 10^{-4}$ sec^{-1} ($\phi = 45°$ N), $g = 9.8$ m sec^{-2}, and $v' \sim u' \sim 10$ m sec^{-1}, so that the left-hand sides of equations (36) and (37) are of order 10^{-2} and thus these conditions are satisfied by most

atmospheric flows. In addition, most atmospheric flows are characterized by $w'/u' \lesssim 1$ and $w'/v' \lesssim 1$, so that we need only investigate the inequalities

$$\frac{2\left\{\Omega_z v'\right\}_M}{\left\{\frac{1}{\bar{\rho}}\frac{\partial p'}{\partial x}\right\}_M} << 1 \tag{38}$$

and

$$\frac{2\left\{\Omega_z u'\right\}_M}{\left\{\frac{1}{\bar{\rho}}\frac{\partial p'}{\partial y}\right\}_M} << 1 \quad . \tag{39}$$

Upon introduction of the length scales

$$L_1 = \frac{\left\{p'\right\}_M}{\left\{\frac{\partial p'}{\partial x}\right\}_M} \quad , \tag{40}$$

$$L_2 = \frac{\left\{p'\right\}_M}{\left\{\frac{\partial p'}{\partial y}\right\}_M} \quad , \tag{41}$$

$$L_3 = \frac{\left\{p'\right\}_M}{\left\{\frac{\partial p'}{\partial z}\right\}_M} \quad , \tag{42}$$

and estimation of the magnitude of the pressure gradient force with the magnitude of the buoyancy force in the vertical equation of motion in equation (30), so that

$$\left\{ \frac{1}{\bar{\rho}} \frac{\partial p'}{\partial z} \right\}_M \sim \left\{ g \frac{\rho'}{\bar{\rho}} \right\}_M \quad , \tag{43}$$

equations (38) and (39) may be written as

$$\frac{L_1}{L_3} << \left\{ \frac{\rho'}{\bar{\rho}} \frac{g}{2\Omega_z v'} \right\}_M \tag{44}$$

and

$$\frac{L_2}{L_3} << \left\{ \frac{\rho'}{\bar{\rho}} \frac{g}{2\Omega_z u'} \right\}_M \quad . \tag{45}$$

We may assume for atmospheric problems that $\rho'/\bar{\rho} \sim 0.01$, $\Omega_z = 0.504 \cdot 10^{-4}$ sec^{-1} ($\phi = 45°$ N), $g = 9.8$ m sec^{-2}, and $u' \sim v' \sim 10$ m sec^{-1}, so that equations (44) and (45) yield

$$\frac{L_1}{L_3} \quad \text{and} \quad \frac{L_2}{L_3} << 10^2 \quad . \tag{46}$$

Most analyses of small-scale perturbations in the absence of Coriolis forces predict $1 \leqq L_1/L_3$ (i = 1, 2) $\leqq 20$ [14, 38]. Accordingly, we will assume as a working hypothesis that equation (46) is satisfied by perturbations in shear layer or jet flows. It will be shown a posteriori that this assumption is valid. An additional condition involving the frequency of the perturbations can be obtained by requiring that the Coriolis forces are small in comparison to the local accelerations, so that the ratio between a typical Coriolis term and a typical acceleration term must be sufficiently less than one to neglect the Coriolis terms. Thus, for example, if we neglect $2\Omega_z \bar{\rho} v'$ against $\partial(\bar{\rho}u')/\partial t$ in equation (28), we obtain the condition that

$$\left\{ 2\Omega_z \bar{\rho} v' \right\}_M \Big/ \left\{ \partial(\bar{\rho}u')/\partial t \right\}_M << 1 \quad .$$

Since $v'/u' \sim 1$, it follows that $\omega_M >> \Omega_z$ where ω_M is a typical frequency of the perturbations. Thus, the frequencies of the perturbations must be very large compared to the rotation rate of the earth. This concludes our analysis of the approximations with regard to the perturbation momentum equations.

Upon eliminating $T'/\bar{T}$ between equation (23) and equation (24), we find

$$\frac{\theta'}{\bar{\theta}} = \frac{C_v}{C_p} \frac{p'}{\bar{p}} - \frac{\rho'}{\bar{\rho}} \quad , \tag{47}$$

where $C_v = C_p - R$. Substitution of equation (47) into equation (32) yields

$$L\rho' - \frac{C_v}{C_p} \frac{\bar{\rho}}{\bar{p}} Lp' - \bar{\rho} w' S = 0 \quad , \tag{48}$$

where

$$S = \frac{1}{\bar{\theta}} \frac{d\bar{\theta}}{dz} \quad . \tag{49}$$

At this point we will invoke the Boussinesq approximation to simplify the mass continuity equation and neglect $L\rho'$ in equation (31). The Boussinesq approximation has been introduced into the momentum conservation equations with the linearization procedure. Equations (28) through (30) without Coriolis terms, equation (31) without $L\rho'$, and equation (48) are the linearized forms of the Boussinesq approximated equations of motion for deep convection. The details of the approximation are contained in a paper by Dutton and Fichtl [39]. The dependent variables are $\bar{\rho}u'$, $\bar{\rho}v'$ $\bar{\rho}w$, p', and ρ'. The equations are suitable for analyzing the stability properties of shear layers and jets in which the frequencies of the perturbations are less than or equal to the Brunt-Vaisala frequency, $(gS)^{1/2}$, and the vertical scales of the perturbations can be of the same order of magnitude as the scale height of the medium. However, these conditions are only sufficient to validate these equations, so that we will relax the length scale requirement and neglect the pressure perturbation term in equation (48) for the sake of mathematical

convenience. According to Dutton and Fichtl [39], this simplification implies that the vertical scales of the perturbations are small compared to the local scale height.

Application of all the above-mentioned approximations to equations (28) through (31) and (48) yields

$$L(\bar{\rho}u') + \bar{\rho}w' \frac{d\bar{u}}{dz} = -\frac{\partial p'}{\partial x} \quad , \tag{50}$$

$$L(\bar{\rho}u') = -\frac{\partial p'}{\partial y} \quad , \tag{51}$$

$$L(\bar{\rho}w') = -\frac{\partial p'}{\partial z} - g\rho' \quad , \tag{52}$$

$$\frac{\partial(\bar{\rho}u')}{\partial x} + \frac{\partial(\bar{\rho}v')}{\partial y} + \frac{\partial(\bar{\rho}w')}{\partial z} = 0 \quad , \tag{53}$$

and

$$L\rho' - \bar{\rho}w'S = 0 \quad . \tag{54}$$

The analysis of shear layer and jet instabilities will be based upon this set of differential equations.

Normal Mode Representation

Earlier in this report we assumed that the time and horizontal length scales of the perturbations are very small in comparison to the associated scales of the unperturbed flow. This assumption permits us to neglect the temporal and horizontal variations of the unperturbed flow in the perturbation equations. Accordingly, we are formally treating the shear layer or jet flow as being a steady-state, horizontally uniform flow, infinite in horizontal extent. This means that we may represent the dependent variables as normal mode solutions with respect to the horizontal and time coordinates. Substitution of these normal mode representations into the simplified perturbation

equations will yield a set of equations that govern the vertical variations of the normal mode amplitudes of the dependent variables.

The normal mode representation of the dependent variables in the horizontal and time coordinates is given by the Fourier integral

$$\phi(x,y,z,t) = \int_0^\infty \int_0^\infty \hat{\phi}(\kappa_1, \kappa_2, \omega, z)\, e^{i(\kappa_1 x + \kappa_2 y + \omega t)}\, d\kappa_1\, d\kappa_2 \quad . \quad (55)$$

In equation (55), ϕ and $\hat{\phi}$ denote a dependent variable and its associated Fourier amplitude and κ_1 and κ_2 denote wave numbers associated with the x and y axes. The frequency of the system, denoted by ω, depends upon κ_1 and κ_2, the structure of the unperturbed flow and the associated boundary conditions.

The dependent variables as represented by equation (55) are constructed from a complete orthogonal function set, so that each Fourier mode can be considered individually. Thus, upon substituting equation (55) into equations (50) through (54), we find

$$i\Omega\, \bar{\hat{\rho}}\vec{u}' + \bar{\hat{\rho}}\hat{w}'\, D\bar{U}\, \vec{i} + i\, \vec{\kappa}\, \hat{p}' + (D\hat{p}' + g\hat{\rho}')\, \vec{k} = 0 \quad , \quad (56)$$

$$i\Omega\, \hat{\rho}' - \bar{\hat{\rho}}\hat{w}'S = 0 \quad , \quad (57)$$

and

$$i\vec{\kappa} \cdot \bar{\hat{\rho}}\vec{u}' + D(\bar{\hat{\rho}}\hat{w}') = 0 \quad , \quad (58)$$

where

$$\Omega = \omega + \kappa_1 \bar{u} \quad , \quad (59)$$

$$\vec{\hat{u}}' = \vec{i}\,\hat{u}' + \vec{j}\,\hat{v}' + \vec{k}\,\hat{w}' \quad , \tag{60}$$

$$D = \frac{d}{dz} \quad , \tag{61}$$

and

$$\vec{\kappa} = \vec{i}\,\kappa_1 + \vec{j}\,\kappa_2 \quad . \tag{62}$$

The symbols $\vec{i}$, $\vec{j}$, and $\vec{k}$ denote unit vectors directed parallel to the x, y, and z axes. The elimination of the horizontal divergence of $\bar{\rho}\vec{\hat{u}}'$ between equations (56) and (58) yields

$$\Omega D\psi - \kappa_1 \psi\, D\bar{u} - i\kappa^2 \hat{p}' = 0 \quad , \tag{63}$$

where

$$\left.\begin{aligned} \psi &= \bar{\rho}\hat{w}' \\ \kappa^2 &= \kappa_1^2 + \kappa_2^2 \end{aligned}\right\} \quad . \tag{64}$$

The elimination of $\hat{\rho}'$ between the $\vec{k}$ component of equation (56) and (57) yields

$$\Omega^2\psi - i\Omega D\hat{p}' - gS\psi = 0 \quad . \tag{65}$$

Further elimination of $\hat{p}'$ between equations (63) and (65) then gives

$$\Omega^2 D^2\psi - \left[k_1\Omega\, D^2\bar{u} - \kappa^2(gS - \Omega^2) \right] \psi = 0 \quad . \tag{66}$$

Equation (66) is a homogeneous second-order ordinary differential equation in the unknown, ψ. In this equation, $\bar{u}$ and $\bar{\theta}$ are known functions of z. The stability analysis in the subsequent portions of this report will be based upon the solution of this equation.

Boundary and Interfacial Conditions

Now we investigate the boundary and interfacial conditions associated with continuous and broken-line jet and shear layer flows in a semi-infinite atmosphere. Equation (66) possesses an infinity of solutions for a given set of $\bar{\theta}$ and $\bar{u}$ profiles; however, the solution for a given set of boundary and interfacial conditions is unique. The general solution to this equation has two arbitrary constants of integration. Upon applying the boundary and interfacial conditions to the general solution, these constants of integration will be known to within a multiplicative constant which depends upon the initial conditions. Because we will examine broken-line jet and shear layer flows, we will obtain solutions to equation (66) valid for various portions of the unperturbed flow and we must ensure that these solutions agree at the interfacial surfaces that separate these regions. The solution in each region will be characterized by two constants of integration; however, the constants of integration must be related because there are only two arbitrary constants of integration for the complete domain of integration. Thus, for each interface in the shear layer or jet flow, we require two interfacial conditions to relate the constants of integration across the interfacial boundaries between adjacent regions of integration.

Rigid Boundaries. We shall require the vertical velocity and thus the vertical component of the perturbation momentum vector to vanish at the lower rigid boundary, so that

$$\int_0^\infty \int_0^\infty \psi \, e^{i(\kappa_1 x + \kappa_2 y + \omega t)} \, d\kappa_1 \, d\kappa_2 = 0 \tag{67}$$

at a rigid boundary. Because this integral must vanish for arbitrary x, y, and t, and because ψ is a complete function set, it follows that

$$\psi = 0 \tag{68}$$

at a rigid boundary. In the subsequent analyses, we will assume that the lower rigid boundary is sufficiently far removed from the jet core or shear layer, so that the lower rigid boundary condition will be applied at $z = -\infty$. The validity of this assumption, which will simplify the study of the permissible eigenstates, will be analyzed by examining a simple Kelvin-Helmholtz shear layer or vortex sheet later in this report.

Free Boundaries at Infinity. The upper boundary, located at infinity, will be considered to be a free surface in which $\bar{p}$ and $\bar{\rho}$ vanish. Since pressure is a single-valued function of position and time, we will require that the pressure perturbations vanish in the limit as we approach the free surface so that

$$\lim_{z \to \infty} \int_0^\infty \int_0^\infty \hat{p}' \, e^{i(\kappa_1 x + \kappa_2 y + \omega t)} \, d\kappa_1 \, d\kappa_2 = 0 \quad . \tag{69}$$

Upon taking the limit operator under the integrals, it follows that

$$\lim_{z \to \infty} \hat{p}' = 0 \quad . \tag{70}$$

This condition may be cast into a statement concerning the behavior of ψ at infinity. If we take the limit of equation (63) as z approaches infinity, and impose equation (70), we find the appropriate condition on ψ is then given by

$$\lim_{z \to \infty} \left\{ \Omega D\psi - \kappa_1 \psi \, D\bar{u} \right\} = 0 \quad . \tag{71}$$

The free boundary equation (71), as well as the rigid boundary equation (68), can be applied to broken-line and continuous shear layer and jet flows.

Interfacial Conditions. Two interfacial conditions are necessary to force agreement of solutions across interfaces in broken-line shear layer and jet flows. One condition will be derived from the requirement that the component of velocity normal to the interface must be continuous across the interface. The other condition will be obtained by integrating equation (66) across an interface.

Consider a horizontal interface which is deformed by perturbations. The perturbations are sufficiently small so that products of perturbation quantities can be neglected in comparison to first-order terms. To prevent infinite accelerations, we require that the component of velocity normal to this surface be continuous. In mathematical terms, this last statement may be expressed as

$$\Delta_s \left\{ u \frac{\partial \Phi}{\partial x} + v \frac{\partial \Phi}{\partial y} + w \frac{\partial \Phi}{\partial z} \right\} = 0 \quad , \tag{72}$$

where

$$\Delta_s(f) = f_2 - f_1 \tag{73}$$

and the subscripts 1 and 2 denote evaluation at the interface from below and above. In equation (72), Φ is a function of x, y, z, and t and it appears in the equation for the interfacial surface given by

$$\Phi(x, y, z, t) = 0 \quad . \tag{74}$$

A function Φ that would describe the instantaneous position of the interface is given by

$$\Phi(x, y, z, t) = z - z_s - \xi'(x, y, t) = 0 \quad , \tag{75}$$

where z_s is the height of the unperturbed position of the interface above a datum plane and ξ' is the height of the interface relative to the unperturbed or equilibrium position. In a particular problem z_s is a constant. Upon substituting equations (75) and (16) into equation (72), and then applying the approximations (25) and (27), we find the perturbation form of equation (72) is given by

$$\Delta_s \left\{ - \bar{u} \frac{\partial \xi'}{\partial x} + w' \right\} = 0 \quad . \tag{76}$$

We may identify ξ' with the vertical component of the Lagrangian displacement vector of a fluid particle located at x, y, and t in the interface, because, by definition, fluid particles can neither leave nor enter the interface. In short, the interface is a material surface. Thus, the vertical velocity of a fluid particle at the point x, y, and t in the interface is given by

$$w'(x,y,z_s + \xi',t) = \frac{d\xi'}{dt} \quad . \tag{77}$$

However, ξ' is a perturbation quantity, so that to within first order

$$w' = \frac{\partial \xi'}{\partial t} + \bar{u} \frac{\partial \xi'}{\partial x} \quad . \tag{78}$$

Substitution of equation (78) into equation (76) yields the result

$$\Delta_s \left(\frac{\partial \xi'}{\partial t} \right) = 0 \quad . \tag{79}$$

If we expand w' in the vertical about the level $z = z_s$ in a Taylor series, then

$$w' = w'(x,y,z_s,t) + \left(\frac{\partial w'}{\partial z} \right)_{z_s} \xi' + \ldots \quad . \tag{80}$$

However, w' and ξ' are perturbation quantities, so that to within first order

$$w'(x,y,z_s + \xi',t) = w'(x,y,z_s,t) \quad . \tag{81}$$

This means we may evaluate the left side of equation (78) at the equilibrium position of the interface.

If we represent ξ' with a Fourier integral of the form

$$\xi' = \int_0^\infty \int_0^\infty \hat{\xi}'(\kappa_1, \kappa_2, \omega)\, e^{i(\kappa_1 x + \kappa_2 y + \omega t)}\, d\kappa_1\, d\kappa_2 \quad , \tag{82}$$

then it follows from equation (78) that

$$\hat{w}'(x, y, z_s, t) = i\Omega\hat{\xi}' \quad . \tag{83}$$

Substitution of equation (82) into equation (79) yields

$$\omega\Delta_s(\hat{\xi}') = 0 \quad , \tag{84}$$

where Δ_s means that we evaluate the "jump" in $\hat{\xi}'$ across the interface at $z = z_s$. In general, ω does not vanish; thus, it may be concluded from equation (84) that the Fourier amplitudes of the vertical component of the Lagrangian displacement vector are continuous across an interface.

We may express equation (84) in terms of $\hat{w}'$ in view of equation (83), so that

$$\Delta_s\left(\frac{\hat{w}'}{\Omega}\right) = 0 \quad . \tag{85}$$

However, since our fundamental differential equation is in terms of ψ, equation (66), we must require

$$\Delta_s\left(\frac{\psi}{\bar{\rho}\Omega}\right) = 0 \quad . \tag{86}$$

Since $\bar{p}$ must be continuous across an interface and $\bar{\rho}$ is inversely proportional to $\bar{\theta}$, it follows that equation (86) can be expressed alternatively in the form

$$\Delta_s \left(\frac{\bar{\theta}\psi}{\Omega} \right) = 0 \quad . \tag{87}$$

This is our first interfacial condition.

Let us now concentrate on developing the second interfacial condition. Equation (66) may be written in the form

$$D \left\{ \Omega D\psi - \kappa_1 \psi \, D\bar{u} \right\} - \kappa^2 g \frac{\psi\bar{\theta}}{\Omega} D \left(\frac{1}{\bar{\theta}} \right) - \kappa^2 \Omega \psi = 0 \quad . \tag{88}$$

If we integrate this expression over an infinitesimal element $(z_s - \epsilon < z < z_s + \epsilon)$ and then pass to the limit, $\epsilon = 0$, it follows that

$$\Delta_s (\Omega D\psi - \kappa_1 \psi \, D\bar{u}) - g\kappa^2 \frac{\psi\bar{\theta}}{\Omega} \Delta_s (\bar{\theta}^{-1}) \quad . \tag{89}$$

In performing this integration, we have used the continuity of $\psi\bar{\theta}/\Omega$ across an interface. Equation (89) may be evaluated on both sides of the interface, thus yielding two conditions. However, one of these conditions and equation (87) yield the other. Thus, we have the option of using the two conditions implied by equation (89), or one of these conditions and equation (87). Equation (89) is merely a statement of the continuity of pressure across an interface.

GENERAL CONSIDERATIONS

Before proceeding to the detailed calculations in the subsequent portions of this report, it is worthwhile to examine the mathematical properties of the governing differential equation (66) and the associated boundary and interfacial conditions that were derived previously. This system is given by

$$\Omega^2 D^2\psi - \left[\kappa_1 \Omega \, D^2\bar{u} - \kappa^2 (gS - \Omega^2) \right] \psi = 0 \quad , \tag{66}$$

$$\psi = 0 \quad \text{at} \quad z = 0 \quad , \tag{68}$$

$$\lim_{z \to \infty} \left\{ \Omega D\psi - \kappa_1 \psi \, D\bar{u} \right\} = 0 \quad , \tag{71}$$

$$\Delta_s \left(\frac{\bar{\theta}\psi}{\Omega} \right) = 0 \quad , \tag{87}$$

and

$$\Delta_s (\Omega D\psi - \kappa_1 \psi \, D\bar{u}) - g\kappa^2 \frac{\psi\bar{\theta}}{\Omega} \Delta_s (\bar{\theta}^{-1}) = 0 \quad . \tag{89}$$

In the following, we will present the method for solving this system for various types of broken-line flows, obtaining two theorems concerning the permissible number of modes this system can possess. Also, we will examine the consequences of two transformations of the dependent variable. These transformations will yield three theorems that were first derived by Miles [31], Howard [33], and Synge [37] for continuous $\bar{\theta}$ and $\bar{u}$ profiles. In addition, a necessary and sufficient condition for the existence of unstable solutions for atmospheres characterized by $S \neq 0$ will be derived. It will be shown that this condition leads to the result that all continuous flows which are statically unstable ($S < 0$) everywhere are dynamically unstable to small perturbations. Finally, the implications of these theorems for broken-line profiles will be examined.

Solutions for Broken-Line Profiles

The purpose of introducing broken-line $\bar{\theta}$ and $\bar{u}$ profiles is to simplify the governing differential equation so that it can be solved with elementary functions. Broken-line profiles are selected so that the coefficients in equation (66) are piecewise constant. The following types of profiles serve this purpose:

(1) Stacked layers in which $\bar{u}$ and $\bar{\theta}$ are constants.

(2) Stacked layers in which $\bar{u}$ and S are constants.

(3) Stacked layers in which $\bar{u}$ is a linear function of z and $\bar{\theta}$ is constant.

Type (1) flows are special cases of the type (3) flows. If $\Omega \neq 0$, then equation (66) reduces to

$$D^2\psi - \kappa^2\psi = 0 \tag{90}$$

for the type (1) and (3) profiles and

$$D^2\psi - \kappa^2\left(1 - \frac{gS}{\Omega^2}\right)\psi = 0 \tag{91}$$

for the type (2) profiles.

Let us now consider a type (1), (2), or (3) flow that possesses N interfacial surfaces and N + 1 layers, where the k^{th} interface is located at $z = z_k$. The solutions to equations (90) and (91) for the k^{th} layer are given by

$$\psi_k = A_k \Psi_k + B_k \Phi_k \quad (k = 1, 2, \ldots, N+1) \quad , \tag{92}$$

where

$$\Psi_k = e^{\kappa \epsilon_k z} \quad , \tag{93}$$

$$\Phi_k = e^{-\kappa \epsilon_k z} \quad , \tag{94}$$

and

$$\epsilon_k = \left(1 - \frac{gS_k}{\Omega_k}\right)^{1/2} \quad . \tag{95}$$

In equation (95), S_k and Ω_k are the values of S and Ω in the k^{th} layer, and A_k and B_k are the associated constants of integration. The solutions

as given by equations (93) and (94) are valid for type (2) flows; the solutions for the type (1) and (3) profiles are obtained by setting $\epsilon_k = 1$. Application of the interfacial equations (87) and (89) to the solutions ψ_k and ψ_{k+1} at the interface yield

$$A_k M^-_{1,k} + B_k M^-_{2,k} + A_{k+1} N_{1,k} + B_{k+1} N_{2,k} = 0 \tag{96}$$

and

$$A_k N_{3,k} + B_k N_{4,k} + A_{k+1} M^+_{1,k} + B_{k+1} M^+_{2,k} = 0 \quad , \tag{97}$$

where

$$\left.\begin{aligned} M^-_{1,k} &= \kappa_1 \Lambda_k \Psi_k(z_k-) - \Omega_k(z_k-)\, D\Psi_k(z_k-) \\ M^-_{2,k} &= \kappa_1 \Lambda_k \Phi_k(z_k-) - \Omega_k(z_k-)\, D\Phi_k(z_k-) \end{aligned}\right\} \quad , \tag{98}$$

$$\left.\begin{aligned} M^+_{1,k} &= \kappa_1 \Lambda_{k+1} \Psi_{k+1}(z_k+) - \Omega_{k+1}(z_k+)\, D\Psi_{k+1}(z_k+) \\ M^+_{2,k} &= \kappa_1 \Lambda_{k+1} \Phi_{k+1}(z_k+) - \Omega_{k+1}(z_k+)\, D\Phi_{k+1}(z_k+) \end{aligned}\right\} \quad , \tag{99}$$

$$N_{1,k} = -\left\{ M^+_{1,k} + g\kappa^2 \frac{\Psi_{k+1}(z_k+)}{\Omega_{k+1}(z_k+)} \left[1 - \frac{\bar{\theta}_{k+1}(z_k+)}{\bar{\theta}_k(z_k-)} \right] \right\} \quad , \tag{100}$$

$$N_{2,k} = -\left\{ M^+_{2,k} + g\kappa^2 \frac{\Phi_{k+1}(z_k+)}{\Omega_{k+1}(z_k+)} \left[1 - \frac{\bar{\theta}_{k+1}(z_k+)}{\bar{\theta}_k(z_k-)} \right] \right\} \quad , \tag{101}$$

$$N_{3,k} = -\left\{ M^-_{1,k} - g\kappa^2 \frac{\Psi_k(z_k-)}{\Omega_k(z_k-)} \left[1 - \frac{\bar{\theta}_k(z_k-)}{\bar{\theta}_{k+1}(z_k+)} \right] \right\} \quad , \tag{102}$$

$$N_{4,k} = -\left\{ M^{-}_{2,k} - g\kappa^2 \frac{\Phi_k(z_k^-)}{\Omega_k(z_k^-)} \left[1 - \frac{\bar{\theta}_k(z_k^-)}{\bar{\theta}_{k+1}(z_k^+)} \right] \right\} \quad , \tag{103}$$

and z_k^- and z_k^+ denote evaluation at the k^{th} interface upon approaching it from below and above. In equations (98) and (99), Λ_k represents the velocity shear of the unperturbed flow in the k^{th} layer.

Equations (96) and (97) represent 2N equations in $2(N + 1)$ variables, namely A_k and B_k ($k = 1, 2, \ldots, N + 1$). This system is underdetermined; however, we have two other conditions at our disposal, namely, equations (68) and (71), which will close the system, so that a solution can be obtained to within an aribtrary multiplicative constant. Evaluation of equation (68) at the lower boundary yields

$$A_1 + B_1 = 0 \quad . \tag{104}$$

Elimination of A_1 from equations (96) and (97) for $k = 1$ with equation (104) yields

$$\left.\begin{aligned} B_1(M^{-}_{2,1} - M^{-}_{1,1}) + A_2N_{1,1} + B_2N_{2,1} &= 0 \\ B_1(N_{4,1} - N_{3,1}) + A_2M^{+}_{1,1} + B_2M^{+}_{2,1} &= 0 \end{aligned}\right\} \quad . \tag{105}$$

At the upper boundary, the linearly independent solutions Ψ_{N+1} and Φ_{N+1} for the types (1) and (3) flows have the limiting values

$$\lim_{z \to \infty} \Psi_{N+1} = \infty \quad \text{and} \quad \lim_{z \to \infty} \Phi_{N+1} = 0 \quad ; \tag{106}$$

therefore, to satisfy equation (71) we must require

$$A_{N+1} = 0 \quad . \tag{107}$$

However, in the case of the type (2) flows, we have

$$\left.\begin{aligned} \lim_{z \to \infty} \Psi_{N+1} &= \infty \quad \text{and} \quad \lim_{z \to \infty} \Phi_{N+1} = 0 \quad \text{for} \quad \mathrm{Re}(\epsilon_{N+1}) > 0 \\ \lim_{z \to \infty} \Psi_{N+1} &= 0 \quad \text{and} \quad \lim_{z \to \infty} \Phi_{N+1} = \infty \quad \text{for} \quad \mathrm{Re}(\epsilon_{N+1}) < 0 \end{aligned}\right\} . \tag{108}$$

To be definite, we will associate Φ_{N+1} with the convergent solution as z approaches infinity; i.e., we will exchange the symbols Φ_{N+1} and Ψ_{N+1} in equations (93) and (94) for $k = N + 1$ if $\mathrm{Re}(\epsilon_{N+1}) < 0$. Thus, equation (107) will be valid for the type (2) profiles. Accordingly, for $k = N$, equations (96) and (97) can be expressed in the form

$$\left.\begin{aligned} A_N M^{-}_{1,N} + B_N M^{-}_{2,N} + B_{N+1} N_{2,N} &= 0 \\ A_N N_{3,N} + B_N N_{4,N} + B_{N+1} M^{+}_{2,N} &= 0 \end{aligned}\right\} . \tag{109}$$

Now, equations (96) and (97), for $k = 2, 3, \ldots, N - 1$, and equations (105) and (109) represent $2N$ linear homogeneous equations in $2N$ unknowns, namely, $A_2, A_3, \ldots, A_N$ and $B_1, B_2, \ldots, B_{N+1}$. Since these equations are homogeneous, the solution can be determined to within only an arbitrary multiplicative constant; this constant is determined by prescribing the initial disturbance at $t = 0$.

According to the theory of linear algebraic equations, we must require the determinant of the coefficients of the A's and B's to vanish, in order for the solution to be nontrivial, so that

$$
\begin{vmatrix}
M^{-}_{2,1} & -M^{-}_{1,1} & N_{1,1} & \cdot & \cdot & 0 & 0 \\
N_{4,1} & -N_{3,1} & M^{+}_{1,1} & \cdot & \cdot & 0 & 0 \\
0 & & M^{-}_{1,2} & \cdot & \cdot & 0 & 0 \\
0 & & N_{3,2} & \cdot & \cdot & 0 & 0 \\
0 & & 0 & \cdot & \cdot & 0 & 0 \\
\cdot & & \cdot & \cdot & \cdot & \cdot & \cdot \\
\cdot & & \cdot & \cdot & \cdot & N_{2,N-1} & 0 \\
0 & & 0 & \cdot & \cdot & M^{+}_{2,N-1} & 0 \\
0 & & 0 & \cdot & \cdot & M^{-}_{2,N} & N_{2,N} \\
0 & & 0 & \cdot & \cdot & N_{4,N} & M^{+}_{2,N}
\end{vmatrix} = 0 \quad . \quad (110)
$$

Equation (110) is the characteristic equation for the problem and the solution of this equation for ω will yield the permissible eigenstates of the perturbations and the stability properties of the unperturbed flow. The expanded form of this equation can be expressed as

$$
\Omega_1^{-1}(z_{1-})\ \Omega_2^{-1}(z_{1+}) \ \ldots\ \Omega_N^{-1}(z_{N-})\ \Omega_{N+1}^{-1}(z_{N^+}) \sum_{k=0}^{2N} a_k\, \omega^k = 0 \quad , \quad (111)
$$

where the a's are functions of the $\bar{u}$'s and the $\bar{\theta}$'s evaluated at the interfaces, the Λ's in the type (3) flows, $e^{\kappa\epsilon_1(z_{1-})z_1}$, $e^{-\kappa\epsilon_1(z_{1-})z_1}$, $e^{\kappa\epsilon_2(z_{1+})z_1}$, $\ldots$, $e^{-\kappa\epsilon_{N+1}(z_{N^+})z_N}$ in the type (2) flows, and κ_1 and κ_2. In deriving equations (90) and (91), it was assumed that $\Omega_k \neq 0$ and thus it follows from equation (111) that

$$
\sum_{k=0}^{2N} a_k\, \omega^k = 0 \quad . \quad (112)
$$

In the type (1) and (3) flows, the a's are independent of ω and equation (112) is a polynomial in ω of degree 2N. Thus, it may be concluded that the permissible number of modes associated with the type (1) and (3) broken-line flows for specified values of κ_1 and κ_2 cannot exceed 2N.

If the basic state is isentropic, then S must vanish everywhere and $\bar{\theta}$ will be continuous across the interfacial surfaces. This means the type (2) flows will reduce to type (1) flows. In addition, the characteristic equation for the type (1), (2), and (3) flows can be written in the form

$$\sum_{k=0}^{2N} b_k \omega^k = 0 \quad , \tag{113}$$

where the b's are functions of the $\bar{u}$'s evaluated at the interfaces, κ_1 and κ_2, and the Λ's in the case of the type (3) flows. Thus, it may be concluded that the permissible number of modes associated with isentropic type (1), (2), and (3) flows for specified values of κ_1 and κ_2 also cannot exceed 2N.

In the type (2) broken-line flows in which S = 0, equation (112) is a transcendental equation in ω. In addition, we have the added restriction that the real part of ϵ_{N+1} must be selected so that the solution in the $(N + 1)^{th}$ layer converges as z approaches infinity. It is extremely difficult to solve this eigenvalue equation for ω, and it appears that no general conclusions can be stated about the permissible number of modes as in the type (1) and (3) flows.

The main objective of this report is to analyze instabilities in shear layer and jet flows with the main emphasis upon the latter. To perform this task, we desire a model that yields a characteristic equation that is amenable to parametric analysis, so that it can be analyzed with relative ease for a wide variety of jet and shear flow configurations. The model best suited for this purpose is a three-layer type (1) flow. The resulting eigenvalue equation is a fourth-order polynomial in ω. Admittedly, the model is somewhat unrealistic since the potential temperature is constant in each layer; nevertheless, the system permits simulation of static instability and stability with "jumps" in the potential temperature across the interfaces. In this respect, the type (2) flows would be more realistic. However, to determine the type (2) eigenvalues we would have to search the complex ω-plane with a trial and error procedure, because of its complicated transcendental nature.

In the type (3) flows, it would be possible to model jets, which are bounded at infinity, with a three-layer model given by

$$\begin{aligned} \bar{u} &= \Lambda_1 z && (0 \leqq z < z_1) \\ \bar{u} &= \Lambda_2(z - z_1) + \Lambda_1 z_1 && (z_1 \leqq z < z_2) \\ \bar{u} &= \Lambda_2(z_2 - z_1) + \Lambda_1 z_1 && (z_2 \leqq z < \infty) \end{aligned} \quad , \tag{114}$$

where $\Lambda_1 > 0$ and $\Lambda_2 < 0$. The characteristic equation for this flow state is a fourth-order polynomial in ω. However, with type (3) flows, it is not possible to model strong jets having large shears with realistic core velocities and still have reasonable unperturbed velocities in the extremities of the velocity profile. This could be remedied by splitting the lower layer into two layers. However, this would complicate the problem, because the characteristic equation would then be a sixth-order polynomial in ω. In the case of the type (1) flows, it is possible to simulate high core velocities and large velocity shears in the form of vortex sheets and still have reasonable velocities in the extremities of the profile, as well as a simple characteristic equation suitable for parametric analysis. Accordingly, later in this report we will confine our attention to an analysis of the three-layer type (1) jet and shear layer flows. Thus, by adjusting the velocities and potential temperature in each layer, we can model a variety of jet and shear layer flows for a variety of thermal stratifications.

Transformation $\psi = \Omega F$

Let us suppose that $\mathrm{Im}(\omega) \neq 0$ and define the function F with the relation

$$\psi = \Omega F \quad . \tag{115}$$

Substitution of the transformation equation (115) into equations (66), (68), (71), (87), and (89) yields

$$D(\Omega^2 DF) - \kappa^2(\Omega^2 - gS)F = 0 \quad , \tag{116}$$

$$\Omega F = 0 \quad \text{at} \quad z = 0 \quad , \tag{117}$$

$$\lim_{z \to \infty} (\Omega^2 DF) = 0 \quad , \tag{118}$$

$$\Delta_s(\bar{\theta} F) = 0 \quad , \tag{119}$$

and

$$\Delta_s (\Omega^2 DF) - g\kappa^2 F \, \bar{\theta} \, \Delta_s(\bar{\theta}^{-1}) \quad . \tag{120}$$

The complex conjugate F^* of F satisfies this system if we replace Ω with Ω^*. Multiplication of equation (115) by F^* and integration over the domain $(0 \leqq z \leqq \infty)$ yields

$$\int_0^\infty F^* D(\Omega^2 DF) \, dz - \int_0^\infty \kappa^2 \Omega^2 \, |F|^2 \, dz + \int_0^\infty \kappa^2 \, gS |F|^2 \, dz = 0 \quad . \tag{121}$$

The first integral on the left-hand side of equation (121) may be integrated by parts, so that

$$\int_0^\infty F^* D(\Omega^2 DF) \, dz = - \int_0^\infty \Omega^2 \, |DF|^2 \, dz + \{\Omega^2 F^* DF\}_0^\infty$$

$$+ \sum_{k=1}^{N} \{\Delta_s (\Omega^2 F^* DF)\}_k \quad . \tag{122}$$

The third term on the right-hand side of equation (122) is the contribution from integration across the interfacial surfaces and $\{\Delta_s(\ )\}_k$ is the "jump" in $(\ )$ across the k^{th} interface. The second term on the right-hand side of the equation is the Riemann concomitant evaluated at the upper and lower boundaries. The contribution at the upper boundary vanishes because of equation (118), while the contribution from the lower boundary will vanish because of equation (117), so that

$$\int_0^\infty F^* D(\Omega^2 DF)dz = -\sum_{k=1}^{N+1} \int_{z_{k-1} < z}^{z < z_k} \Omega^2 |DF|^2 dz$$

$$+\sum_{k=1}^{N} \left\{ \Delta_s(\Omega^2 F^* DF) \right\}_k , \qquad (123)$$

where z_k $(k = 1, 2, 3, \ldots, N)$ is the height of the k^{th} interface, $z_o = 0$, and $z_{N+1} = \infty$. The third integral on the left-hand side of equation (121) can be partitioned into two parts so that

$$\int_0^\infty \kappa^2 gS|F|^2 dz = \sum_{k=1}^{N+1} \int_{z_{k-1} < z}^{z < z_k} \kappa^2 gS|F|^2 dz$$

$$-\kappa^2 g \sum_{k=1}^{N} \left\{ \frac{\bar{\theta}^2 |F|^2}{2} \Delta_s(\bar{\theta}^{-2}) \right\}_k . \qquad (124)$$

The first term on the right side of equation (124) is the contribution from integration across each layer of the broken-line jet or shear layer flow; the integration bounds do not include the end points of the intervals. The second term on the right side of equation (124) is the contribution from integration across the interfacial surfaces. In deriving equation (124) we have used the continuity of $\bar{\theta}F$ across the interfacial surfaces, see condition (119). Combination of equations (121), (123), and (124) yields

$$\sum_{k=1}^{N+1} \int_{z_{k-1} < z}^{z < z_k} \Omega^2 |G|^2 dz - \kappa^2 g \sum_{k=1}^{N+1} \int_{z_{k-1} < z}^{z < z_k} S|F|^2 dz$$

$$- \sum_{k=1}^{N} \left\{ \Delta_s (\Omega^2 F^* DF) - \kappa^2 g \frac{\bar{\theta} |F|^2}{2} \Delta_s (\bar{\theta}^{-2}) \right\}_k = 0 \quad , \tag{125}$$

where

$$|G|^2 = |DF|^2 + \kappa^2 |F|^2 \quad . \tag{126}$$

Continuous Jets and Shear Layers. For continuous profiles of $\bar{\theta}$ and $\bar{u}$ we have $N = 0$, so that the interfacial term in equation (125) vanishes and the summation signs can be removed from the first and second terms. Thus, we may write equation (125) in the form

$$\int_0^\infty \Omega^2 |G|^2 dz - \kappa^2 g \int_0^\infty S|F|^2 dz = 0 \quad . \tag{127}$$

From this result, we may conclude that the eigenvalue equation for continuous flows will have two and only two branches in the complex ω-plane. This result means that the eigenvalues of ω occur in complex conjugate pairs so that unstable and stable modes coexist. The reason for this apparent contradiction is that the diffusive effects of viscosity and heat conduction have been neglected. However, it is known that in the case of the Orr-Sommerfeld equation, the unstable solution is the physically relevant one, and the associated stable or decaying mode that occurs in the inviscid limit can be removed by asymptotic expansions involving a Reynolds number and then letting the Reynolds number approach infinity. In view of the fact that equation (66) reduces to the inviscid Orr-Sommerfeld equation for the special case of $S = 0$, we will assume that the unstable solution is the physically relevant one. Equation (127) enables us to derive a necessary and sufficient condition for instability and obtain bounds on the eigenvalues of ω.

a. A Necessary and Sufficient Condition for Instability. Expansion of Ω^2 in equation (127) yields

$$\omega^2 I_2 + 2\omega I_1 + I_o = 0 \quad , \tag{128}$$

where

$$I_o = \int_o^\infty \left\{ (\kappa_1 \bar{u})^2 |G|^2 - \kappa^2 g S |F|^2 \right\} dz \quad , \tag{129}$$

$$I_1 = \int_o^\infty \kappa_1 \bar{u} \, |G|^2 \, dz \quad , \tag{130}$$

and

$$I_2 = \int_o^\infty |G|^2 \, dz \quad . \tag{131}$$

Upon solving equation (128) for ω, we find

$$\omega = -\frac{I_1}{I_2} \pm \left(\frac{I_1^2}{I_2^2} - \frac{I_o}{I_2} \right)^{1/2} \quad . \tag{132}$$

The integrals I_o, I_1, and I_2 are real quantities, so that it may be concluded from equation (132) that the necessary and sufficient condition for ω to be complex and thus for instability $(\mathrm{Im}(\omega) < 0)$ to exist is

$$I_1^2 < I_o I_2 \quad , \tag{133}$$

or

$$\left\{ \int_0^\infty \kappa_1 \bar{u} |G|^2 \, dz \right\}^2 < \int_0^\infty \left\{ (\kappa_1 \bar{u})^2 |G|^2 - \kappa^2 g S |F|^2 \right\} dz \int_0^\infty |G|^2 \, dz \quad . \tag{134}$$

If $S = 0$, then inequality in equation (134) reduces to the form

$$\left\{ \int_0^\infty \kappa_1 \bar{u} |G|^2 dz \right\}^2 < \int_0^\infty |G|^2 \, dz \int_0^\infty (\kappa_1 \bar{u})^2 |G|^2 \, dz \quad . \tag{135}$$

According to the Schwarz inequality, the inequality in equation (135) will be satisfied for all continuous distributions of $\bar{u}$, except in the special case of $\bar{u}$ = constant, where we then have an equality. This result implies that isentropic atmospheres ($S = 0$) characterized by distributions of $\bar{u}(z)$ that vary, however slightly, are always unstable.

Equation (134) is always satisfied for $S < 0$ everywhere, and thus, all continuous statically unstable shear layer and jet flows are dynamically unstable. If $S > 0$ everywhere, only special distributions of $\bar{u}$ will satisfy equation (134). If S is too large locally or globally, then inequality (134) will be reversed and the unperturbed flow will be dynamically stable. On the other hand, if S is sufficiently small for $S > 0$, then the flow can be dynamically unstable.

b. Inviscid Orr-Sommerfeld Equation. Let us now concentrate on the special case $S = 0$. In this case,

$$\Omega \left\{ \Omega D^2 \psi - (\kappa_1 D^2 \bar{u} + \kappa^2 \Omega) \psi \right\} = 0 \quad . \tag{136}$$

In general, $\Omega \neq 0$, except perhaps at selected points on the velocity profile, and thus, equation (136) implies that

$$\Omega D^2 \psi - (\kappa_1 D^2 \bar{u} + \kappa^2 \Omega) \psi = 0 \quad . \tag{137}$$

This equation is the inviscid Orr-Sommerfeld equation (Rayleigh equation) and it can be derived directly from equations (56) through (58) by setting $S = 0$ ab initio in equation (57). Now, equation (137) has a singularity of multiplicity one at $\Omega = 0$, while equation (66) has a singularity of multiplicity two at the same point, and because of this reduction in the multiplicity of the singularity, the necessary and sufficient equation (133) is not valid for $S = 0$.

It should be noted that if $S = 0$, then equation (57) implies that $\hat{\rho}'$ will vanish if Ω is nontrivial. This result implies the Eulerian density fluctuations, ρ', vanish, because ρ' is constructed from the $\hat{\rho}'$ function set through the Fourier integral, equation (55). However, it should not be concluded that the Lagrangian density fluctuations vanish. To clarify this point, we write equation (54) in the form

$$L\rho' = -w' \left\{ D\bar{\rho} + \frac{c_v}{c_p} \frac{g\bar{\rho}}{R\bar{T}} \right\} , \tag{138}$$

where

$$D\bar{\rho} + \frac{c_v}{c_p} \frac{g\bar{\rho}}{R\bar{T}} = \frac{\bar{\rho}}{\bar{\theta}} D\bar{\theta} . \tag{139}$$

The quantity

$$- \frac{c_v}{c_p} \frac{g\bar{\rho}}{R\bar{T}}$$

is the value of $D\bar{\rho}$ associated with an isentropic atmosphere; i.e.,

$$(D\bar{\rho})_{\bar{\theta}=\text{const}} = - \frac{c_v}{c_p} \frac{g\bar{\rho}}{R\bar{T}} . \tag{140}$$

Thus, we may write equation (138) as

$$L\rho' = -w' \left\{ D\bar{\rho} - (D\bar{\rho})_{\bar{\theta}=\text{const}} \right\} \quad . \tag{141}$$

Now, ascending and descending fluid particles will experience changes in density due to adiabatic expansions or compressions. These changes correspond to the Lagrangian density changes and are given by $w'(D\bar{\rho})_{\theta=\text{const}}$. In addition to these changes, we have the density changes due to vertical advection which are given by $w'D\bar{\rho}$. The net local change in density due to vertical motions at a point translating with the mean flow at a given level is equal to the Lagrangian changes minus the vertical advection changes, so that the local changes relative to the mean flow are thus given by equation (141). We have the following situations:

Statically stable atmosphere: $D\bar{\rho} > (D\bar{\rho})_{\bar{\theta}=\text{const}}$

Statically neutral atmosphere: $D\bar{\rho} = (D\bar{\rho})_{\bar{\theta}=\text{const}}$

Statically unstable atmosphere: $D\bar{\rho} < (D\bar{\rho})_{\bar{\theta}=\text{const}}$.

Thus, we may conclude from equation (141) that in a stable stratification the local density changes relative to the mean flow are positive for ascending motions and negative for descending motions, while the reverse is true for unstable stratifications. In a neutral stratification, the local density changes will vanish because the Lagrangian changes are balanced by the vertical advection changes.

Lin [40, 41, 42] and Foote and Lin [43] have discussed equation (137) in detail for boundary layer and jet velocity profiles for $\kappa_2 = 0$. According to Squire's [44] theorem, $\kappa_2 = 0$ corresponds to those marginal states in configuration space that bound all possible unstable states. Lin and Foote explain that the necessary and sufficient condition for the existence of an unstable mode is that $D^2\bar{u}$ vanish somewhere within the fluid. In addition, they note that the neutral modes contiguous to the unstable modes are characterized by

$$D^2\bar{u}(z_c) = 0 \tag{142}$$

and

$$\omega = -\kappa_1 \bar{u}(z_c) \quad , \tag{143}$$

where z_c is that value of z at which equation (137) has a singularity. To determine the critical solution, we merely solve equation (142) for z_c, calculate ω with equation (143), and then determine the critical wave number by solving equation (137). We can then calculate the eigenvalues of ω in the vicinity of the marginal neutral solution by expanding ψ and ω in a Taylor series in terms of κ_1^2 about the marginal solution, paying proper attention to the solution in the vicinity of the singularities. Lipps [45,46] has used this technique to examine barotropic instability in the westerlies. The important point of this discussion is that in the case of the inviscid Orr-Sommerfeld equation we have necessary and sufficient conditions for the instability associated with jets and boundary layer flows which are useful because one may proceed in a straightforward fashion to calculate the critical neutral solution. We are not so fortunate in the case of barotropic instability in stratified fluids characterized by nonvanishing S. Equation (133) does not provide for a straightforward procedure for determining the critical solutions because it depends upon the solution. Thus, it appears that in order to obtain the critical solution for stratified flows we must examine the complete set of Fourier amplitudes associated with given distributions of $\bar{\theta}$ and $\bar{u}$. This can be extremely difficult in view of the fact that relatively simple continuous distributions of $\bar{\theta}$ and $\bar{u}$ make equation (66) very difficult to solve. One way to avoid these difficulties is to employ broken-line representations of jets and shear layers.

c. Semicircle Theorem. It is possible to derive additional information from equation (127) by separating the real and imaginary parts so that

$$\int_0^\infty \left[(\kappa_1 \bar{u} + \omega_r)^2 - \omega_i^2 \right] |G|^2 \, dz - \kappa^2 g \int_0^\infty S |F|^2 \, dz = 0 \tag{144}$$

and

$$i\, 2\omega_i \int_0^\infty (\kappa_1 \bar{u} + \omega_r) \, |G|^2 \, dz = 0 \quad , \tag{145}$$

where $\omega_i = \mathrm{Im}(\omega)$ and $\omega_r = \mathrm{Re}(\omega)$. It may be concluded from equation (145) that if $\omega_i < 0$ (dynamically unstable perturbations), then $\kappa_1\bar{u} + \omega_r$ must vanish at least once in the interval $0 \leqq z \leqq \infty$. This result was first obtained by Synge [37].

Let us now assume $\omega_i \neq 0$, so that equations (144) and (145) may be written

$$\kappa_1^2 \int_0^\infty \bar{u}^2 |G|^2 \, dz = (\omega_r^2 + \omega_i^2) \int_0^\infty |G|^2 dz + \kappa^2 \int_0^\infty gS|F|^2 dz \tag{146}$$

and

$$\kappa_1 \int_0^\infty \bar{u}|G|^2 \, dz = -\omega_r \int_0^\infty |G|^2 \, dz \quad . \tag{147}$$

If we assume $a \leqq \kappa_1 \bar{u} \leqq b$, then

$$\int_0^\infty (\kappa_1\bar{u} - a)(\kappa_1\bar{u} - b)|G|^2 \, dz \leqq 0 \quad . \tag{148}$$

Combination of equations (146), (147), and (148) yields the result that

$$\left\{ \left[\omega_r + \frac{1}{2}(a+b) \right]^2 + \omega_i^2 - \left[\frac{1}{2}(a-b) \right]^2 \right\} \int_0^\infty |G|^2 dz + \int_0^\infty gS|F|^2 dz \leqq 0 \quad . \tag{149}$$

If we consider media that possess positive static stability $(S > 0)$, then equation (149) implies

$$\left[\omega_r + \frac{1}{2} (a + b) \right]^2 + \omega_i^2 \leqq \left[\frac{1}{2} (a - b) \right]^2 \tag{150}$$

because $|G|^2$ and $|F|^2$ are positive definite. Thus, the complex wave frequency ω for any unstable mode, associated with $S > 0$, must lie inside the semicircle in the lower half of the complex ω-plane, which has the range of $\kappa_1 \bar{u}$ for diameter. This result was first obtained by Howard [33].

Broken-Line Profiles. The stability criteria in equation (133) and the semicircle theorem do not necessarily apply to an arbitrary broken-line flow because the function F does not occur in a positive definite form in the third term on the left-hand side of equation (125). In the other terms, F and DF occur in absolute value forms and it is possible to fix the signs of the various terms without explicitly knowing F, while this is not true for the term in question. However, it is possible to make this term vanish by restricting the flows to those characterized by $\bar{\theta}$ being continuous across the interfacial surfaces.

If we require $\bar{\theta}$ to be continuous across the interfacial surfaces, then it follows that equations (119) and (120) can be written as

$$\Delta_s(F) = 0 \tag{151}$$

and

$$\Delta_s(\Omega^2 DF) = 0 \quad . \tag{152}$$

Equation (151) implies that F is continuous across an interface if $\bar{\theta}$ is continuous across the interface, so that we may conclude from equation (152) that

$$\Delta_s(\Omega^2 F^* DF) = 0 \quad . \tag{153}$$

Accordingly, equation (125) reduces to

$$\sum_{k=1}^{N+1} \int_{z_{k-1} < z}^{z < z_k} \Omega^2 |G|^2 dz - \kappa^2 g \sum_{k=1}^{N+1} \int_{z_{k-1} < z}^{z < z_k} S|F|^2 \, dz = 0 \quad . \quad (154)$$

This equation is valid only for those flows in which $S \neq 0$ in at least one layer. If S vanishes everywhere, then the basic state is isentropic and the governing differential equation is a Rayleigh equation, so that equation (154) would be invalid for the same reason the continuous counterpart was invalid. Upon expanding Ω^2 in equation (154) and rearranging the terms, we find

$$\omega^2 I_2' + 2\omega I_1' + I_o' = 0 \quad , \quad (155)$$

and

$$I_o' = \sum_{k=1}^{N+1} \int_{z_{k-1} < z}^{z < z_k} \left\{ (\kappa_1 \bar{u})^2 |G|^2 - \kappa^2 g S |F|^2 \right\} dz \quad . \quad (156)$$

$$I_1' = \sum_{k=1}^{N+1} \int_{z_{k-1} < z}^{z < z_k} \kappa_1 \bar{u} |G|^2 \, dz \quad , \quad (157)$$

where

$$I_2' = \sum_{k=1}^{N+1} \int_{z_{k-1} < z}^{z < z_k} |G|^2 \, dz \quad , \quad (158)$$

If we identify the I''s with the I's in equation (128), it follows that the stability criterion in equation (133) is valid for the broken-line profiles characterized by $\bar{\theta}$ being continuous across the interfacial surfaces. Upon separating the real and imaginary parts of equation (154), we find

$$\sum_{k=1}^{N+1} \left\{ \int_{z_{k-1} < z}^{z < z_k} \left[(\kappa_1 \bar{u} + \omega_r)^2 - \omega_i^2 \right] |G|^2 dz \right.$$

$$\left. - \kappa^2 g \int_{z_{k-1} < z}^{z < z_k} S|F|^2 \, dz \right\} = 0 \qquad (159)$$

and

$$i\, 2\omega_i \sum_{k=1}^{N+1} \int_{z_{k-1} < z}^{z < z_k} (\kappa_1 \bar{u} + \omega_r) |G|^2 \, dz = 0 \quad . \qquad (160)$$

Thus, it may be concluded from equation (160) that if $\omega_i < 0$, then $\kappa_1 \bar{u} + \omega_r$ must vanish at least once in the interval $0 \leqq z \leqq \infty$, so that Synge's theorem is valid for any broken-line flow in which $\bar{\theta}$ is continuous across the interfaces. In addition to this theorem, it can be shown that Howard's semicircle theorem is valid. The details are similar to those presented earlier for the continuous case. The only difference between these proofs is that the integration bounds in equations (159) and (160) do not contain the points $z = z_1, z_2, \ldots, z_N$ (the heights of the interfacial surfaces). In the case of the continuous profiles, these points have a measure of zero, so that we can integrate across them.

Transformation $\psi = \Omega^{1/2} H$

Let us now suppose that $\mathrm{Im}(\omega) \neq 0$ and define a function H such that

$$\psi = \Omega^{1/2} H \quad . \qquad (161)$$

With this transformation, equation (66) becomes

$$D(\Omega DH) - \left[\frac{\kappa_1}{2} D^2\bar{u} + \kappa^2\Omega + \frac{1}{\Omega}\left(\frac{\kappa_1^2}{4} (D\bar{u})^2 - \kappa^2 gS \right) \right] H = 0 \quad , \tag{162}$$

and the associated boundary and interfacial conditions are given by

$$\Omega^{1/2} H = 0 \quad \text{at} \quad z = 0 \quad , \tag{163}$$

$$\lim_{z \to \infty} \left\{ \Omega^{3/2} DH - \frac{1}{2} \kappa_1 D\bar{u}\, \Omega^{1/2} H \right\} = 0 \quad , \tag{164}$$

$$\Delta_s \left(\frac{\bar{\theta} H}{\Omega^{1/2}} \right) \quad , \tag{165}$$

and

$$\Delta_s \left(\Omega^{3/2} DH - \frac{1}{2} \kappa_1 D\bar{u}\, \Omega^{1/2} H \right) - g\kappa^2 \frac{H\bar{\theta}}{\Omega^{1/2}} \Delta_s (\bar{\theta}^{-1}) \quad . \tag{166}$$

Upon multiplying equation (162) by H^* and integrating over the domain $(0 \leq z \leq \infty)$, we find

$$\sum_{k=1}^{N+1} \int_{z_{k-1} < z}^{z < z_k} \left\{ \Omega |K|^2 + \frac{\kappa_1}{2} D^2\bar{u} |G|^2 + \frac{|H|^2}{|\Omega|^2} \Omega^* \left[\frac{\kappa_1^2}{4} (D\bar{u})^2 - \kappa^2 gS \right] \right\} dz \,\cdot$$

$$+ \sum_{k=1}^{N} \left\{ \left[\frac{|H|^2}{|\Omega|} \bar{\theta}^2 \right]_k \lim_{\epsilon_k \to \infty} \int_{z_k - \epsilon_k}^{z_k + \epsilon_k} \left[\frac{|\Omega| \kappa_1 D^2\bar{u}}{2\bar{\theta}^2} \right. \right.$$

$$\left. \left. + \left(\frac{\Omega^*}{\Omega} \right)^{1/2} \frac{1}{\bar{\theta}^2} \left(\frac{\kappa_1^2}{4} (D\bar{u})^2 - \kappa^2 gS \right) \right] dz \right\}$$

$$- \sum_{k=1}^{N} \left[\Delta_s (H^* \Omega DH) \right]_k - \lim_{z \to \infty} \Omega H^* DH = 0 \quad , \tag{167}$$

where

$$|K|^2 = |DH|^2 + \kappa^2 |H|^2 \quad , \tag{168}$$

and we have applied equation (163) and used the continuity of $\bar{\theta}\, H/\Omega^{1/2}$ across the interfacial surfaces, equation (165). The second and third terms in equation (167) are the contributions from integrating equation (162) across the interfacial surfaces. The fourth term in equation (167) results from integrating $H^* D(\Omega DH)$ by parts, and if we restrict our analysis to flows characterized by

$$\lim_{z \to \infty} (D\bar{u}) = 0 \quad ,$$

then this boundary term will vanish according to equation (164).

Continuous Jets and Shear Layers. In the case of continuous unperturbe flows, the interfacial terms in equation (167) vanish and the summation represented by the first term in this equation collapses to one term and we find that

$$\int_0^\infty \left\{ \Omega |K|^2 + \frac{\kappa_1}{2} D^2\bar{u} |H|^2 + \frac{|H|^2}{|\Omega|^2} \Omega^* \left[\frac{\kappa_1^2}{4} (D\bar{u})^2 - \kappa^2 gS \right] \right\} dz = 0 \quad . \tag{169}$$

The imaginary part of equation (169) is given by

$$\omega_i \int_0^\infty \left\{ |K|^2 + \frac{|H|^2}{|\Omega|^2} \left[\kappa^2 gS - \frac{\kappa_1^2}{4} (D\bar{u})^2 \right] \right\} dz = 0 \quad . \tag{170}$$

Because $\omega_i \neq 0$, this result is impossible if

$$gS - \frac{1}{4} \frac{\kappa_1^2}{\kappa^2} (D\bar{u})^2 \geq 0 \quad \text{(everywhere in } 0 \leq z \leq \infty) \quad . \tag{171}$$

Inequality equation (171) is a sufficient condition for stability in the sense that the perturbations are neutral oscillations that neither decay nor amplify in time. Equation (171) reduces to Miles' [31] result if $\kappa_1 = \kappa$. If $\kappa_1 = 0$, then equation (171) is satisfied for all transverse disturbances provided that $S > 0$ and the stability properties of the perturbations are independent of $\bar{u}$. This can be verified by noting that $\bar{u}$ does not occur in equation (66) and the associated boundary conditions if $\kappa_1 = 0$.

If the perturbations are dynamically unstable, then it follows from equation (170) that we must have

$$gS - \frac{1}{4}\frac{\kappa_1^2}{\kappa^2}(D\bar{u})^2 < 0 \quad \text{(over a finite measure in } 0 \leqq z \leqq \infty\text{)} \qquad (172)$$

The condition on the static stability gS for hydrodynamic instability is made more severe by letting κ approach κ_1. This means that if we reduce the static stability of a flow which is hydrodynamically stable, and if we allow it to tend toward dynamic instability, then the first hydrodynamic instabilities will occur via longitudinal eddies ($\kappa_1 = \kappa$). Thus, from a stability point of view, the relevant solutions are the longitudinal solutions, because the associated critical eigenstates will bound all the unstable eigenstates in configuration space.

Broken-Line Profiles. In the case of the type (1), (2), and (3) flows, it is not possible to eliminate the interfacial contributions that occur in equation (167). Thus, we cannot formally conclude, without analyzing special cases, that the results for the continuous profiles should be valid for the broken-line flows, or at least carry over to the broken-line case in a modified form, because H does not occur in a positive definite form in the third term on the left-hand side of equation (167). However, there is one class of profiles for which equations (171) and (172) are valid. These profiles are characterized by continuous $\bar{\theta}$, $\bar{u}$, and $D\bar{u}$ across the interfacial surfaces which permits us to conclude from equations (165) and (166) that

$$\Delta_s(\Omega DH) = 0 \quad , \qquad (173)$$

and

$$\Delta_s(H^*) = 0 \quad . \qquad (174)$$

Combination of equations (173) and (174) implies that $\Delta_s(H^*\Omega DH) = 0$ and thus it follows that the third term on the left-hand side of equation (167) vanishes. The continuity of $\bar{\theta}$, $\bar{u}$, and $D\bar{u}$ across the interfacial surfaces implies that

$$\sum_{k=1}^{N} \left\{ \left[\frac{|H|^2}{|\Omega|} \bar{\theta}^2 \right]_k \lim_{\epsilon_k \to 0} \int_{z_k - \epsilon_k}^{z_k + \epsilon_k} \left[\frac{|\Omega| \kappa_1 D^2\bar{u}}{2\bar{\theta}^2} \right] + \left(\frac{\Omega^*}{\Omega} \right)^{1/2} \frac{1}{\bar{\theta}^2} \left[\frac{\kappa_1^2}{4} (D\bar{u})^2 - \kappa^2 gS \right] \right\} dz = 0 \quad . \tag{175}$$

In view of the above considerations, it follows from equation (167) that

$$\sum_{k=1}^{N+1} \int_{z_{k-1} < z}^{z < z_k} \left\{ \Omega |K|^2 + \frac{\kappa_1}{2} D^2\bar{u} |G|^2 + \frac{|H|^2}{|\Omega|^2} \Omega^* \left[\frac{\kappa_1^2}{4} (D\bar{u})^2 - \kappa^2 gS \right] \right\} dz = 0 \quad . \tag{176}$$

The imaginary part of equation (176) is given by

$$\omega_i \sum_{k=1}^{N+1} \int_{z_{k-1} < z}^{z < z_k} \left\{ |K|^2 + \frac{|H|^2}{|\Omega|^2} \left[\kappa^2 gS - \frac{\kappa_1^2}{4} (D\bar{u})^2 \right] \right\} dz = 0 \quad . \tag{177}$$

This expression is identical to equation (170) except that the points at the interfacial surfaces are not included in the integration. However, at these points, the continuity of $\bar{\theta}$, $\bar{u}$, and $D\bar{u}$ and the continuity of $\bar{\theta}H/\Omega^{1/2}$, equation (165), implies that

$$\frac{|H|^2}{|\Omega|^2} \left[\kappa^2 gS - \frac{\kappa_1^2}{4} (D\bar{u})^2 \right]$$

has a measure of zero at the interfaces, so that there is no contribution to the integration at these points and we may write equation (177) in the form

$$\omega_i \left\{ \sum_{k=1}^{N+1} \int_{z_{k-1} < z}^{z < z_k} |K|^2 dz + \int_0^\infty \frac{|H|^2}{|\Omega|^2} \left[\kappa^2 gS - \frac{\kappa_1^2}{4} (D\bar{u})^2 \right] dz \right\} = 0 \quad . \tag{178}$$

It is clear that equations (171) and (172) follow from this result.

Let us now concentrate on the broken-line type (1) profiles. It was explained earlier that a result like equation (171) or equation (172) for the type (1) profiles cannot be obtained formally from equation (167) without analyzing special cases. However, it is possible to present plausible arguments that lead to modified forms of equations (171) and (172) for the broken-line type (1) profiles.

Later in this report, it will be shown that the broken-line solutions are the long-wave approximations of the associated continuous profile solutions. The philosophy of how one selects a broken-line flow to represent a continuous flow will be discussed later. However, it is worth noting that, for the bounded velocity profiles, one selects the extremes of the velocity profile to obtain the broken-line counterpart, while the potential temperature broken-line representation is obtained by a spatial average of the continuous $\bar{\theta}$ distribution in each layer. The broken-line approach for solving equation (66) works best for the long waves, because the long waves "feel" only the gross features of the basic state. The solutions will tend to fail as the wavelength decreases, because the waves will be sensitive to the details of the basic state profiles. Accordingly, the broken-line solutions are the antitheses of the short-wave WKBJ solutions.

In the broken-line limit, S and $D\bar{u}$ are not defined at the interfaces, so that equations (171) and (172) are not formally valid. However, we must realize that, in layering the basic state to obtain a broken-line representation, we really are considering the gross features of $\bar{u}$ and $\bar{\theta}$ that occur over the vertical length scale of the waves. Accordingly, if we estimate S and $D\bar{u}$ over this length scale, then it is possible to obtain an estimate of a sufficient condition for stability from equation (171).

The type (1) broken-line solutions of equation (66) in the k^{th} layer are given by

$$\psi_k = A_k e^{\kappa z} + B_k e^{-\kappa z} \quad . \tag{179}$$

If we define the vertical length scale of the wave to be

$$L_\psi = \frac{|\psi|}{\left|\frac{d\psi}{dz}\right|} \quad , \tag{180}$$

then the length scale in the k^{th} layer is

$$L_{\psi,k} = \kappa^{-1} \left| \frac{A_k e^{\kappa z} + B_k e^{-\kappa z}}{A_k e^{\kappa z} - B_k e^{-\kappa z}} \right| \quad . \tag{181}$$

In the lowest layer, $A_1 = -B_1$, and equation (181) yields the result

$$L_{\psi,1} = \kappa^{-1} |\tanh \kappa z| \quad , \tag{182}$$

while in the upper layer, $A_{N+1} = 0$, and thus the associated length scale is given by

$$L_{\psi,N+1} = \kappa^{-1} \quad . \tag{183}$$

According to equation (182) the vertical scale of the wave vanishes at the surface of the earth, increases as the distance z from the lower boundary increases, and tends to a limiting value κ^{-1}. In the uppermost layer, the vertical length scale is κ^{-1} everywhere. In the intermediate layers, $L_{\psi,k}$ is proportional to κ^{-1} ($k = 2, 3, \ldots, N$). An overall estimate of the vertical scale for the entire wave could be represented by

$$L_{\psi} = a\kappa^{-1} \quad , \tag{184}$$

where a is a positive constant. The estimates of S and $D\bar{u}$ over this length scale across an interface are given by

$$\left.\begin{aligned} S &\sim 2\frac{\kappa}{a}\frac{\bar{\theta}_2 - \bar{\theta}_1}{\bar{\theta}_2 + \bar{\theta}_1} \\ D\bar{u} &\sim \frac{\kappa}{a}(\bar{u}_2 - \bar{u}_1) \end{aligned}\right\} \quad , \tag{185}$$

where the subscripts 1 and 2 denote evaluation below and above the interface. Substitution of equations (185) into equation (171) leads to an estimate of a sufficient condition for stability in the type (1) broken-line case, namely,

$$g\frac{\bar{\theta}_2 - \bar{\theta}_1}{\bar{\theta}_2 + \bar{\theta}_1} - \frac{\kappa_1^2}{8a\kappa}(\bar{u}_2 - \bar{u}_1)^2 \geqq 0 \quad \text{(at all interfaces)} \quad . \tag{186}$$

The corresponding estimate of a necessary condition for instability based on equation (172) is given by

$$g\frac{\bar{\theta}_2 - \bar{\theta}_1}{\bar{\theta}_2 + \bar{\theta}_1} - \frac{\kappa_1^2}{8a\kappa}(\bar{u}_2 - \bar{u}_1)^2 < 0 \quad \text{(at a sufficient number of interfaces)} \quad . \tag{187}$$

If $\kappa_1 = 0$, then these results imply that the stability properties of the flow are independent of $\bar{u}$ for pure lateral perturbations, and the flow must possess a sufficient number of interfaces characterized by $\bar{\theta}_2 < \bar{\theta}_1$ to be unstable. If κ_1 approaches infinity with κ_2 fixed, then the term

$$\frac{\kappa_1^2}{8a\kappa}(\bar{u}_2 - \bar{u}_1)$$

will grow without bound, so that equation (187) will be satisfied for sufficiently small wavelengths. Thus, we may tentatively conclude that all type (1) broken-line flows will tend to be unstable to perturbations with sufficiently

small wavelengths. It is not possible to obtain this result from equations (171) or (172) for continuous profiles, so that the tendency toward short wave instability in the broken-line flows could, in some instances, be spurious, resulting from the discontinuous stratification of the basic state. However, this result does not preclude the usefulness of the broken-line representations. From the inequality (187), it would appear that, if we reduce the static stability of a broken-line flow which is hydrodynamically stable, and if we allow it to tend toward dynamic stability, then the first hydrodynamic instabilities will occur via longitudinal eddies, as in the continuous flows.

Later in this report, it will be shown that the necessary and sufficient condition for longitudinal ($\kappa_1 = \kappa$) instability in a two-layer Kelvin-Helmholtz vortex sheet with the lower boundary at $z = -\infty$ is given by

$$g \frac{\bar{\theta}_2 + \bar{\theta}_1}{\bar{\theta}_2 \bar{\theta}_1} (\bar{\theta}_2 - \bar{\theta}_1) - \kappa (\bar{u}_2 - \bar{u}_1)^2 < 0 \quad . \tag{188}$$

This relationship is similar to equation (187) for $\kappa_1 = \kappa$. In fact, for sufficiently small $|\bar{\theta}_1 - \bar{\theta}_2|$, we have

$$\frac{\bar{\theta}_2 + \bar{\theta}_1}{\bar{\theta}_2 \bar{\theta}_1} (\bar{\theta}_2 - \bar{\theta}_1) \simeq 4 \frac{\bar{\theta}_2 - \bar{\theta}_1}{\bar{\theta}_2 + \bar{\theta}_1} \quad . \tag{189}$$

Accordingly, if we combine equations (187) and (189) and set $a = 0.5$, then we obtain the result equation (188), so that out estimates of S and $D\bar{u}$ are valid a posteriori.

THREE-LAYER MODEL

We will now examine the three-layer type (1) flows in detail. More specifically, the solution to the governing differential equation (66) will be presented and the associated dispersion or eigenvalue equation for ω will be determined. This equation is a fourth-degree polynomial in ω. Also, we will examine the solutions to this eigenvalue equation and thus determine the stability properties of jet and shear layer flows.

The Model

In this section we will present the three-layer type (1) flow model and the solutions in each layer. This material will be similar to that previously discussed. However, at the risk of repetition we will develop the solution in detail to demonstrate the mathematical machinery of the broken-line flows.

We consider a broken-line flow composed of three layers. Within each layer we treat the unperturbed potential temperature $\bar{\theta}$ and velocity $\bar{u}$ as constants. Figure 1 shows a diagram of this flow configuration. The unperturbed velocity and potential temperature in each layer are denoted by $\bar{u}_i$ and $\bar{\theta}_i$ $(i = 1, 2, 3)$. The vertical extent of layer 2 will be $-h < z < h$, while layer 3 will extend over the region $h < z < \infty$. We assume that the jet core, or center of the shear layer, is sufficiently far removed from the surface of the earth so that the lower rigid boundary condition can be applied at $z = -\infty$. Thus, the lower layer will extend over the region $-\infty < z < -h$. This assumption will simplify the analysis of the dispersion relation. In addition, this assumption does not negate the major results obtained previously, because the theorems will be valid with the lower boundary located at $z = -\infty$. Ramm and Warren [47] have used this approximation in an analysis of pressure fluctuations at the surface of the earth and found that the solution did not differ significantly from that associated with the rigid boundary located at $z = -H$, where H is the location of the surface of the earth with respect to the jet core (Fig. 1). We will examine this approximation later in this report with the aid of a Kelvin-Helmholtz vortex sheet. In addition to this approximation, we will restrict our analysis to longitudinal $(\kappa_1 = \kappa)$ perturbations. The calculation will then yield the critical stability states in configuration space which bound all unstable states, and thus we will determine the most statically stable state for a given basic state flow configuration that is hydrodynamically unstable.

The layer approximation implies that within each layer the governing differential equation (66) takes the simplified form

$$D^2\psi - \kappa^2\psi = 0 \quad . \tag{190}$$

The general solution of equation (190) in each layer is a linear combination of the functions

$$e^{\kappa z} \quad \text{and} \quad e^{-\kappa z} \quad .$$

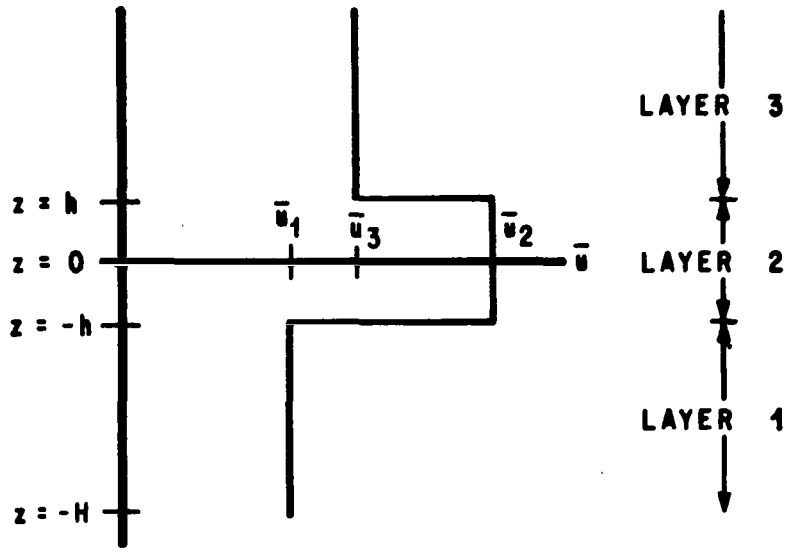

BASIC STATE VELOCITY DISTRIBUTION

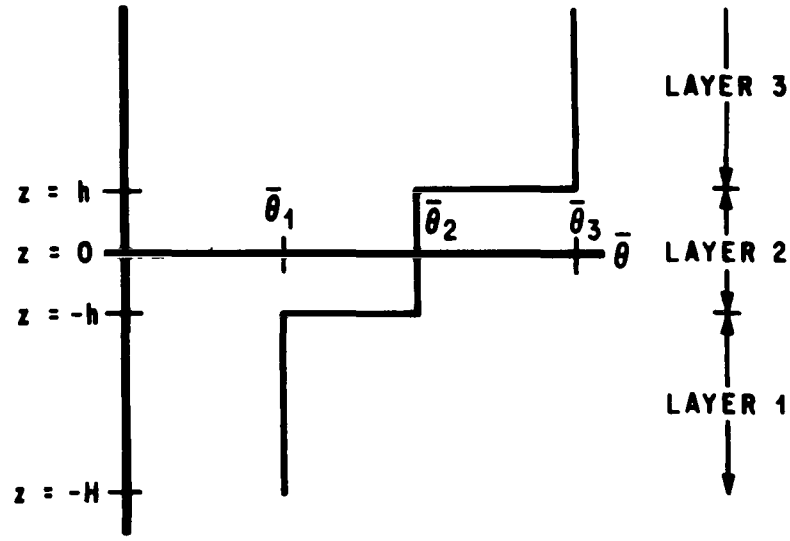

BASIC STATE POTENTIAL TEMPERATURE DISTRIBUTION

Figure 1. Distributions of basic state velocity and potential temperature.

In type (1) broken-line flows, $D\bar{u}$ vanishes in each layer, so that the upper boundary condition (71) reduces to

$$\lim_{z \to \infty} \Omega D\psi = 0 \quad . \tag{191}$$

The solution that satisfies the modified boundary condition (191) and the lower boundary condition $\psi = 0$ at $z = -\infty$ is given by

$$\psi = A_1 e^{\kappa z} \qquad (-\infty < z < -h) \quad , \tag{192}$$

$$\psi = A_2 e^{\kappa z} + B_2 e^{-\kappa z} \qquad (-h < z < h) \quad , \tag{193}$$

and

$$\psi = B_3 e^{-\kappa z} \qquad (h < z < \infty) \quad , \tag{194}$$

where A_1, A_2, B_2, and B_3 are constants of integration of which only one is arbitrary, because of the interfacial conditions which permit us to join the solution together across the interfaces.

Characteristic Equation

We will derive the characteristic equation of the system from equations (192) through (194) and the interfacial conditions (87) and (89).

Upon applying equation (87), we find that at the lower interface

$$\beta_1 \frac{e^{-k/2}}{\Omega_1} A_1 - \frac{e^{-k/2}}{\Omega_2} A_2 - \frac{e^{+k/2}}{\Omega_2} B_2 = 0 \quad , \tag{195}$$

while at the upper interface we have

$$\frac{e^{k/2}}{\Omega_2} A_2 + \frac{e^{-k/2}}{\Omega_2} B_2 - \frac{e^{-k/2}}{\beta_2 \Omega_3} B_3 = 0 \quad . \tag{196}$$

Application of equation (89) at the lower interface from below yields the result

$$\left(-k\Omega_1 + \frac{k^2}{\Omega_1} R_1 \right) e^{-k/2} A_1 + \Omega_2 k e^{-k/2} A_2 - \Omega_2 k e^{k/2} B_3 = 0 \quad , \tag{197}$$

while application of the same condition at the upper interface from above gives the result

$$-\Omega_2 k e^{k/2} A_2 + \Omega_2 k e^{-k/2} B_2 + \left(\frac{k^2 R_2}{\Omega_3 \beta_2} - k\Omega_3 \right) e^{-k/2} B_3 = 0 \quad . \tag{198}$$

The various quantities in equations (195) through (198) are defined by the following relationships:

$$\Omega_1 = \nu + k\lambda_1 \quad , \tag{199}$$

$$\Omega_2 = \nu + k \quad , \tag{200}$$

$$\Omega_3 = \nu + k\lambda_2 \quad , \tag{201}$$

$$k = 2\kappa h \quad , \tag{202}$$

$$R_1 = \frac{2hg}{\bar{u}_2^2} \left(\frac{\bar{\theta}_2 - \bar{\theta}_1}{\bar{\theta}_2} \right) \quad , \tag{203}$$

$$R_2 = \frac{2hg}{\bar{u}_2^2}\left(\frac{\bar{\theta}_3 - \bar{\theta}_2}{\bar{\theta}_3}\right) \quad , \tag{204}$$

$$\nu = \frac{\omega 2h}{\bar{u}_2} \quad , \tag{205}$$

$$\lambda_1 = \frac{\bar{u}_1}{\bar{u}_2} \quad , \tag{206}$$

$$\lambda_2 = \frac{\bar{u}_3}{\bar{u}_2} \quad , \tag{207}$$

$$\beta_1 = \frac{\bar{\theta}_1}{\bar{\theta}_2} \quad , \tag{208}$$

and

$$\beta_2 = \frac{\bar{\theta}_2}{\bar{\theta}_3} \, . \tag{209}$$

The quantities R_1 and R_2 are the Richardson numbers of the problem. Equations (195) through (198) constitute a set of four independent equations with four unknowns, namely, A_1, A_2, B_2, and B_3. It should be noted that a set of conditions can be obtained by applying equation (89) at the lower interface from above and at the upper interface from below. However, these conditions can also be obtained by combining equations (195) and (197), and equations (196) and (198), but they do not yield extra information.

If the solution of equations (195) through (198) is to be nontrivial, then the determinant of the coefficients of the dependent variables must vanish so that

$$\begin{vmatrix} \left(\frac{k}{\Omega_1} R_1 - \Omega_1\right) e^{-k/2} & \Omega_2 e^{-k/2} & -\Omega_2 e^{k/2} & 0 \\ \frac{\beta_1 e^{-k/2}}{\Omega_2} & -\frac{e^{-k/2}}{\Omega_2} & -\frac{e^{k/2}}{\Omega_2} & 0 \\ 0 & -\Omega_2 e^{k/2} & \Omega_2 e^{-k/2} & \left(\frac{kR_2}{\beta_2\Omega_2} - \Omega_2\right) e^{-k/2} \\ 0 & -\frac{e^{k/2}}{\Omega_2} & -\frac{e^{-k/2}}{\Omega_2} & \frac{e^{-k/2}}{\beta_2\Omega_3} \end{vmatrix} = 0. \tag{210}$$

Upon expanding this determinant, we find

$$(\beta_1\Omega_2^2 + \Omega_1^2 - kR_1)(\Omega_2^2 + \beta_2\Omega_3^2 - kR_2)$$

$$- e^{-2k}(\beta_1\Omega_2^2 - \Omega_1^2 + kR_1)(\Omega_2^2 - \beta_2\Omega_3^2 + kR_2) = 0 \quad , \tag{211}$$

which is the characteristic equation for the system.

It is only possible to obtain the solution to equations (195) through (198) to within a multiplicative constant, because these equations are homogeneous. Thus, upon solving them for A_2, B_2, and B_3 in terms of A_1, we find

$$A_2 = \frac{\Omega_1^2 + \beta_1\Omega_2^2 - kR_1}{2\Omega_1\Omega_2} A_1 \quad , \tag{212}$$

$$B_2 = -\left\{\frac{\Omega_1^2 - \beta_1\Omega_2^2 - kR_1}{2\Omega_1\Omega_2}\right\} e^{-k} A_1 \quad , \tag{213}$$

and

$$B_3 = \frac{\beta_2\Omega_3}{\Omega_1\Omega_2^2}\left\{ \Omega_1^2 \sinh k + \beta_1\Omega_2^2 \cosh k - kR_1 \sinh k \right\} A_1 \quad . \tag{214}$$

A_1 is an arbitrary constant which is specified by the initial conditions.

The eigenvalue equation for the Kelvin-Helmholtz instability can be obtained as a special case of equation (211) by setting $\beta_2 = 1$ and $R_2 = 0$ and noting that in this case $\Omega_2 = \Omega_3$ so that

$$\beta_1\Omega_2^2 + \Omega_1^2 - kR_1 = 0 \quad . \tag{215}$$

Upon solving this equation for ω we find

$$\omega = -\kappa\left(\frac{\bar{\theta}_2\bar{u}_1 + \bar{\theta}_1\bar{u}_2}{\bar{\theta}_1 + \bar{\theta}_2} \right) \pm \left[g\kappa \frac{\bar{\theta}_2 - \bar{\theta}_1}{\bar{\theta}_2 + \bar{\theta}_1} - \frac{\bar{\theta}_1\bar{\theta}_2}{(\bar{\theta}_1 + \bar{\theta}_2)^2} \kappa^2 (\bar{u}_2 - \bar{u}_1)^2 \right]^{1/2} . \tag{216}$$

We have written this expression in dimensional form, because the only length scale available is the disturbance size.

Since $\bar{p}$ must be continuous across an interface, we may rewrite equation (216) in the more familiar form

$$\omega = -\kappa\left[\frac{\bar{\rho}_1(0-)\bar{u}_1 + \bar{\rho}_2(0+)\bar{u}_2}{\bar{\rho}_1(0-) + \bar{\rho}_2(0+)} \right] \tag{217}$$

$$\pm \left\{ g\kappa \frac{\bar{\rho}_1(0-) - \bar{\rho}_2(0+)}{\bar{\rho}_1(0-) + \bar{\rho}_2(0+)} - \frac{\bar{\rho}_1(0-)\,\bar{\rho}_2(0+)\,\kappa^2}{[\rho_1(0-) + \rho_2(0+)]^2} (\bar{u}_2 - \bar{u}_1)^2 \right\}^{1/2} .$$

Equation (217) was first obtained by Kelvin [6] for two superposed incompressible layers of fluid. The difference between his result and that for two compressible layers is that in the former, the unperturbed density is a constant in each layer, while in the latter, the densities are evaluated at the interfaces.

In most regions of the troposphere and the lower stratosphere, $1.05 \geqq \beta_i \geqq 0.95$ $(i = 1,2)$. Accordingly, in our subsequent calculations we will set $\beta_i = 1$ $(i = 1,2)$ in all terms that do not contain g in each of the embraced expressions in equation (211). The effect of this approximation upon the solution can be determined by examining the eigenvalues associated with the Kelvin-Helmholtz instability. Thus, the counterpart of equation (216) for $\beta_1 = 1$ is

$$\omega = -\kappa\left(\frac{\bar{u}_1 + \bar{u}_2}{2}\right) \pm \left[g\kappa\left(\frac{\bar{\theta}_2 - \bar{\theta}_1}{2\bar{\theta}_2}\right) - \left(\frac{\bar{u}_2 - \bar{u}_1}{2}\right)^2 \kappa^2 \right]^{1/2} \quad . \tag{218}$$

If the flow were unstable, then the wave frequency would be estimated by an arithmetic mean of the basic flow, rather than a density-weighted mean of the basic flow and the condition for instability would read

$$R_a = \frac{2g}{(\bar{u}_2 - \bar{u}_1)^2 \kappa}\left(\frac{\bar{\theta}_2 - \bar{\theta}_1}{\bar{\theta}_2}\right) < 1 \quad , \tag{219}$$

as compared to the exact form

$$R_{K.H.} = \frac{g(\bar{\theta}_2 + \bar{\theta}_1)}{\theta_1\theta_2\kappa}\,\frac{\bar{\theta}_2 - \bar{\theta}_1}{(\bar{u}_2 - \bar{u}_1)} < 1 \quad . \tag{220}$$

Forming the ratio

$$\frac{R_a}{R_{K.H.}} = \frac{2\bar{\theta}_1}{\bar{\theta}_1 + \bar{\theta}_2} \quad , \tag{221}$$

we find that for $\beta_1 = 0.95$, $R_a/R_{K.H.} = 0.974$. Thus, it would appear that this approximation has a negligible effect upon the wave frequency and the critical Richardson numbers.

If we expand equation (211) and apply the approximation $\beta_i = 1$ $(i = 1,2)$ in all terms that do not contain g, then we find that

$$\nu^4 + c_3\nu^3 + c_2\nu^2 + c_1\nu + c_o = 0 \quad , \tag{222}$$

where

$$c_3 = k(\lambda_1 + \lambda_2 + 2) \quad , \tag{223}$$

$$c_2 = \frac{1}{2} k^2(\lambda_1^2 + \lambda_2^2 + 2) + k^2(\lambda_1 + 1)(\lambda_2 + 1) - \frac{1}{2} k(R_1 + R_2)$$

$$- k^2(1 - \lambda_1)(1 - \lambda_2)e^{-2k} \quad , \tag{224}$$

$$c_1 = \frac{1}{2}\Bigg\{ k^3\left[(\lambda_1^2 + 1)(\lambda_2 + 1) + (\lambda_2^2 + 1)(\lambda_1 + 1)\right]$$

$$- k^2\left[R_1(\lambda_2 + 1) + R_2(\lambda_1 + 1)\right]$$

$$- k^3\left[(\lambda_2 - 1)(\lambda_1^2 - 1) + (\lambda_1 - 1)(\lambda_2^2 - 1)\right]e^{-2k}$$

$$- k^2\left[R_1(1 - \lambda_2) + R_2(1 - \lambda_1)\right]e^{-2k}\Bigg\} \quad , \tag{225}$$

and

$$c_o = \frac{1}{4}\Bigg\{ k^4(\lambda_1^2 + 1)(\lambda_2^2 + 1) - k^3\left[R_1(1 + \lambda_2^2) + R_2(1 + \lambda_1^2)\right]$$

$$+ k^2R_1R_2 - k^4(\lambda_1^2 - 1)(\lambda_2^2 - 1)e^{-2k}$$

$$- k^3\left[R_1(1 - \lambda_2^2) + R_2(1 - \lambda_1^2)\right]e^{-2k} - k^2R_1R_2e^{-2k}\Bigg\} \quad . \tag{226}$$

The analysis to be discussed later, based upon equation (222), will be performed by extracting the roots of this equation for various jet and shear layer configurations. The jets and shear layers will be simulated by varying R_1, R_2, λ_1, and λ_2.

THE EIGENVALUES

We will now consider the secular or characteristic equation (222) which relates the parameters of the perturbations, k and ν, to the basic state flow parameters, namely, λ_1, λ_2, R_1, and R_2. The stability properties of a multitude of jets and shear layers can be analyzed by varying the basic state parameters and then determining the values of k and ν which satisfy the secular equation (222). The goal of stability calculations is to determine which basic state flows lead to unstable perturbations, because it is plausible that these instabilities could ultimately result in turbulence. However, this may not be true in every case, because it is also possible that the instabilities could lead to an organized finite amplitude motion that is nonturbulent; e.g., Stuart [2] and Landau and Lifshitz [48]. In either event, the Reynolds stresses will be important after the instability begins. The Reynolds stresses are the result of nonlinear interaction between the various components of the perturbations, as well as between the perturbations and the basic state flow. In our analysis, we will not account for these interactions; therefore, the results are valid for only the initial stages of the instability.

Without loss of generality, we will assume $k > 0$. The left-hand side of equation (222) is a fourth-degree polynomial in ν, and the roots of this equation may be complex. The theory of equations predicts that, if complex eigenvalues, roots of equation (222), occur for specified values of k, λ_1, λ_2, R_1, and R_2, then the complex roots will appear in complex conjugate pairs. If the eigenvalues of ν are real, then the solutions to equation (66) will be characterized by neutral ($\mathrm{Im}(\nu) = 0$) oscillations that neither decay nor grow in time [see equation (82)]. However, if ν is complex, then the perturbations will be either damped ($\mathrm{Im}(\nu) > 0$) in time, or grow temporally without bound ($\mathrm{Im}(\nu) < 0$). If $\mathrm{Im}(\nu) < 0$, then the motion is said to be unstable. Clearly, (ν_r, λ_1, λ_2, R_1, R_2, k)-space (configuration space) will be partitioned into two subsets; one set will contain neutrally-stable modes ($\nu_i = 0$), while the other will contain the unstable and damped modes, where $\nu_r = \mathrm{Re}(\nu)$ and $\nu_i = \mathrm{Im}(\nu)$. The surface in configuration space characterized by $\nu_i = 0$ that exists contiguously to a domain characterized by $\nu_i < 0$ will

be a stability boundary. One of the objectives of this discussion will be to determine this boundary.

Later, we will analyze shear layer and jet instability in the context of the Kelvin-Helmholtz instability. Also, we will consider the stability properties of two types of flows: (1) jet flows characterized by even distributions of λ and R, and (2) shear layer flows that possess an odd distribution λ and an even distribution of R. The latter case was developed by Howard [34]; the former is believed to be a new case. A general analysis of jets and shear layers in the context of the three-layer model will be presented. In this analysis, we consider flows with asymmetric and symmetric distributions of λ and R.

Kelvin-Helmholtz Limit

As k tends to infinity, the second term on the left-hand side of equation (211) approaches zero, because of the presence of the multiplicative factor e^{-2k}. Thus, for sufficiently large k we obtain

$$(\beta_1\Omega_2^2 + \Omega_1^2 - kR_1)\ (\Omega_2^2 + \beta_2\Omega_3^2 - kR_2) \simeq 0 \quad . \tag{227}$$

Since the left-hand side of this equation is a fourth-degree polynomial in ν, it possesses four roots for each configuration of k, λ_1, λ_2, R_1, and R_2. One set of these roots must satisfy the equation

$$\beta_1\Omega_2^2 + \Omega_1^2 - kR_1 \simeq 0 \quad , \tag{228}$$

and the other set must satisfy

$$\Omega_2^2 + \beta_2\Omega_3^2 - kR_2 \simeq 0 \quad . \tag{229}$$

Equations (228) and (229) correspond to characteristic equations for perturbations in Kelvin-Helmholtz sheets in unbounded stratified media.

Upon solving equation (228) for ν we find

$$\nu = -k\frac{(1+\lambda_1)}{2} \pm \left[\frac{kR_1}{2} - \frac{(1-\lambda_1)^2k^2}{4}\right]^{1/2} , \tag{230}$$

while equation (229) yields the result

$$\nu = -k\frac{(1+\lambda_2)}{2} \pm \left[\frac{kR_2}{2} - \frac{(1-\lambda_2)^2k^2}{4}\right]^{1/2} , \tag{231}$$

where we have used the approximations $\beta_1 \simeq 1$ and $\beta_2 \simeq 1$. The pair of eigenvalues given by equation (230) will be termed the A modes and they depend upon the basic state flow through the "jumps" in $\bar{\theta}$ and $\bar{u}$ across the lower interface. The eigenvalues given by equation (231) will be termed the B modes and they depend upon the "jumps" in $\bar{\theta}$ and $\bar{u}$ across the upper interface.

We may identify the A and B modes with perturbations which propagate locally at the lower and upper interfaces, respectively. This can be verified by examining the ψ field given by equation (192) through equation (194). Let us first consider the A modes. As k becomes large, A_2, equation (212), will approach zero because A_2 is proportional to the left-hand side of equation (228). In addition, B_3, equation (214), will approach zero, because cosh k and sinh k both approach $e^{k/2}$ as k approaches infinity, so that B_3 is essentially proportional to the left-hand side of equation (228) for sufficiently large k. This means that in the case of the A modes we have the asymptotic relations

$$\begin{aligned}
\psi &\sim A_1 e^{k\eta} && \left(-\infty < \eta < -\frac{1}{2}\right) \\
\psi &\sim -A_1\left\{\frac{\Omega_1^2 - \beta_1\Omega_2^2 - kR_1}{2\Omega_1\Omega_2}\right\} e^{-k(\ +1)} && \left(-\frac{1}{2} < \eta < \frac{1}{2}\right) \\
\psi &\sim 0 && \left(\frac{1}{2} < \eta < \infty\right)
\end{aligned} , \tag{232}$$

where $\eta = z/2h$. The A-mode solutions decay spatially in the vertical above and below the lower interface at a rate proportional to $e^{-k|\eta^*|}$, where $\eta^* = \eta + \frac{1}{2}$. Thus, the A modes propagate locally in the vicinity of the lower interface..

To determine the behavior of the solution in the case of the B modes as k approaches infinity, it is expedient to solve equations (195) through (198) for A_1, A_2, and B_2 in terms of B_3. Thus, we have

$$A_1 = \frac{\Omega_1}{\beta_1\beta_2\,\Omega_3\Omega_2^2}\left\{\Omega_3^2\beta_2 \sinh k + \Omega_2^2 \cosh k - kR_2 \sinh k\right\} B_3 \tag{233}$$

$$A_2 = -\left\{\frac{\Omega_3^2\beta_2 - \Omega_2^2 - kR_2}{2\beta_2\Omega_2\Omega_3}\right\} e^{-k}\, B_3 \tag{234}$$

$$B_2 = \left\{\frac{\Omega_2^2 + \beta_2\Omega_3^2 - kR_2}{2\beta_2\Omega_2\Omega_3}\right\} B_3 \quad . \tag{235}$$

Thus, for the B modes, B_2 and A_1 will approach zero as k becomes large because of equation (229), so that the solution is asymptotically given by

$$\begin{aligned}
\psi &\sim 0 && \left(-\infty < \eta < -\frac{1}{2}\right) \\
\psi &\sim -B_3\left\{\frac{\Omega_3^2\beta_2 - \Omega_2^2 - kR_2}{2\beta_2\Omega_2\Omega_3}\right\} e^{-k(1-\eta)} && \left(-\frac{1}{2} < \eta < \frac{1}{2}\right) \\
\psi &\sim B_3 e^{-k\eta} && \left(\frac{1}{2} < \eta < \infty\right) \quad .
\end{aligned} \tag{236}$$

In this case, the solutions decay spatially in the vertical above and below the upper interface at a rate proportional to $e^{-k|\eta^*|}$. Thus, the B modes propagate locally in the vicinity of the upper interface.

If ν is complex, then according to equations (230) and (231), we must have

$$\text{A modes: } \frac{R_1}{(1-\lambda_1)^2} < \frac{k}{2} \tag{237}$$

$$\text{B modes: } \frac{R_2}{(1-\lambda_2)^2} < \frac{k}{2} \quad . \tag{238}$$

If these conditions are satisfied, then equations (230) and (231) yield a complex eigenvalue characterized by $\nu_i < 0$. These eigenvalues correspond to the dynamically unstable solutions. However, if the perturbations satisfy only one of these conditions, then the instability will be confined to one interface, the interface that satisfies either equation (237) or equation (238).

If $R_1 < 0$ and $R_2 < 0$, then equations (237) and (238) will be satisfied for all values of k; therefore, for large k or small wavelengths, there will be an unstable wave at both the upper and lower interfaces. This means that the short wave solutions will always be unstable in statically unstable atmospheres. Calculations with equation (222) also showed that the small wave number Fourier components are dynamically unstable in statically unstable atmospheres.

The critical A mode state with wave number k_1^* which bounds all unstable A modes in configuration space is given by

$$\text{A modes: } k_1^* = \frac{2R_1}{(1-\lambda_1)^2} \quad . \tag{239}$$

This condition is obtained by making equation (237) an equality. Thus, if k is the wave number of an A-mode disturbance and $k > k_1^*$, then the disturbance is unstable. Similarly, the critical B-mode state with wave number k_2^* which bounds all unstable B modes in configuration space is given by

$$\text{B modes: } k_2^* = \frac{2R_2}{(1-\lambda_1)^2} \quad . \tag{240}$$

As k approaches infinity, the terms involving k^2 under the radicals in equations (230) and (231) will increase faster than the linear term in k. Thus, the eigenvalues will be complex for sufficiently large k and the imaginary parts of equations (230) and (231) will tend toward $\pm ik|1-\lambda_1|/2$ and $\pm ik|1-\lambda_2|/2$. This means that, as k tends toward infinity, the imaginary part of ν will increase without bound. Thus, for inviscid flows, the most unstable mode is infinitesimally small. In reality, eddy viscosity (nonlinear interactions) and molecular viscosity would check the unboundedness of ν_i as k approaches infinity.

In synoptic scale jet streams λ_1, R_1 and λ_2, R_2 characterize conditions below and above the jet core, respectively. The typical situation that can be found in these jets is $R_1 > 0$, $R_2 > 0$, and $R_1/(1-\lambda_1)^2 < R_2/(1-\lambda_2)^2$, so that $k_1^* < k_2^*$. This means that in the context of the Kelvin-Helmholtz instability the critical wavelength of the perturbations below the jet core is larger than the critical wavelength of the perturbations above the core. If we identify these instabilities with clear air turbulence, then it might be inferred that the spectrum of clear air turbulence extends over a broader band of wave numbers below the jet core. It might also be inferred that there is a greater probability of encountering clear air turbulence below the core in comparison to conditions above the core. Recent observations of clear air turbulence [Reiter, 49] appear to support these theoretical speculations.

The Kelvin-Helmholtz limit is valid only for sufficiently large k. If the wavelengths of the perturbations are too large (small k), then we must consider all the terms in equation (222). The remainder of this discussion is devoted to the analysis of this equation.

Two Special Cases

Before proceeding to a general numerical analysis of equation (222), it is worthwhile to analyze two special cases. One case corresponds to a jet with symmetric basic state vertical distributions of fluid velocity and static stability. In this case, $\lambda_1 = \lambda_2 = \lambda$ and $R_1 = R_2 = R$. The other case corresponds to a shear layer characterized by an odd distribution of fluid velocity and an even distribution of static stability. We will call these flows the symmetric jet and the odd shear layer.

Symmetric Jet ($\lambda_1 = \lambda_2 = \lambda$, $R_1 = R_2 = R$). Without loss of generality we may set $\lambda = 0$, which implies the frame of reference will be moving with a velocity equal to that in the upper and lower layers. This has the advantage that $\bar{u}_2$ represents the velocity differential across the two interfaces and thus the interpretation of R as a Richardson number is justified. In this case, equation (211) becomes

$$\left\{ (\nu + k)^2 + \nu^2 - kR + e^{-k}\left[(\nu + k)^2 - \nu^2 + kR \right] \right\}$$
$$\times \left\{ (\nu + k)^2 + \nu^2 - kR - e^{-k}\left[(\nu + k)^2 - \nu^2 + kR \right] \right\} = 0 \quad . \qquad (241)$$

This equation is a fourth-degree polynomial in ν, so that this jet is characterized by four eigenvalues for each pair of values of k and R. Accordingly, one pair of eigenvalues, which we will term the C modes, must satisfy the quadratic equation:

$$\text{C modes:} \quad (\nu + k)^2 + \nu^2 - kR + e^{-k}\left[(\nu + k)^2 - \nu^2 + kR \right] = 0 \quad . \qquad (242)$$

The other pair of eigenvalues, the D modes, must satisfy the equation:

$$\text{D modes:} \quad (\nu + k)^2 + \nu^2 - kR - e^{-k}\left[(\nu + k)^2 - \nu^2 + kR \right] = 0. \quad . \qquad (243)$$

Thus, upon solving equation (242), we find that the C modes are given by

$$\nu = -\frac{k}{2}\left(1 + e^{-k}\right) \pm \frac{1}{2}\left\{ \left[k\left(e^{-k} + 1\right) - 2R \right] k\left(e^{-k} - 1 \right) \right\}^{1/2} , \qquad (244)$$

while the other pair of eigenvalues, the D modes, are given by

$$\nu = -\frac{k}{2}\left(1 - e^{-k}\right) \pm \frac{1}{2}\left\{ \left[k\left(e^{-k} - 1\right) + 2R \right] k\left(e^{-k} + 1\right) \right\}^{1/2} , \qquad (245)$$

Since $1 \pm e^{-k} > 0$, it is clear that the necessary and sufficient conditions for instability to set in are given by

$$\text{C modes: } R < \frac{k}{2}\left(1 + e^{-k}\right) \quad , \tag{246}$$

$$\text{D modes: } R < \frac{k}{2}\left(1 - e^{-k}\right) \quad . \tag{247}$$

The C modes are the most unstable since the critical value of R, in this case, is greater than that of the D modes; i.e., the C modes in comparison to the D modes will experience instability over a wider band of wave numbers for a given value of R. Thus, as we increase the wave number of the disturbance, the C modes will first destabilize at the wave number that first satisfies equation (246) and, upon further increasing the wave number, the D modes will destabilize at the wave number that first satisfies equation (247). In view of these comments, equation (246) is the relevant stability criterion for this case. If instability sets in, the waves will propagate unidirectionally with phase velocities $-\left(1 + e^{-k}\right)/2$ and $-\left(1 - e^{-k}\right)/2$ for the C and D modes, respectively.

The solution to equation (66) for the case of the C modes is given by

$$\begin{aligned}
\psi &= A_1 e^{k\eta} && \left(-\infty < \eta < -\frac{1}{2}\right) \\
\psi &= A_1 \frac{\nu^2 - (\nu + k)^2 - kR}{\nu(\nu + k)}\, e^{-k} \sinh k\eta && \left(-\frac{1}{2} < \eta < \frac{1}{2}\right) \\
\psi &= -A_1 e^{-k\eta} && \left(\frac{1}{2} < \eta < \infty\right) \quad .
\end{aligned} \tag{248}$$

This can be verified by combining equation (242) with equations (212) through (214) and, in turn, combining the resulting relationships with equations (192) through (194). Similarly, the solution for the D modes is given by

$$\psi = A_1 e^{k\eta} \qquad \left(-\infty < \eta < -\frac{1}{2}\right)$$

$$\psi = -A_1 \frac{\nu^2 - (\nu + k)^2 - kR}{\nu(\nu + k)} e^{-k} \cosh k\eta \qquad \left(-\frac{1}{2} < \eta < \frac{1}{2}\right) \tag{249}$$

$$\psi = A_1 e^{-k\eta} \qquad \left(\frac{1}{2} < \eta < \infty\right) \quad .$$

The C modes are odd solutions, while the D modes are even solutions.

The Fourier amplitudes of the Lagrangian displacements of the interfaces are related to the vertical velocity through the relationship

$$\hat{\xi}' = -i \frac{\hat{w}'}{\Omega} \quad , \tag{250}$$

equation (83). Upon evaluating equation (250) at the lower interface from below and combining this relationship with the solution of the C modes valid in the region $-\infty < \eta < -\frac{1}{2}$, equation (248), we find that the amplitude of the Lagrangian displacement at the lower interface for the C modes is given by

$$\hat{\xi}_1' = -\frac{i A_1 e^{-k/2}}{\bar{\rho}_-(-1/2)\nu} \quad . \tag{251}$$

Similarly, we find that at the upper interface, the amplitude of the C-mode Lagrangian displacement is given by

$$\hat{\xi}_2' = \frac{i A_1 e^{-k/2}}{\rho_+(1/2)\nu} \quad . \tag{252}$$

The subscripts 1 and 2 on $\hat{\xi}'$ denote evaluation at the lower and upper interfaces, respectively, and $\bar{\rho}_-(-1/2)$ and $\bar{\rho}_+(1/2)$ denote the density at

the lower and upper interfaces evaluated from below at the lower interface and from above at the upper interface. In the case of the D modes, the Lagrangian displacements are given by

$$\hat{\xi}_1' = -\frac{i A_1 e^{-k/2}}{\bar{\rho}_-(-1/2)\nu} \tag{253}$$

and

$$\hat{\xi}_2' = -\frac{i A_1 e^{-k/2}}{\bar{\rho}_+(1/2)\nu} \quad . \tag{254}$$

It may be concluded from equations (251) and (252) that the C-mode Lagrangian displacements at the upper and lower interfaces are out of phase by 180 degrees, because $\hat{\xi}_1'/\hat{\xi}_2' < 0$. However, it may be concluded from equations (253) and (254) that the D-mode Lagrangian displacements are in phase because $\hat{\xi}_1'/\hat{\xi}_2' > 0$. Figure 2 depicts the interface configurations associated with the C and D modes. Earlier in this section we concluded that the critical wave number of the C modes is less than that of the D modes. Thus, if a symmetric jet is excited by disturbances with ever-decreasing wavelengths, then the first instability will set in via an asymmetric mode (odd C modes). Thus, the odd solutions are the most unstable solutions.

The asymptotic behavior of ψ for large k in the case of the C modes is given by

$$\begin{aligned}
\psi &\sim A_1 e^{k\eta} && \left(-\infty < \eta < -\frac{1}{2}\right) \\
\psi &\sim -A_1 \frac{\nu^2 - (\nu + k)^2 - kR}{\nu(\nu + k)} e^{-k(\eta+1)} && \left(-\frac{1}{2} < \eta < 0\right) \\
\psi &\sim A_1 \frac{\nu^2 - (\nu + k)^2 - kR}{\nu(\nu + k)} e^{-k(1-\eta)} && \left(0 < \eta < \frac{1}{2}\right) \\
\psi &\sim -A_1 e^{-k\eta} && \left(\frac{1}{2} < \eta < \infty\right) \quad ,
\end{aligned} \tag{255}$$

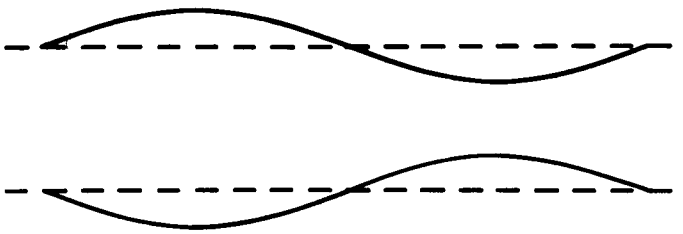

C MODES (ODD SOLUTIONS)

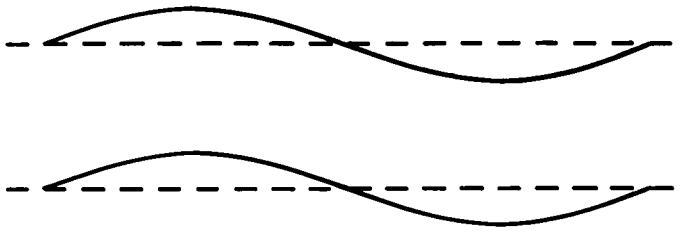

D MODES (EVEN SOLUTIONS)

Note: The dashed lines represent the equilibrium interface configurations and the solid lines are the perturbed interfaces.

Figure 2. Interface configurations associated with the C and D modes.

while the D modes have the behavior

$$
\begin{aligned}
\psi &\sim A_1 e^{k\eta} && \left(-\infty < \eta < -\frac{1}{2}\right) \\
\psi &\sim -A_1 \frac{\nu^2 - (\nu + k)^2 - kR}{\nu(\nu + k)} e^{-k(\eta+1)} && \left(-\frac{1}{2} < \eta < 0\right) \\
\psi &\sim -A_1 \frac{\nu^2 - (\nu + k)^2 - kR}{\nu(\nu + k)} e^{-k(1-\eta)} && \left(0 < \eta < \frac{1}{2}\right) \\
\psi &\sim A_1 e^{-k\eta} && \left(\frac{1}{2} < \eta < \infty\right) .
\end{aligned}
\tag{256}
$$

Now the limiting C modes should correspond to the A modes, while the limiting D modes should correspond to the B modes. However, upon comparing equation (232) with equation (255) and equation (236) with equation (256), we find the correspondence is not exact. The difference between these results can be explained by an examination of the limit procedures that were used to obtain each result. First, since B_3 is arbitrary in equation (236), we may replace it with A_1. In obtaining equations (232) and (236), we first obtained an approximate eigenvalue equation (227) and then deduced equations (228) and (229). We then concluded from equations (228), (212), and (214) that $A_2 \to 0$ and $B_3 \to 0$ as $k \to \infty$ for the A modes, while equations (229), (233), and (235) permitted us to conclude that $A_1 \to 0$ and $B_2 \to 0$ as $k \to \infty$ for the B modes. Now in the case of the symmetric jet we first obtained the exact solutions of equations (248) and (249) with the aid of the characteristic equations (244) and (245) and then took the limit of the solution as $k \to \infty$. In short, the limit procedure, discussed previously, is the reverse of the one used to obtain the limiting solution for the symmetric jet. It appears that we lose half of the limiting solution with the limit procedure discussed previously. The difficulty can be resolved as follows. First the A_1's in equations (248) and (249) are functions of the initial conditions and the A_1's in these solutions are different, because they are derived from the odd and even parts of the initial conditions. This is also true for the limiting solutions of equations (255) and (256). Now as $k \to \infty$, the limiting solutions of equations (255) and (256) differ by a multiplicative constant, K, say, in the domain $-\infty < \eta < 0$, while the solutions in the domain $0 < \eta < \infty$ differ by the multiplicative constant -K. This means the complete solution for large k can be constructed with the C modes in the domain $-\infty < \eta < 0$ and the D modes in the domain $0 < \eta < \infty$, or vice versa. If the complete solution for large k is odd, even, or neither of these, the symmetry or asymmetry properties will automatically be taken into account, because two constants of integration will be available for each pair of modes (a C mode and a D mode) for each k. This means the limiting solutions of equations (232) and (236) are valid for the symmetric jet, in addition to being valid for asymmetric basic state flows.

Odd Shear Layer ($\lambda_1 = 0$, $\lambda_2 = 2$, $R_1 = R_2 = R$). Upon setting $\lambda_1 = 0$, $\lambda_2 = 2$ and $R_1 = R_2 = R$, equation (211) reduces to the form

$$\left[(\nu + k)^2 + \nu^2 - kR\right]\left[(\nu + k)^2 + (\nu + 2k)^2 - kR\right]$$

$$- e^{-2k}\left[(\nu + k)^2 - \nu^2 + kR\right]\left[(\nu + k)^2 - (\nu + 2k)^2 + kR\right] = 0 \quad . \quad (257)$$

Upon setting $\nu = \gamma - k$, we find that equation (257) can be written as

$$\left[\gamma^2 - (\Gamma_1 + \Gamma_2)^2\right]\left[\gamma^2 - (\Gamma_1 - \Gamma_2)^2\right] = 0 \quad , \tag{258}$$

where

$$\Gamma_1^2 = \frac{1}{4}\left\{kR - k^2e^{-2k} - \left(1 - e^{-2k}\right)^{1/2}(kR - k^2)\right\} \tag{259}$$

and

$$\Gamma_2^2 = \frac{1}{4}\left\{kR - k^2e^{-2k} + \left(1 - e^{-2k}\right)^{1/2}(kR - k^2)\right\} \quad . \tag{260}$$

The symbol γ represents the complex wave frequency relative to a frame of reference which is translating with the basic state flow in the middle layer. In the sequel, all considerations with regard to this shear layer will be referenced to this coordinate system. It should be noted that $\bar{u}$ measured in this relative frame of reference is an odd function. It is clear that the four roots of equation (258) are all given by

$$\gamma = \pm (\Gamma_1 \pm \Gamma_2) \quad . \tag{261}$$

Now the following statements concerning the stability properties of the flow can be concluded from equation (261):

(i) Stability (four real roots) if

$$R > k\,\frac{e^{-2k} + \left(1 - e^{-2k}\right)^{1/2}}{1 + \left(1 - e^{-2k}\right)^{1/2}} \quad . \tag{262}$$

(ii) Instability (two pairs of conjugate complex roots with nonzero real parts) if

$$k\,\frac{e^{-2k} - \left(1 - e^{-2k}\right)^{1/2}}{1 - \left(1 - e^{-2k}\right)^{1/2}} < R < k\,\frac{e^{-2k} + \left(1 - e^{-2k}\right)}{1 + \left(1 - e^{-2k}\right)^{1/2}} \quad . \tag{263}$$

(iii) Instability (two pairs of conjugate pure imaginary roots) if

$$R < k\,\frac{e^{-2k} - \left(1 - e^{-2k}\right)^{1/2}}{1 - \left(1 - e^{-2k}\right)^{1/2}} \quad . \tag{264}$$

provided

$$k < \frac{1}{8} \ln \frac{1}{2}\left(\sqrt{5} + 1\right) \quad \text{for} \quad R > 0 \quad .$$

This example was constructed by Howard [34] to show that the principle of the exchange of stabilities is not necessarily valid for odd profiles of $\bar{u}$ associated with even distributions of S or static stability. A discussion of the principle of the exchange of stabilities can be found in Reference 50. The argument for applying this principle is based upon the symmetry properties of equation (66). If ω is an eigenvalue belonging to a proper solution $\psi(z)$ for assigned values of κ_1 and κ_2, then ω^* is also an eigenvalue for the same values of κ_1 and κ_2 and belongs to the eigenfunction $\psi(z)^*$. In other words, conjugation does not change equation (66). In addition, since $\bar{u}$ is an odd function of z and S is an even function, then $-\omega$ is also an eigenvalue and belongs to $\psi(-z)$. Thus, we might infer that the transition state in passing from stability to instability should be characterized by $\omega = 0$ if it is unique. Howard explains that this means that neither left nor right is preferred as a direction of propagation of the instability, so that the wave apparently must stand still, unless the transition state, as well as all other states, occurs in mirror image pairs with respect to the real axis of the complex ω- or ν-plane. Thus, if an unsteady marginal state $(\mathrm{Re}(\nu) \neq 0$ and $(\mathrm{Im}(\nu) = 0)$ exists, it will be characterized by two unstable waves moving in opposite directions with the same speed. This last alternative is predicted by equation (261). This should be compared with the case of the symmetric jet which predicts that the transition state C and D modes are characterized by

unidirectionally propagating waves with phase velocities $\left(1 - e^{-k}\right)/2$ and $\left(1 + e^{-k}\right)/2$ with respect to a frame of reference translating with the jet core basic state flow. In addition, the symmetric jet instability first sets in via a single unstable wave (C mode) and it is only for sufficiently large k that two unstable waves exist [see equations (246) and (247)], while the odd shear layer is characterized by two unstable waves for all unstable states in configuration space. Thus, the odd shear layer and the symmetric jet are characterized by fundamentally different destabilization phenomena, in spite of the fact that the sources of the instability are similar, namely, the shearing action of the unperturbed wind profile.

The amplitudes of the Lagrangian displacements at the lower interface are given by

$$\hat{\xi}_1' = -\frac{i A_1}{\bar{\rho}_-(-1/2)\Omega_1} e^{-k/2} \quad , \tag{265}$$

while the Lagrangian amplitudes associated with the upper interfaces are given by

$$\hat{\xi}_2' = -\frac{i A_1 \beta_2}{\bar{\rho}_+(1/2)\Omega_1\Omega_2^2}\left\{\Omega_1^2 \sinh k + \beta_1\Omega_2^2 \cosh k - kR \sinh k\right\} e^{-k/2} \quad . \tag{266}$$

Equation (265) was obtained by substituting equation (192) into equation (250) and equation (266) was obtained by combining equations (194), (214), and (250). Let us now consider the behavior of these functions for sufficiently small k, for $R > 0$, so that equation (262) is satisfied. This means we will consider neutral motions.

Upon expanding Γ_1 and Γ_2 in a Taylor series expansion in k about the point $k = 0$, and using the definition $\nu = \gamma - k$ and equation (261), we find that the four eigenvalues can be expressed in the forms

$$\nu \sim -k \pm R^{1/2}k^{1/2}\left\{1 - \frac{k}{2R} + \ldots\right\} \qquad (k \to 0) \quad , \tag{267}$$

and

$$\nu \sim -k \pm R^{1/2}k^{1/2}\left\{\frac{k^{1/2}}{2^{1/2}} + \frac{1}{2^{1/2}}\left(\frac{R-2}{2R}\right)k^{3/2} + \ldots\right\} \qquad (k \to 0) \quad . \tag{268}$$

The modes associated with equations (267) and (268) will be termed the E and F modes, respectively. Since we are now analyzing the neutral modes, it follows that ν is real and $\Omega_2^2 > 0$. Thus, the phase angle between the Lagrangian displacements at the upper and lower interfaces for a given mode will be determined by the sign of

$$\Upsilon = \Omega_1^2 \sinh k + \beta_1\Omega_2^2 \cosh k - kR \sinh k \quad , \tag{269}$$

where Υ is the quantity within the braces in equation (266). If $\Upsilon > 0$, then the Lagrangian displacements will be in phase (phase angle equal to 0 deg), while if $\Upsilon < 0$ then the displacements will be 180 deg out of phase. Upon retaining only the first two terms in equations (267) and (268), we find for the E modes that

$$\Upsilon = \left(1 \mp \frac{R^{1/2}}{2^{1/2}}\right)^2 k^3 + \beta_1 \frac{Rk^2}{2} - k^2R \quad , \tag{270}$$

while in the case of the F modes we have

$$\Upsilon = \left(k \mp R^{1/2}k^{1/2}\right)^2 k + \beta_1 Rk - k^2R \quad . \tag{271}$$

If k is sufficiently small, then we need only consider the terms involving k^2 in equation (270), so that in the case of the E modes $\Upsilon < 0$, because β_1 is approximately equal to unity and $R > 0$. This means the E modes for $R > 0$ are the odd solutions and the phase angle between the Lagrangian displacements is 180 deg. In this case, the interface configuration will be like that of the C modes as shown in Figure 1. Similarly, if k is sufficiently small, the term $\beta_1 Rk$ in equation (271) will be an order of magnitude greater than the magnitudes of the other terms in the same equation, so that $\Upsilon > 0$ in the case of the F modes. Thus, the F modes for $R > 0$ are the even solutions,

the phase angle between the Lagrangian displacements will be equal to 0 deg, and the interface configuration will be like that of the D modes as shown in Figure 2. Calculations with equations (265) and (266) appeared to show that these phase relationships are true for all neutral odd shear layer solutions.

In the case of the symmetric jet, we found that as k increases, the first unstable solution is odd and a further increase in k results in a destabilization of one mode of the even solutions. The first unstable solution in the odd shear layer will be a linear combination of an even and an odd mode as we increase k and pass through the critical state. These modes propagate in opposite directions relative to a frame of reference translating with the basic velocity in the middle layer, and the magnitude of the phase velocities of these modes are equal. Thus, the interaction of these modes results in a stationary wave instability in a frame of reference translating with the mean flow in the middle layer of the three-layer model.

As k increases beyond the critical wave number, the phase angle between the Lagrangian displacements departs from 0 deg in the F modes and 180 deg in the E modes. The phase angles of the C and D modes are equal to 180 deg and 0 deg, respectively, for all values of k.

General Eigenvalue Analysis

In the previous paragraph, we discussed the stability properties of two special cases: the symmetric jet and the odd shear layer. These special cases proved to be both interesting and instructive; however, they do not exhaust the many possibilities that could exist in the atmosphere. Accordingly, the purpose of this section is to analyze the eigenvalues and thus the stability properties of other types of jets and shear layers. The analysis will be valid for microscale shear layers and jets imbedded in the synoptic scale vertical wind profile and mesoscale and synoptic scale jets and shear layers.

Eigenvalue Diagrams. The essential features of six types of basic state flows to be considered are tabulated as follows:

Basic State Flows

Flow Number	λ_1	λ_2	R_1	R_2
1	0.5	0	0.4	0.2
2	0.5	0	0.2	0.2
3	0.5	0	0.2	0.4
4	0.5	0.4	0.2	0.2
5	0.5	0.8	0.2	0.2
6	0.5	1.3	0.2	0.2

In the subsequent discussion, we will refer to these flows by number, as listed in the above tabulation.

Flows 1, 2, and 3 are jet flows with asymmetric velocity distributions, where the velocity in layer 3 is equal to zero, and that in layer 1 is equal to $0.5\,\bar{u}_2$. Flows 1 and 3 have asymmetric distributions of static stability. Flow 3 is hydrostatically more stable above the jet core, while flow 1 is hydrostatically more stable below the jet core. Flow 2 has a symmetric distribution of static stability. The distribution of static stability associated with flow 3 could correspond to that associated with a synoptic scale jet stream in which one would expect to find the relatively more stable fluid above the jet core in the stratosphere; i.e., $R_1 < R_2$, while flows 1 and 3 could correspond to meso- and micro-scale jets imbedded in a synoptic scale wind profile. Of course, it is also possible to associate flow 2 with meso- and micro-scale flows. Flows 1, 2, 3 were selected to determine the effects of the distribution of static stability upon jet stability.

Flows 4 and 5 correspond to jet flows, while flow 6 corresponds to a shear layer flow. These flows have asymmetric velocity distributions and the associated distributions of static stability are symmetric. Flows 2, 4, 5, and 6 were selected to determine the effects of the distribution of velocity upon jet and shear layer instability. These flows could correspond to micro- and meso-scale flows.

Figures 3 through 8 are eigenvalue diagrams of perturbations that could occur in flows 1 through 6, respectively. These diagrams illustrate the magnitudes of the real and imaginary parts of ν calculated with equation (222). If the real part of ν, denoted by ν_r, is negative, then the quantity

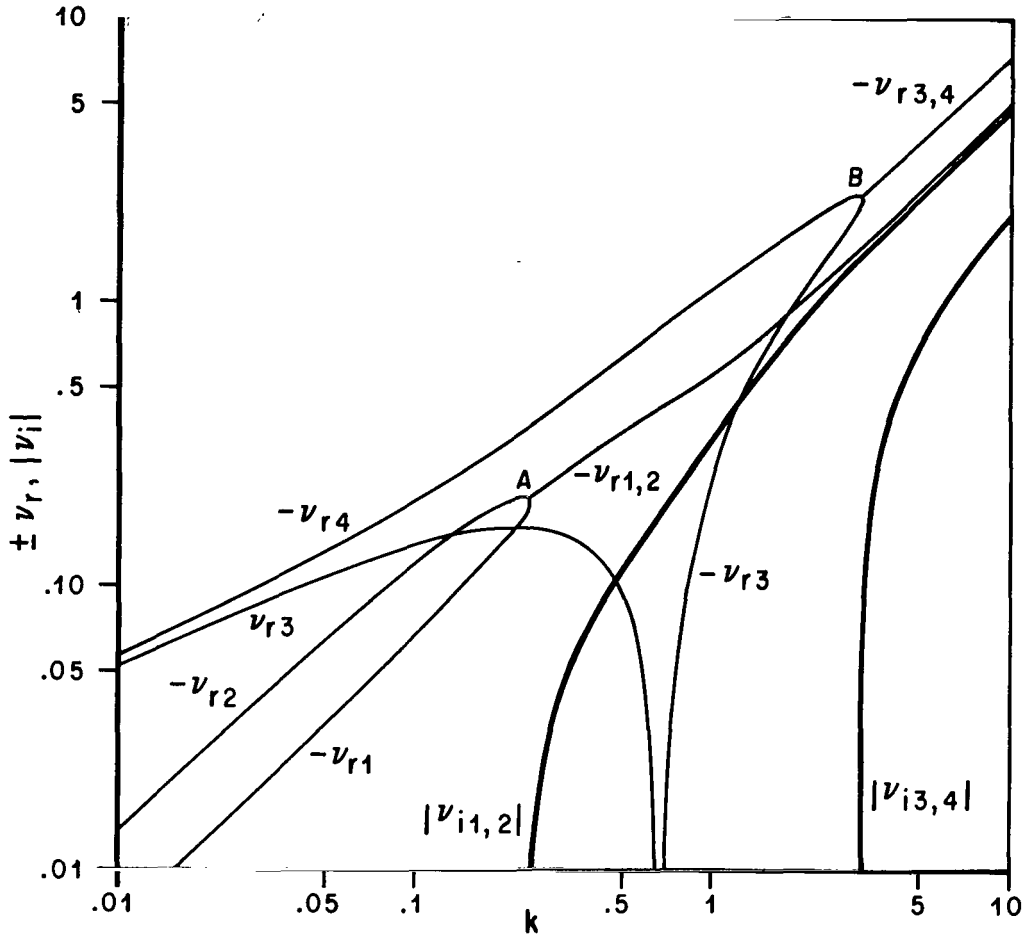

Note: Both negative and positive values of ν_r are plotted in this figure, negative values of ν_r being indicated with a minus sign. Now, the imaginary parts of ν occur in complex conjugate pairs. Thus, the absolute value of ν_i has been plotted and the appropriate mode numbers have been indicated. The critical eigenstates occur at the points A and B. The ν_r curve for modes 1 and 2 branches at point A. To the left of this point, modes 1 and 2 are neutral and $|\nu_{i1,2}| = 0$, while to the right of this point, modes 1 and 2 are unstable and $\nu_{r1} = \nu_{r2}$ and $|\nu_{i1,2}| > 0$. Similar comments can be made about branch point B in relation to modes 3 and 4.

Figure 3. Eigenvalue diagram for $\lambda_1 = 0.5$, $\lambda_2 = 0$, $R_1 = 0.4$, and $R_2 = 0.2$.

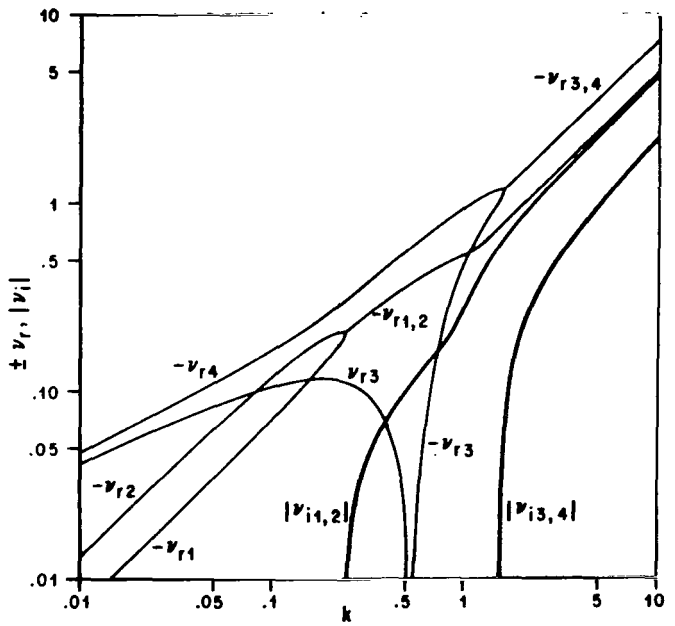

Figure 4. Eigenvalue diagram for $\lambda_1 = 0.5$, $\lambda_2 = 0$, $R_1 = 0.2$, and $R_2 = 0.2$. (See Fig. 3 for explanation of the symbols.)

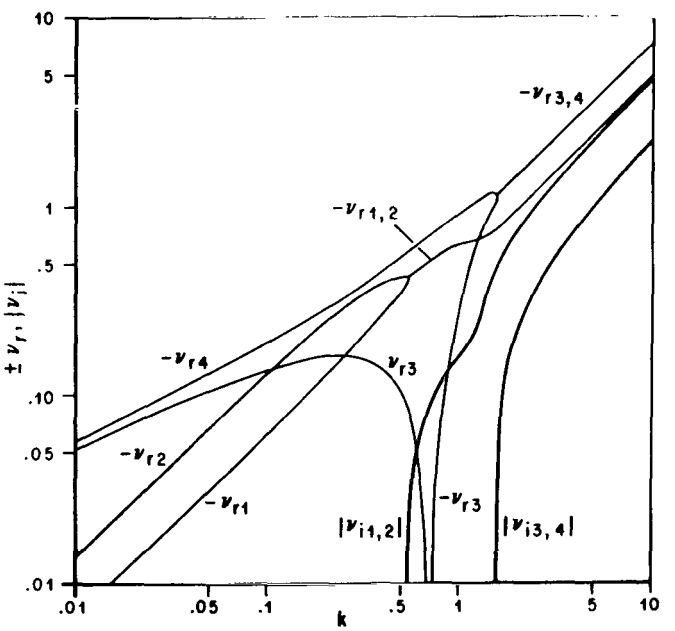

Figure 5. Eigenvalue diagram for $\lambda_1 = 0.5$, $\lambda_2 = 0$, $R_1 = 0.2$, and $R_2 = 0.4$. (See Fig. 3 for explanation of the symbols.)

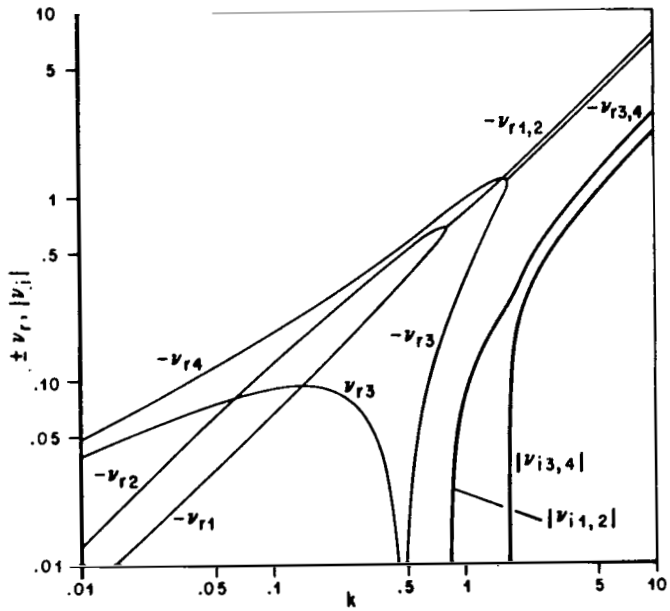

Figure 6. Eigenvalue diagram for $\lambda_1 = 0.5$, $\lambda_2 = 0.4$, $R_1 = 0.2$, and $R_2 = 0.2$. (See Fig. 3 for explanation of the symbols.)

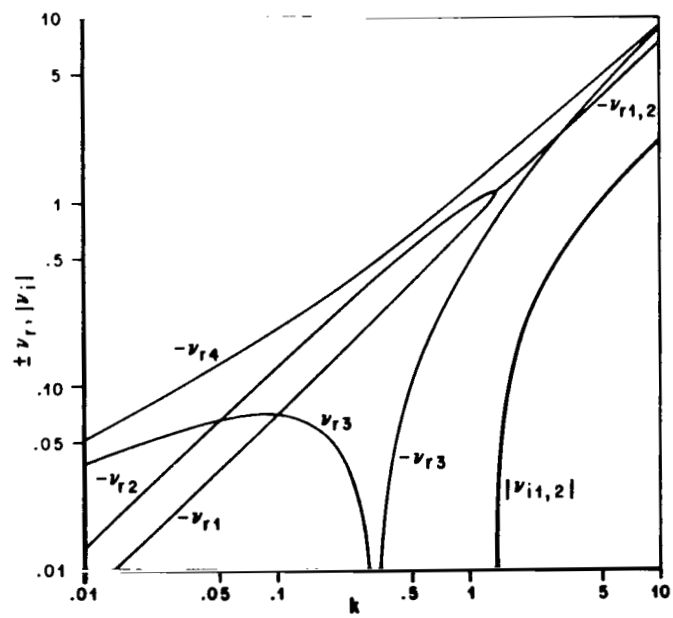

Figure 7. Eigenvalue diagram for $\lambda_1 = 0.5$, $\lambda_2 = 0.8$, $R_1 = 0.2$, and $R_2 = 0.2$. (See Fig. 3 for explanation of the symbols.)

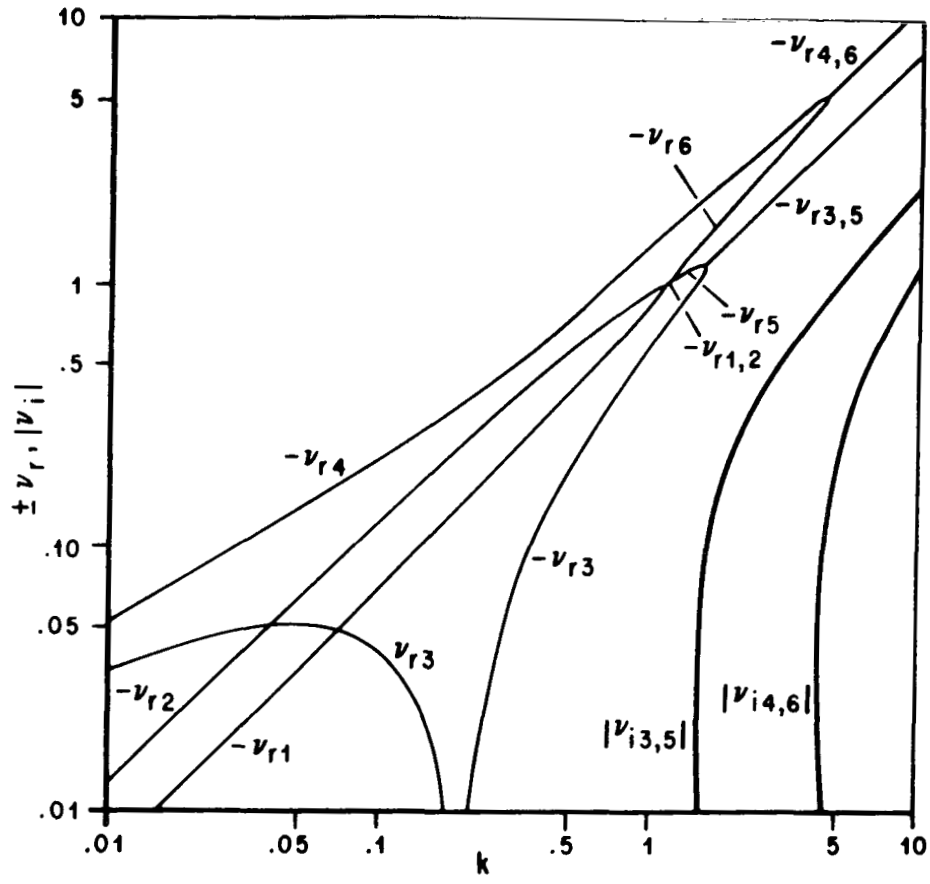

Figure 8. Eigenvalue diagram for $\lambda_1 = 0.5$, $\lambda_2 = 1.3$, $R_1 = 0.2$, and $R_2 = 0.2$. (See Fig. 3 for explanation of the symbols.)

$-\nu_r$ was plotted. If ν is complex, then the eigenvalues will occur in complex conjugate pairs; thus, we have plotted the magnitude of the imaginary part of ν, denoted by ν_i, and it will be understood that both positive and negative values of ν_i occur. The left side of the characteristic equation (222) is a fourth-degree polynomial in ν, so that for each configuration of λ_1, λ_2, R_1, R_2, and k, there will exist four modes, each with its own value of ν. Accordingly, the modes are indicated with numerical subscripts (1, 2, 3, and 4) on ν_r and ν_i in Figures 3 through 7. In Figure 8 we have departed from this notation to label the various features on the ν_r curves, so that the

additional subscripts (5 and 6) do not imply that the number of modes exceed four for any particular value of k. In discussing Figure 8, we will refer to six modes; however, four of these modes (1, 2, 5, and 6) do not occur over the complete spectrum of wave numbers.

The critical state, the neutral state contiguous to an unstable state, occurs at a branch point in the complex ν-plane. In Figures 3 through 8, these critical states occur at a branch point in the (ν_r, k)-plane; e.g., points A and B in Figure 3 are critical points. To the left of point A, the eigenvalues of ν for modes 1 and 2 are real, so that ν_{i1} and ν_{i2} vanish and ν_{r1} and ν_{r2} are the eigenvalues of modes 1 and 2. As we approach point A from the left, ν_{r1} and ν_{r2} approach the same value. At point A, $\nu_{r1} = \nu_{r2}$ and $\nu_{i1} = \nu_{i2} = 0$. As we proceed away from point A toward the right, we then have $\nu_{r1} = \nu_{r2}$ and $|\nu_{i1,2}| > 0$, and the roots of equation (222) associated with modes 1 and 2 occur in complex conjugate pairs. Thus, one mode is unstable, while the other is damped in time. Similar comments can be made about branch point B in relation to modes 3 and 4. The branch points of modes 1 and 2 (branch point A) and 3 and 4 (branch point B) are points on a stability boundary in configuration space. In each case, the growth rate (ν_i) increases rapidly as the wave number increases for $k > k^*$, where k^* denotes the wave number associated with a stability boundary. Branch point A is the relevant point on the stability boundary because it corresponds to the mode with the smallest wave number or largest wavelength which is neutrally stable. In the situations considered in Figures 3 and 4, the marginal wavelength is approximately equal to 24d, while in Figure 5 it is approximately equal to 12d, where $d = 2h$. If we interpret d to be the vertical halfwidth of a jet, then the marginal wavelength for $d = 1$ km is equal to 24 km for the situations considered in Figures 3 and 4, and 12 km for the case considered in Figure 5.

If $\nu_r < 0$, then the solution to equation (66) is proportional to $e^{i(kx-|\nu_r|t)}$, which corresponds to a wave that propagates toward increasing values of x with a wave speed equal to $|\nu_r|k^{-1}$. Similarly, if $\nu_r > 0$, then the solution is proportional to $e^{i(kx+\nu_r t)}$ which corresponds to a wave that propagates toward decreasing values of x with a wave speed also equal to $|\nu_r|k^{-1}$.

Figures 3 through 8 appear to show that, as k approaches zero, the eigenvalues behave as follows:

$$\nu = \nu_{r1,2} \sim k \qquad (k \to 0) \tag{272}$$

and

$$\nu = \nu_{r3,4} \sim k^{1/2} \qquad (k \to 0) \quad . \tag{273}$$

The precise asymptotic behavior can be deduced from equation (211), namely,

$$(\Omega_2^2 + \Omega_1^2 - kR_1)\ (\Omega_2^2 + \Omega_3^2 - kR_2)$$

$$-e^{-2k}(\Omega_2^2 - \Omega_1^2 + kR_1)\ (\Omega_2^2 - \Omega_3^2 + kR_2) = 0 \quad , \tag{274}$$

where we have set $\beta_1 = \beta_2 = 1$. As k approaches zero, e^{-2k} behaves like $1 - 2k$, so that for sufficiently small k we may cast equation (274) into the form

$$\Omega_2^2(\Omega_1^2 + \Omega_3^2) - k(R_1 + R_2)\Omega_2^2 + k^3R_1R_2 + k^2\left[R_1(\Omega_2^2 - \Omega_3^2) + R_2(\Omega_2^2 - \Omega_1^2)\right]$$

$$+ k(\Omega_2^2 - \Omega_1^2)\ (\Omega_2^2 - \Omega_3^2) \simeq 0 \quad . \tag{275}$$

In modes 1 and 2, $\nu_{r1,2}$ behaves like k as $k \to 0$. This means Ω_1, Ω_2, and Ω_3 are asymptotically proportional to k, so that the second and third terms on the left-hand side of equation (275) are at least one order of magnitude greater than the remaining terms. Thus, we may conclude that the asymptotic behavior of the eigenvalues associated with modes 1 and 2 are given by

$$\nu_{1,2} \sim -k \pm \left(\frac{R_1R_2}{R_1 + R_2}\right)^{1/2} k \qquad (k \to 0) \quad , \tag{276}$$

where the positive and negative signs are associated with modes 1 and 2, respectively. Upon dividing equation (276) by k, we find that the wave velocity or phase velocity has the asymptotic behavior

$$c_{p1,2} \sim -1 \pm \left(\frac{R_1 R_2}{R_1 + R_2} \right)^{1/2} \qquad (k \to 0) \tag{277}$$

where c_p is the phase velocity measured in units of $\bar{u}_2$. The basic state dimensionless velocity in the middle layer of the three-layer model is equal to unity. Thus, it may be concluded from equation (277) that mode 1 will propagate upstream, while mode 2 will propagate downstream with a velocity equal in magnitude and opposite in sign to mode 1 with respect to a frame of reference attached to the basic state flow in the middle layer. This will be true for both jets and shear layers.

In the case of modes 3 and 4, $\nu_{r3,4}$ behaves like $k^{1/2}$ as $k \to 0$. This means that Ω_1, Ω_2, and Ω_3 will approach ν as $k \to 0$. Thus, the last three terms in equation (275) will asymptotically vanish and the first and second terms in the same equation will be of order k^2, while the third term will be of order k^3. Thus, the first two terms in equation (275) are the significant terms, so that we have

$$\nu^2 \left[\nu^2 - k \left(\frac{R_1 + R_2}{2} \right) \right] \to 0 \qquad (k \to 0) \quad . \tag{278}$$

We may conclude from equation (278) that

$$\nu_{3,4} \sim \pm \left(\frac{R_1 + R_2}{2} \right)^{1/2} k^{1/2} \qquad (k \to 0) \tag{279}$$

because ν^2 is nontrivial. The associated phase velocity is given by

$$c_{p3,4} \sim \pm \left(\frac{R_1 + R_2}{2} \right)^{1/2} k^{-1/2} \qquad (k \to 0) \quad . \tag{280}$$

We may conclude from equation (280) that $c_{p3,4} \to \pm \infty$ as $k \to 0$.

For the two-layer Kelvin-Helmholtz model, it may be concluded from equation (230) or equation (231) that

$$\nu_{K.H.} \sim \pm \left(\frac{R}{2}\right)^{1/2} k^{1/2} \qquad (k \to 0) \qquad , \tag{281}$$

where R denotes R_1 or R_2. It has been common practice in meteorology to consider the region below the synoptic scale jet streams as a Kelvin-Helmholtz shear layer, so that $R = R_1$ in equation (281). Upon forming the ratio of equations (279) and (281) we find

$$\frac{\nu_{3,4}}{\nu_{K.H.}} = \left(1 + \frac{R_2}{R_1}\right)^{1/2} \qquad (k \to 0) \qquad . \tag{282}$$

In synoptic scale jets $R_2 \geqq R_1$; thus, it may be concluded that the three-layer model predicts phase velocities for small k which are greater than those predicted by the two-layer model by a factor of at least 1.4. The result is also true for two-layer model estimates of ν above the jet core. It might be concluded that if we accept the three-layer model as being more realistic than the two-layer one, then static stability conditions above the jet core do affect wave propagation below the jet core and vice versa.

At this point in the discussion it is worthwhile to introduce the group velocity of the waves. The group velocity, in units of $\bar{u}_2$, is given by

$$c_g = \frac{\partial \nu_r}{\partial k} \qquad , \tag{283}$$

and is equal to the slope of the ν_r curve in a (ν_r, k)-plane. If $c_g > 0$, then the wave energy of a wave packet with wave numbers between k and k + dk will propagate toward decreasing values of x, while $c_g < 0$ corresponds to wave energy propagation toward increasing values of x. The coordinates in Figures 3 through 8 are $\ln|\nu_r|$ and ln k; thus it is desirable to write equation (283) in the form

$$|c_g| = |c_p| \frac{\partial \ln |\nu_r|}{\partial \ln k} \quad , \tag{284}$$

where the sign of c_g must be determined with the aid of equation (283).

The asymptotic behavior of the group velocity for modes 1 and 2 is given by

$$c_g \sim -1 \pm \left(\frac{R_1 R_2}{R_1 + R_2} \right)^{1/2} \qquad (k \to 0) \quad , \tag{285}$$

where the positive and negative signs are associated with modes 1 and 2, respectively. Similarly, the asymptotic behavior for modes 3 and 4 is given by

$$c_g \sim \pm \frac{1}{2} \left(\frac{R_1 + R_2}{2} \right)^{1/2} k^{-1/2} \qquad (k \to 0) \quad , \tag{286}$$

where the positive and negative signs are associated with modes 3 and 4, respectively. Thus, it may be concluded from equations (277) and (285) that the phase and group velocities are asymptotically equal as k approaches zero for modes 1 and 2. In modes 3 and 4, equations (280) and (286) permit us to conclude that the group velocity is one-half the phase velocity.

Let us now concentrate on the behavior of the eigenvalues as k approaches infinity. The asymptotic behavior of the eigenvalues can be obtained from equations (230) and (231). As k approaches infinity, the terms under the radicals that involve λ_1 and λ_2 will dominate the terms that contain R_1 and R_2, respectively, so that

$$\nu \sim -\left(\frac{1 + \lambda}{2} \right) k \pm i \frac{|1 - \lambda|}{2} k \qquad (k \to \infty) \quad , \tag{287}$$

where λ denotes λ_1 or λ_2. Thus, the eigenvalues will be complex for sufficiently large k. An examination of Figures 3 through 8 will show that equation (287) is the correct asymptotic behavior for large k.

The quantity $|1 - \lambda|$ is a measure of the basic state velocity shear across the lower interface if $\lambda = \lambda_1$ or the upper interface if $\lambda = \lambda_2$, viz., $|1 - \lambda_i| = |(\bar{u}_2 - \bar{u}_i)/\bar{u}_2|$ $(i = 1, 3)$. Thus, we may conclude from equation (287) that the growth rate of the perturbations will increase in absolute value as the basic state shear increases. If $\lambda = 1$, then equation (287) predicts that ν_i is asymptotically equal to zero. This is an incorrect result. In this case, the correct asymptotic relation is given by

$$\left[\nu \sim -k \pm i \left(-\frac{R}{2} \right)^{1/2} k^{1/2} \right] \qquad (k \to \infty) \quad , \tag{288}$$

where R denotes R_1 or R_2. Relation (288) is an obvious consequence of the Kelvin-Helmholtz limit; see equations (230) and (231). If $R \geqq 0$, then the eigenvalues given by equation (288) are real, and the basic state flow is neutral to small perturbations. However, if $R < 0$, then the eigenvalues are complex, and the absolute values of the growth rates increase as the static stability decreases.

The quantity $(1 + \lambda)/2$ is equal to the dimensionless average velocity between layers 1 and 2 if $\lambda = \lambda_1$ or layers 2 and 3 if $\lambda = \lambda_2$, viz., $(1 + \lambda_i)/2 = (\bar{u}_i + \bar{u}_2)/2\bar{u}_2$ $(i = 1, 3)$. The phase and group velocities associated with equation (287) are given by

$$c_p = c_g \sim -\frac{1 + \lambda}{2} \qquad (k \to \infty) \quad , \tag{289}$$

while the phase and group velocities associated with equation (288) are given by

$$\left.\begin{aligned} c_p &\sim -1 \pm i \left(-\frac{R}{2} \right)^{1/2} k^{-1/2} \, \delta_1 \\ c_g &\sim -1 \pm i \left(-\frac{R}{2} \right)^{1/2} \frac{k^{-1/2}}{2} \, \delta_1 \end{aligned}\right\} \tag{290}$$

where

$$\delta_1 = \begin{cases} 0 & \text{if } R \leqq 0 \\ 1 & \text{if } R > 0 \end{cases} \quad .$$

It was shown previously that for sufficiently large k, the modes associated with the eigenvalue equations (230) and (231) propagate locally at the lower and upper interfaces, respectively. Equation (289) predicts that the perturbations at the lower and upper interfaces propagate their phase and energy with speeds equal to the average speeds between layers 1 and 2 and layers 2 and 3, respectively. The direction of propagation with respect to the basic state flow in the middle layer of the three-layer model is downstream if $1 + \lambda > 0$, or upstream if $1 + \lambda < 0$, while $\lambda = -1$ corresponds to a standing wave perturbation. In Figures 3 through 6, the short wave Fourier components associated with modes 3 and 4 and modes 1 and 2 propagate at the lower and upper interfaces, respectively, while the reverse is true for the modes in Figure 7. In Figure 8, the short wave Fourier components associated with modes 4 and 6 and modes 3 and 5 propagate at the upper and lower interfaces, respectively.

The modes associated with equation (290) are unstable if $R < 0$ and neutral if $R \geqq 0$, the equation (290) predicts that the perturbations propagate their phase and energy locally at the appropriate interface (R_1 and R_2 correspond to the lower and upper interfaces) with velocities equal to the basic flow. If $R > 0$, then each interface will be characterized by two modes that propagate both their phase and energy in opposite directions, relative to a frame of reference translating with a speed equal to $\bar{u}_2$.

Let us now concentrate on the regions of the eigenvalue diagrams in which k is neither very small nor extremely large. In most of the cases in Figures 3 through 8, these regions occur in the domain $0.05 < k < 5$. In the preceding paragraphs, we were able to analyze the behavior of the eigenvalues for sufficiently large and sufficiently small k with the aid of asymptotic expansions in the neighborhood of $k = 0$ and $k = \infty$. The asymptotic behavior was obtained by examining the behavior of the various terms in equation (211) as k approaches zero and infinity. We found that certain terms vanished or increased faster than other terms. This permitted us to neglect certain terms and restrict the analysis to a few important terms and thus simplify the analysis considerably. However, if k is neither small nor large, all the terms in equation (211) are of the same order of magnitude, so that all the terms must be retained. Now the left-hand side of equation (211) is a fourth-order polynomial in ν and all odd and even powers of ν between zero and four are present. In principle, it is possible to factor equation (211) and thus obtain expressions for the roots as functions of k, λ_1, λ_2, R_1, and R_2. However, from a practical point of view, it is virtually impossible,

except in a few special cases, to extract the roots of equation (211) and express them as functions of k, λ_1, λ_2, R_1, and R_2 without resorting to the use of numerical methods. The eigenvalues in Figures 3 through 8 were obtained from equation (211) by using standard numerical methods; e.g., Hartree [51].

As k increases away from $k = 0.01$, in Figures 3 through 7, $|\nu_{r1}|$ and $|\nu_{r2}|$ increase faster and slower than k, respectively, so that the absolute values of the phase and group velocities are increasing functions of k for mode 1 and decreasing functions of k for mode 2. The signs of these velocities are negative, so that the phase and energy are propagated downstream with respect to the basic state flow in the middle layer. To the left in the immediate vicinity of the branch point associated with modes 1 and 2 there exists a point on the $|\nu_{r2}|$ curve characterized by

$$\frac{\partial \ln |\nu_{r2}|}{\partial \ln k} = 0$$

and thus $c_g = 0$. To the left of this point $c_g < 0$, while to the right $c_g > 0$. As we approach the branch point we find

$$\lim_{k \to k^*} \frac{\partial \nu_{r1}}{\partial k} = +\infty, \quad \lim_{k \to k^*} \frac{\partial \nu_{r2}}{\partial k} = -\infty \quad \text{and} \quad \nu_{r1} = \nu_{r2} \quad ,$$

so that the critical state is characterized by two modes with the same phase velocity which is less than zero. However, the group velocities are infinite, but opposite in sign. This result is also valid for all the other branch points in Figures 3 through 8. To the right of the branch point, $\nu_{r1} = \nu_{r2} < 0$ and $\nu_{i1} = -\nu_{i2}$. As k increases away from the branch point, $|\nu_{r1,2}|$ increases slower than k, so that the phase and group speeds are decreasing functions of k; however, the rates of decrease of these functions approach zero as k approaches infinity, and $c_{p1,2}$ and $c_{g1,2}$ approach constant values, equation (289). In the immediate vicinity of the branch point, $|\nu_{i1,2}|$ is a rapidly increasing function of k and tends toward infinity as k approaches infinity, equation (287), so that the most unstable state is associated with $k = \infty$.

Let us now concentrate on modes 3 and 4 in Figures 3 through 7. As k increases away from $k = 0.01$, $|\nu_{r4}|$ increases faster than ν_{r3}, and $\nu_{r4} < 0$, $\nu_{r3} > 0$, and $\nu_{r3} < |\nu_{r4}|$. In the vicinity of $k = 0.3$, a point exists on the ν_{r3} curve characterized by $\partial\nu_{r3}/\partial k = 0$. To the left of this point, $c_{g3} > 0$, so that the energy is propagated upstream with respect to the basic state flow in the middle layer, while to the right $c_{g3} < 0$, so that the energy is propagated downstream. In both cases, the phase velocity c_{p3} is positive, and thus the phase is propagated upstream. In mode 4 in the vicinity of the maximum of ν_{r3}, the phase and energy is propagated downstream. As k continues to increase, ν_{r3} experiences a sign change in the vicinity of $k = 0.5$. In this region, the associated group velocity of mode 3 is extremely large and positive, while the phase velocity vanishes at the wave number associated with $\nu_{r3} = 0$. The behavior of $|\nu_{r3}|$, $|\nu_{r4}|$, and $|\nu_{i3,4}|$ for $k > 1$ is qualitatively the same as the corresponding parameters of modes 1 and 2.

In Figure 8, the configuration of the eigenvalues is similar to those in Figures 3 through 7, except in the neighborhood of $k = 1.0$ where the eigenvalues show multiple branching. For the cases shown in Figures 3 through 7, we found that unstable modes existed for all wave numbers greater than some critical value; thus, it would appear that the critical wave number k^* is a single-valued function of λ_1, λ_2, R_1, and R_2. However, Figure 8 shows that the critical wave number is a multivalued function of λ_1, λ_2, R_1, and R_2. If k_1^*, k_2^*, and k_3^* denote the wave numbers of the branch points associated with modes 1 and 2, 5 and 6, and 3 and 5, respectively, then we have neutral modes if $k \leqq k_1^*$ or $k_2^* \leqq k \leqq k_3^*$, while we have instability if $k_1^* < k < k_2^*$ or $k_2^* < k$. We will pursue this point later in this discussion. Goldstein [16] obtained somewhat similar results in considering the stability properties of the broken-line flow given by

$$\frac{\bar{u}(z)}{\bar{u}(h)} = \begin{cases} 1 & y > \infty \\ z/h & -h < y < h \\ -1 & y < -\infty \end{cases} \tag{291}$$

$$\bar{\rho}(z) = \begin{cases} \rho_o - \sigma & y > \infty \\ \rho_o & -h < y < h \\ \rho_o + \sigma & y < -\infty \end{cases} , \tag{292}$$

where ρ_o and σ are positive constants.

As explained earlier in this report Miles [31] and Howard [33] have shown that, for continuous basic state flows, the complex wave frequency ω for any unstable mode associated with $S > 0$ must occur within the semicircle which has the range of $\kappa_1\bar{u}$ for diameter in the lower half of the ω-plane, so that

$$\left[\omega_r + \frac{1}{2}(a + b)\right]^2 + \omega_i^2 \leq \left(\frac{a - b}{2}\right)^2 , \tag{293}$$

where a and b are the upper and lower bounds on $\kappa_1\bar{u}$. However, for broken-line flows, it was possible only to prove that equation (293) is valid for those flows in which $\bar{\theta}$ is continuous across the interfacial surfaces. In addition to equation (293), Miles [31] has also shown that, for statically stable $(S > 0)$ continuous basic state flows, the critical eigenstates are characterized by

$$\kappa_1 a < -\omega < \kappa_1 b . \tag{294}$$

The eigenvalues given by the asymptotic relationship (287) satisfy equation (293). In addition, numerical calculations with the results in Figures 3 through 8 show that critical state and unstable eigenvalues satisfy equations (294) and (293), respectively. Thus, in view of these conditions, it would appear that the eigenvalues of the three-layer model behave like the ones from the continuous counterpart.

Absolute Stability Boundaries. In the previous paragraph, we presented the eigenvalues associated with six types of basic state flows. We determined the asymptotic behavior of the eigenvalues for both large and small values of k. We also analyzed the eigenvalues for intermediate values of k. In our analysis, we found that there exists a critical wave number k* such that if

$k \leqq k^*$, the solutions are neutral oscillations. On the other hand, if $k^* < k < \infty$, then the solutions are unstable, except possibly for a small band of wave numbers, contained within the domain $k^* < k < \infty$, in which the solutions are neutral oscillations. Thus, for example, for flows 1 through 5, we found that the absolute stability boundary was characterized by one critical wave number in each case, while for flow 6 the absolute stability boundary was characterized by three critical wave numbers. The critical wave numbers associated with an absolute stability boundary are functions of λ_1, λ_2, R_1, and R_2. The purpose of this discussion is to show the behavior of these functions.

a. Homentropic Flows. In the following paragraphs, we will discuss jet and shear layer instability in a homentropic atmosphere ($R_1 = R_2 = 0$). The characteristic equation for homentropic flows can be obtained from equation (211) by setting $R_1 = R_2 = 0$ and $\beta_1 = \beta_2 = 1$, so that

$$(\Omega_2^2 + \Omega_1^2)(\Omega_2^2 + \Omega_3^2) - e^{-2k}(\Omega_2^2 - \Omega_1^2)(\Omega_2^2 - \Omega_3^2) = 0 \quad . \tag{295}$$

We will examine this equation in the context of three special cases, namely, the symmetric jet ($\lambda_1 = \lambda_2 = 0$), the Kelvin-Helmholtz vortex sheet ($\lambda_1 = 0$, $\lambda_2 = 1$), and the odd shear layer ($\lambda_1 = 0$, $\lambda_2 = 2$).

The eigenvalues associated with the homentropic symmetric jet can be obtained from equations (244) and (245) by setting $R = 0$, so that one pair of eigenvalues is given by

$$\nu = -\frac{k}{2}\left(1 + e^{-k}\right) \pm \frac{k}{2}\left\{\left(e^{-k} + 1\right)\left(e^{-k} - 1\right)\right\}^{1/2} \quad , \tag{296}$$

while the other pair is given by

$$\nu = -\frac{k}{2}\left(1 - e^{-k}\right) \pm \frac{k}{2}\left\{\left(e^{-k} + 1\right)\left(e^{-k} - 1\right)\right\}^{1/2} \quad . \tag{297}$$

We may conclude from these equations that the eigenvalues are complex for all values of k in the domain $0 < k \leqq \infty$ because $e^{-k} - 1 < 0$. Thus, the symmetric jet is unstable to all disturbances with wave numbers in the domain $0 < k \leqq \infty$. This means the stability boundary is given by $k^* = 0$.

As k approaches zero, the eigenvalues (296) asymptotically behave like

$$\nu \sim -k \pm i \frac{k^{3/2}}{2^{1/2}} \qquad (k \to 0) \tag{298}$$

and the asymptotic behavior of equation (297) is given by

$$\nu \sim -\frac{k^2}{2} \pm i \frac{k^{3/2}}{2^{1/2}} \qquad (k \to 0) \quad . \tag{299}$$

Lord Rayleigh, cf. Drazin and Howard [52], has termed the modes of disturbance associated with equations (298) and (299) as varicosities and sinuousities, respectively. The varicosities are traveling wave disturbances that propagate with a velocity equal to that in the jet core. The phase velocity of the sinuousities tends to zero as k approaches zero, so that these instabilities to within first-order in k are temporally nonoscillatory amplifying waves.

The characteristic equation (295) for the Kelvin-Helmholtz vortex sheet is given by

$$(\nu + k)^2 \left[(\nu + k)^2 + \nu^2 \right] = 0 \quad . \tag{300}$$

In this case, the broken-line flow is characterized by one interfacial surface, so that the eigenvalue equation should be a quadratic equation in ν. It can be shown that $(\nu + k)^2$ is a superfluous multiplicative factor in equation (300); thus, the eigenvalues are given by

$$\nu = -\frac{k}{2} \pm i \frac{k}{2} \quad . \tag{301}$$

It may be concluded from this equation that we have instability for all wave numbers in the domain $0 < k \leqq \infty$ as is true for the symmetric jet, and the stability boundary is given by $k^* = 0$. These disturbances propagate downstream with the average velocity in the shear layer.

The eigenvalues for the odd shear layer can be obtained from equation (261) by setting $R = 0$ in equations (259) and (260), so that

$$\nu = -k \pm i\frac{k}{2}\left\{\left[e^{-2k} - \left(1 - e^{-2k}\right)^{1/2}\right]^{1/2} \pm \left[e^{-2k} + \left(1 - e^{-2k}\right)^{1/2}\right]^{1/2}\right\} \quad . \tag{302}$$

The quantity under the braces is real for sufficiently small k, while the first term under the braces will be pure imaginary and the second real for sufficiently large k, so that it may be concluded that the homentropic odd shear layer is unstable to all disturbances with wave numbers in the interval $0 < k \leqq \infty$ and the stability boundary is given by $k^* = 0$. The asymptotic behavior of the four eigenvalues implied by equation (302) is given by

$$\nu \sim -k \pm ik \qquad (k \to 0) \tag{303}$$

and

$$\nu \sim -k \pm i\frac{k^{3/2}}{2^{1/2}} \qquad (k \to 0) \quad . \tag{304}$$

The modes of disturbance associated with equation (303) "feel" the shear layer as a Kelvin-Helmholtz vortex sheet [see equation (301)]. The phase velocity of these disturbances is equal to the basic state velocity in the middle layer and the disturbances propagate downstream. The disturbances associated with equation (304) are identical to Rayleigh's varicosities in the symmetric jet [see equation (298)].

The shear layer flows are more unstable than the symmetric jet with respect to small wave number disturbances. This fact can be verified by noting that the Kelvin-Helmholtz vortex sheet and the odd shear layer have modes of disturbance with growth rates proportional to k for small values of k, while the growth rates associated with the symmetric jet are proportional to $k^{3/2}$. The odd shear layer also has one mode of disturbance that possesses a growth rate proportional to $k^{3/2}$. As k approaches infinity, the growth

rates in all three cases asymptotically approach $-k/2$, so that the stability properties of these flows are asymptotically equivalent as k approaches infinity.

In view of the above results, it would appear that homentropic jet and shear layer flows are unstable to all disturbances with wave numbers in the interval $0 < k \leqq \infty$. Drazin and Howard [52] have analyzed the stability properties of continuous jet and shear layer flows with regard to small wave number perturbations. They obtained eigenvalue equations in terms of integrals in which the integrands were functions of the basic state velocity and density distributions and the characteristic value ν. In their analysis, they considered homentropic flows, and the results presented in this section are consistent with their results. Accordingly, it would appear that, in the context of long wave disturbances, the broken-line profiles are behaving like continuous ones.

Finally, the asymptotic behaviors of the eigenvalues given by equations (276) and (279) do not agree with the results in this section for the case $R_1 = R_2 = 0$. This means that equations (276) and (279) are not uniformly valid as R_1 and R_2 approach zero. However, equations (276) and (279) and the results in this section show that the introduction of static stability into the system tends to promote stability in the low wave number Fourier components of the perturbations. In the section that follows it will be shown that the static stability must be introduced into the system at both interfaces to promote dynamic stability at low wave numbers.

b. Statically Stable Flows. In this section, we will analyze statically stable jet and shear layer flows. The analysis will be in the form of a parametric analysis of the eigenvalue equation (222). It will be shown that, for certain values of λ_1, λ_2, R_1, and R_2, the absolute stability boundaries behave like those of the Kelvin-Helmholtz two-layer model. However, it will also be shown that a large class of basic state flows exist which do not exhibit stability properties like those of a Kelvin-Helmholtz vortex sheet.

The critical wave number is a function of λ_1, λ_2, R_1, and R_2. To depict this function, we must construct a series of graphs. In each of these graphs, k^* is plotted against a selected basic state parameter, while the other parameters are held fixed. To perform this task we could use one or all of four possible types of plots, viz., k^* versus λ_2 for fixed values of λ_1, R_1, and R_2, k^* versus R_2 for fixed values of λ_1, λ_2, and R_1, etc. However, the fact that the eigenvalue equation (222) possesses certain symmetry properties permits us to reduce the required number of figures

by one-half. This equation is invariant to an interchange of the parameters λ_1, λ_2, and R_1, R_2. The reason for this result can be traced to the symmetric way the basic state parameters occur in equation (211) with respect to Ω_2^2 if we use the approximation in which we set β_1 and β_2 equal to unity in all terms that do not contain g. For example, a plot of k^* versus λ_2 for fixed values of λ_1, R_1, and R_2 can also be used as a plot of k^* versus λ_1 for fixed values of λ_2, R_1, and R_2 if we interchange λ_1 and λ_2, and R_1 and R_2; similarly, a plot of k^* versus R_1 can be used as a plot of k^* versus R_2. In this section, we will consider two types of plots of the critical conditions, namely, k^* versus λ_2 and k^* versus R_2 for the appropriate fixed basic state variables.

Figures 9 through 12 are plots of k^* versus λ_2 for $\lambda_2 \geqq 0$, and Figures 13 through 16 are the corresponding plots of k^* versus $-\lambda_2$ for $\lambda_2 < 0$, respectively. In these figures, $\lambda_2 < 1$ and $\lambda_2 \geqq 1$ correspond to jet and shear layer flows, respectively. The regions associated with the unstable and neutral solutions are labelled in the figures. The boundaries (the curves) that separate these regions represent neutral mode configurations. Thus, for example, in Figure 9, $\lambda_2 = 0.2$ implies that all perturbations with $k \leqq 0.4$ are neutral oscillations, while those perturbations that have $k > 0.4$ are unstable.

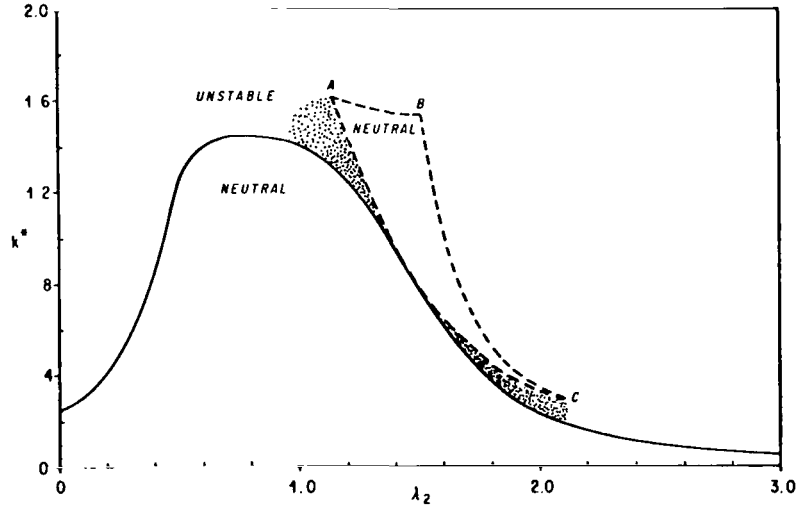

Note: The regions associated with the unstable and neutral solutions are indicated in the figure. The upper dashed curve ABC is predicted by the two-layer Kelvin-Helmholtz theory, while the shaded region of unstable solutions is unique to the three-layer model.

Figure 9. k^* versus λ_2 for $\lambda_1 = 0.5$, $R_1 = 0.2$, and $R_2 = 0.2$.

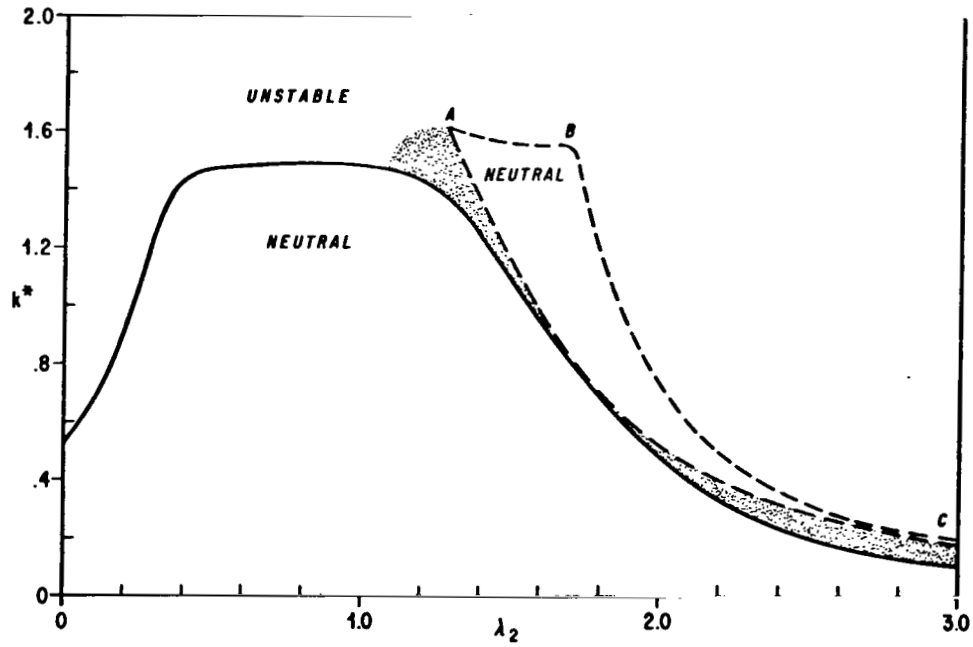

Figure 10. k^* versus λ_1 for $\lambda_2 = 0.5$, $R_1 = 0.2$, and $R_2 = 0.4$. (See Fig. 9 for an explanation of the curves.)

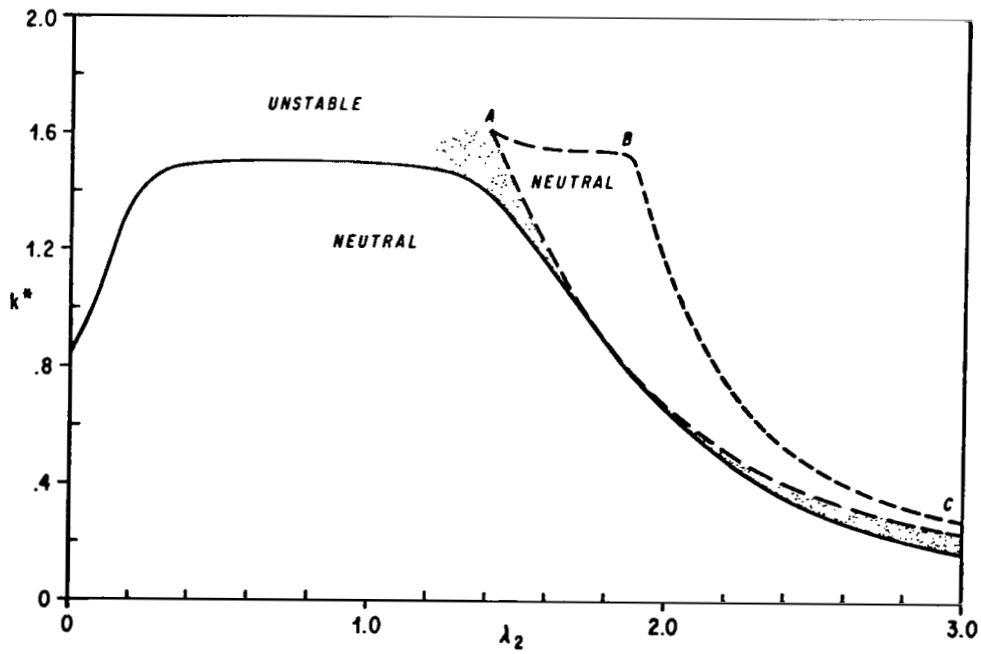

Figure 11. k^* versus λ_2 for $\lambda_1 = 0.5$, $R_1 = 0.2$, and $R_2 = 0.6$. (See Fig. 9 for an explanation of the curves.)

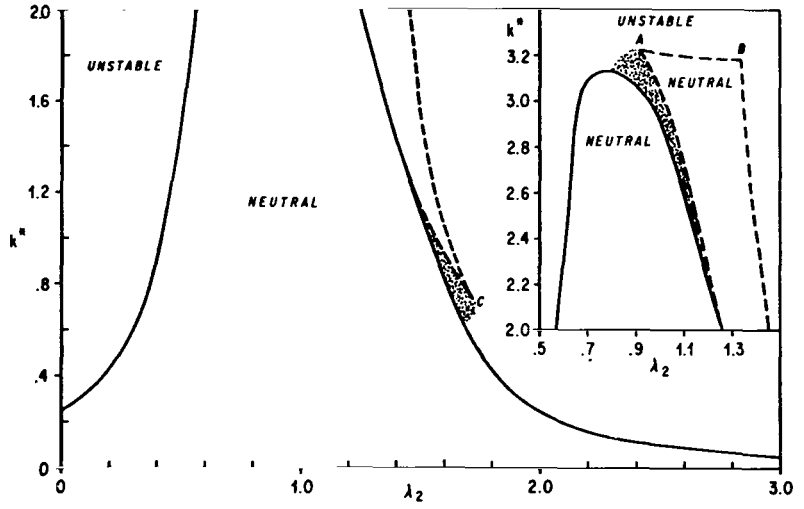

Figure 12. k^* versus λ_2 for $\lambda_1 = 0.5$, $R_1 = 0.4$, and $R_2 = 0.2$. (See Fig. 9 for an explanation of the curves.)

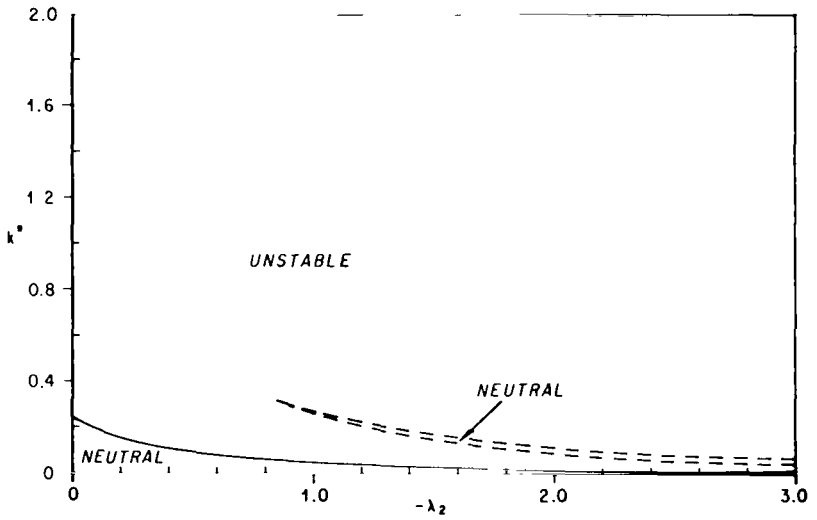

Note: The regions associated with the unstable and neutral solutions are indicated in the figure. The solid stability boundary falls below the Kelvin-Helmholtz estimate of the stability curve (Fig. 18). The region of neutral solutions contained within the dashed curves lies above the Kelvin-Helmholtz critical curve.

Figure 13. k^* versus $-\lambda_2$ for $\lambda_1 = 0.5$, $R_1 = 0.2$, and $R_2 = 0.2$.

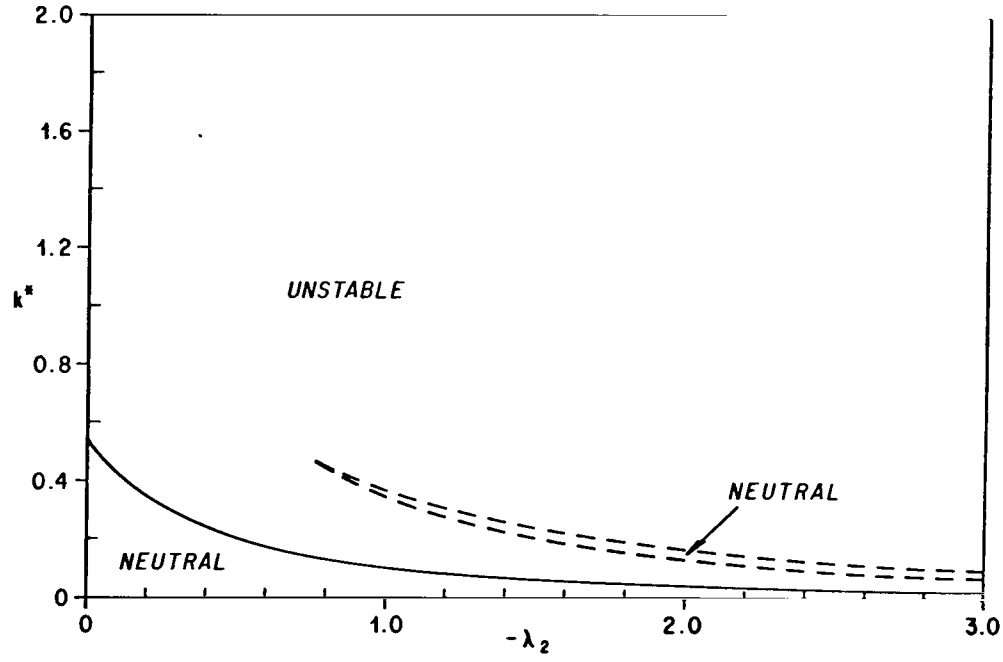

Figure 14. k^* versus $-\lambda_2$ for $\lambda_1 = 0.5$, $R_1 = 0.2$, and $R_2 = 0.4$. (See Fig. 13 for an explanation of the curves.)

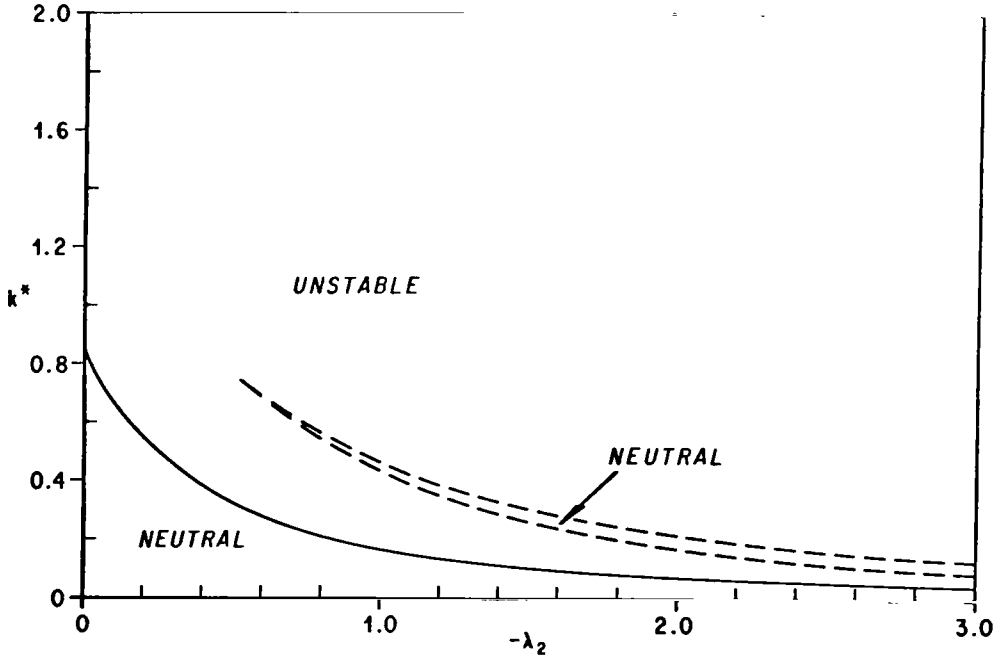

Figure 15. k^* versus $-\lambda_2$ for $\lambda_1 = 0.5$, $R_1 = 0.2$, and $R_2 = 0.6$. (See Fig. 13 for an explanation of the curves.)

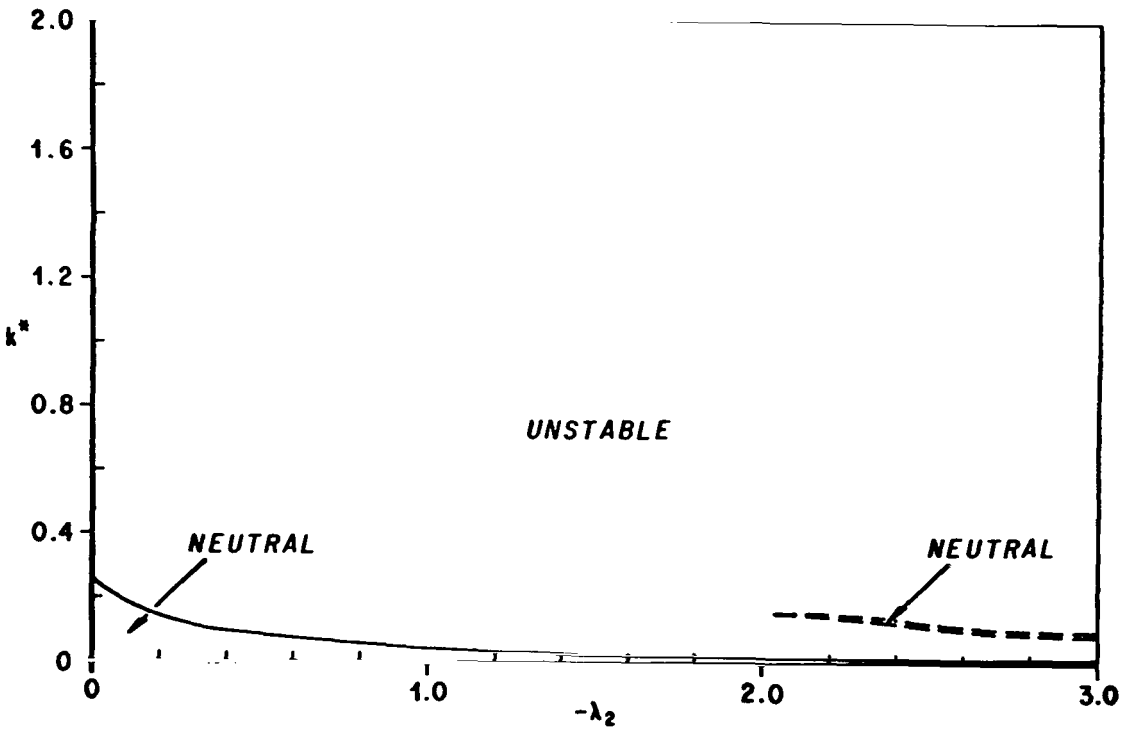

Figure 16. k^* versus $-\lambda_2$ for $\lambda_1 = 0.5$, $R_1 = 0.4$, and $R_2 = 0.2$. (See Fig. 13 for an explanation of the curves.)

In each figure, a region of neutral solutions, bounded by the dashed curve, exists within the unstable region above the solid stability curves. Thus, for example, in Figure 9, $\lambda_2 = 1.2$ implies that the solutions with wave numbers in the intervals $0 \leqq k \leqq 1.25$ and $1.45 \leqq k \leqq 1.58$ are neutral oscillations; otherwise, the solutions are unstable. This extra neutral region is associated with flows that have eigenvalue diagrams like that of flow 6 in the preceding section (Fig. 8).

Approximate stability boundaries for the three-layer model can be constructed from the two-layer Kelvin-Helmholtz theory. The two-layer estimates of the critical wave numbers associated with the lower interface are given by

$$k_1^* = \frac{2R_1}{(1 - \lambda_1)^2} \quad , \tag{305}$$

while the two-layer critical wave numbers associated with conditions at the upper interface are given by

$$k_2^* = \frac{2R_2}{(1 - \lambda_2)^2} \quad , \tag{306}$$

[see equations (239) and (240)]. The two-layer solutions that have $k > k_1^*$ at the lower interface and $k > k_2^*$ at the upper interface are unstable. Earlier, we found that certain types of three-layer flows have perturbations characterized by two branch points (Figs. 3 through 7), while certain other types of flows have perturbations characterized by four-branch points (Fig. 8). The two-branch point flows have one absolute stability boundary, and the four-branch point flows have three absolute stability boundaries. The remaining branch point in each case does not correspond to an absolute stability boundary because it exists within a band of wave numbers associated with an unstable mode of disturbance, and for purposes of discussion, we will term these points the unstable branch points. However, it is possible to have flows that do not possess unstable branch points. The odd shear layer is an example of this type of flow. The critical wave numbers associated with the absolute stability boundaries of the three-layer flows can be estimated by selecting the least of the two Kelvin-Helmholtz estimates given by equations (305) and (306). We select the smaller of the two values because the other wave number exists within a band of unstable solutions and thus corresponds to an estimate of the critical wave number associated with a three-layer unstable branch point. Thus, if $k_1^* > k_2^*$, then k_2^* is the two-layer estimate of the critical wave number associated with the three-layer counterpart, while k_1^* is an estimate of the associated unstable branch point and vice versa.

Two-layer estimates of the three-layer stability boundaries in Figures 9 through 11 and 13 through 15 are given in Figures 17 and 18, respectively. Except for a very small portion of the stability boundary in the vicinity of the point A, the three-layer stability boundaries in Figures 9 through 11 fall below the two-layer estimates in Figure 17. However, only the solid stability boundaries in Figures 13 through 15 fall below the two-layer estimates in Figure 18. From the point of view of the solid-three-layer stability curves, it might be concluded that the three-layer flows are more unstable than the Kelvin-Helmholtz flows with respect to the long wave modes of disturbance. The two-layer estimates depart from the upper dashed curves, labelled ABC, in Figures 9 through 11 by no more than 7 percent. However, the two-layer estimates are greater than the three-layer values by approximately 15 percent

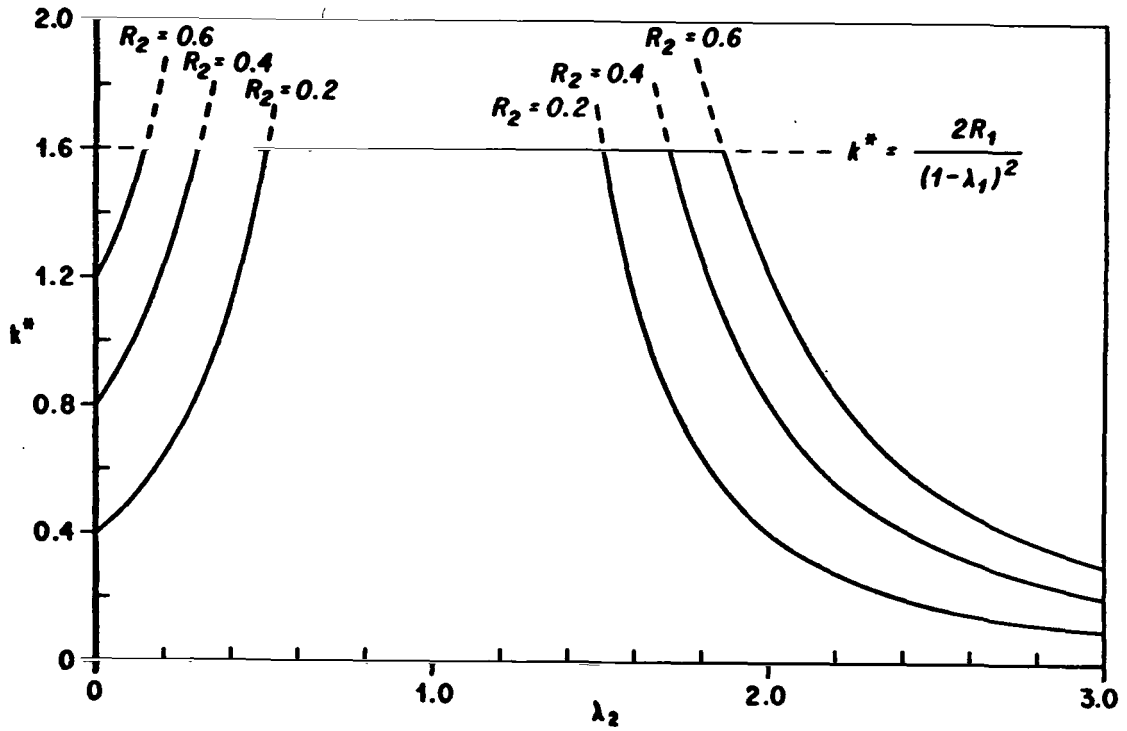

Note: The curves denoted by the various values of R_2 were calculated with the Kelvin-Helmholtz critical wave number equation $k^* = 2R_2/(1 - \lambda_2)^2$, while the straight line was calculated with the equation $k^* = 2R_1/(1 - \lambda_1)^2$. The solid portions of these curves represent the two-layer model estimates of the stability boundaries associated with the three-layer model.

Figure 17. k^* versus λ_2 estimated from the two-layer theory for $\lambda_1 = 0.5$, $R_1 = 0.2$, and $R_2 = 0.2, 0.4, 0.6$.

at the peak of the solid k^* curve, 40 percent at $\lambda_2 = 0$, and 50 percent at $\lambda_2 = 3.0$ in Figures 9 through 11. In Figures 13 through 15, the two-layer estimates are greater than the three-layer values of the solid stability boundary by approximately 50 percent at $\lambda_2 = -1.0$ and 30 percent at $\lambda_2 = -3.0$. Thus, the three-layer stability criterion differs significantly from the Kelvin-Helmholtz criterion. However, the most significant difference between the two theories is the number of branch points associated with the absolute stability boundaries in each case. In the case of the Kelvin-Helmholtz

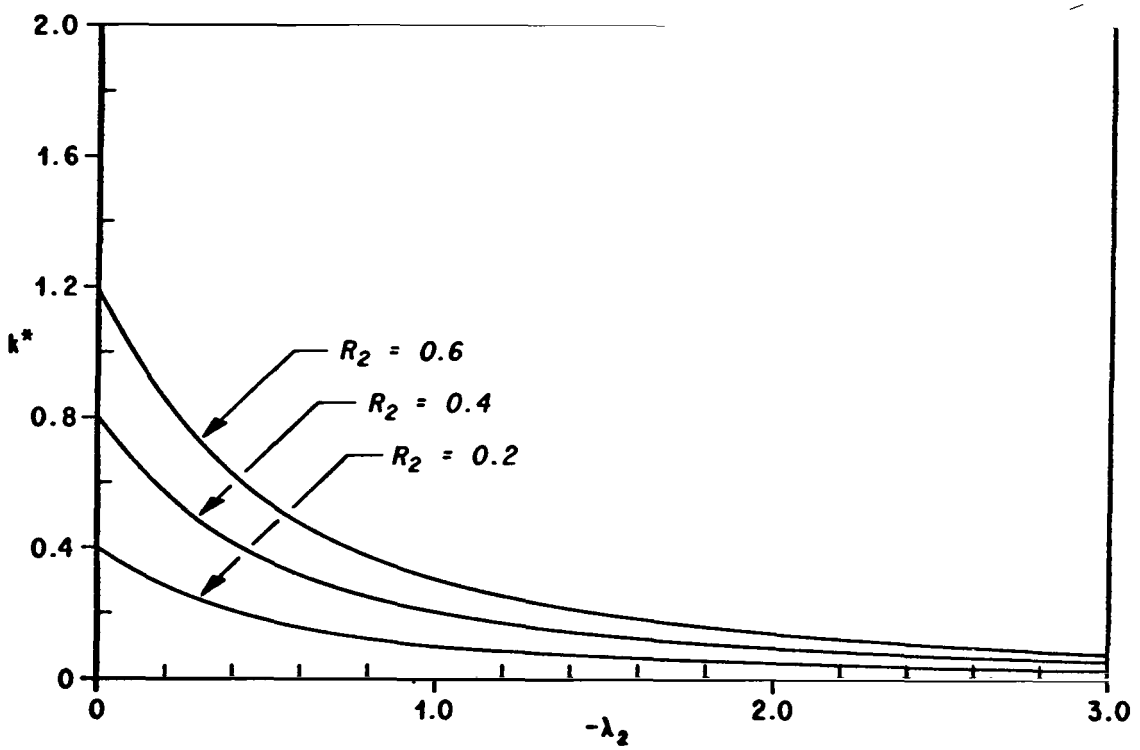

Note: The curves denoted by the various values of R_2 were calculated with the Kelvin-Helmholtz critical wave number equation $k^* = 2R_2/(1 - \lambda_2)^2$.

Figure 18. k^* versus $-\lambda_2$ estimated from the two-layer theory for $\lambda_1 = 0.5$, $R_1 = 0.2$, and $R_2 = 0.2$, 0.4., 0.6.

theory, all perturbations with wave numbers greater than some critical value are unstable, so that the unstable solutions occur in a semi-infinite band of wave numbers. The three-layer theory predicts that certain types of basic state flows have unstable perturbations that occur in semi-infinite bands of wave numbers as in the Kelvin-Helmholtz flows, while certain other flows possess unstable solutions in both semi-infinite and finite bands of wave numbers.

The introduction of a second interface into a broken-line shear layer produces a band of unstable solutions within the two-layer neutral region for certain values of λ_1, λ_2, R_1, and R_2. These bands of unstable solutions, located in the shaded regions in Figures 9 through 11, appear to be associated

primarily with shear flows. On the other hand, certain three-layer jets possess neutral solutions within the unstable regions above the solid stability curves in Figures 13 through 15, and these neutral regions also lie above the two-layer estimates of the solid stability curves.

It is noteworthy that the solid stability boundaries in Figures 9 through 11 fall below the Kelvin-Helmholtz estimate at $\lambda_2 = 1.0$. The basic state flow associated with this point has no velocity differential across the upper interface, and thus, the velocity field is identical to that of the Kelvin-Helmholtz shear layer. However, the three-layer flow possesses a positive static stability at both the upper and lower interfaces. The results in Figures 9 through 11 and Figure 17 imply that the introduction of static stability above or below the Kelvin-Helmholtz vortex sheet leads to a broadening of the spectrum of unstable perturbations and thus promotes instability in the long wave Fourier components. This destabilization is generated by a sort of resonance phenomenon. Perturbations are generated by the basic state vorticity at the shearing interface. Because of the inherent coupling between the two interfaces, a gravity wave motion is induced at the shear free interface, and these waves tend to enhance the perturbations at the shearing interface. V. Bjerknes and Höiland [13, 14] have examined a similar phenomenon in a two-layer system bounded by lower and upper rigid surfaces. Their system consisted of two isothermal layers of fluid in which the basic state velocities took on constant but different values in each layer. Each layer was characterized by a positive static stability because of the isothermal condition in each layer. The "jumps" in potential temperature across the lower and upper interfaces in the three-layer model are analogous to the static stabilities in the model of Bjerknes and Höiland; however, the velocity distributions are somewhat different. Nevertheless, some comparisons can be made between the two models. These investigators found that the existence of an internal static stability has a destabilizing effect insofar as it promotes instability in some of the long wave Fourier components. However, Bjerknes also found that dynamic stabilization occurs in the perturbations that have wave numbers near the critical wave number predicted by the two-layer Kelvin-Helmholtz theory (two layers with constant but different values of density and velocity in each layer). This type of stabilization is also predicted by the three-layer model. Earlier in this section, we found that the upper dashed curves, labelled ABC in Figures 9 through 11, were within a few percent of the stability boundaries predicted by the two-layer theory. Thus, the neutral solutions in the region bounded by the dashed curves in Figures 9 through 11 are analogous to the stabilized waves of Bjerknes.

At this point, it is worthwhile to mention the work of Goldstein [16] and Taylor [15]. Goldstein and Taylor analyzed the dynamic stability properties of a finite layer of fluid in which the density was constant and the velocity distribution was linear in z. This layer of fluid was sandwiched between two semi-infinite layers of fluid in which the basic state density and velocity had constant but different values in each layer. The resulting velocity distribution was a piecewise continuous odd distribution, and the associated density profile was an odd discontinuous function. These distributions are given by equations (291) and (292). Taylor examined a similar case; however, in his model he permitted the distribution of density to be other than odd. Goldstein's shear layer is a special case of Taylor's model. Goldstein and Taylor found that their odd shear layer is characterized by two absolute stability boundaries and the unstable perturbations satisfy the condition

$$\frac{k}{1+e^{-k}} < J + 1 < \frac{k}{1-e^{-k}} \quad , \tag{307}$$

where

$$J = \frac{g}{\rho_o} \frac{\sigma h}{\bar{u}(h)^2} \quad . \tag{308}$$

σ is the density differential across the lower and upper interfaces, $\bar{u}(h)$ is the basic state velocity at the upper interface and $-\bar{u}(-h) = \bar{u}(h)$, and ρ_o is the density in the middle layer.

If we replace the layers of constant density in the Goldstein-Taylor model with layers of constant potential temperature, then a calculation would show that the instability criterion is also given by equation (307); however, in this case, J is given by

$$J = \frac{g}{\bar{\theta}_2} \frac{(\bar{\theta}_3 - \bar{\theta}_1)\,2h}{[2\bar{u}(h)]^2} \quad . \tag{309}$$

To obtain this criterion, one must assume that β_1 and β_2 can be set equal to unity in all terms that do not contain g. This assumption is consistent with our analysis of the three-layer model.

Howard's odd shear layer should be the three-layer model analogue of the Goldstein-Taylor shear layer. However, it will be shown that this is not the case. In Figure 9, the point $\lambda_2 = 1.5$ corresponds to an odd shear layer flow. In the paragraph "Two Special Cases," we set $\lambda_1 = 0$ and $\lambda_2 = 2$ so that the velocity differential across each interface was equal to unity. In Figure 9, the corresponding parameters are $\lambda_1 = 0.5$ and $\lambda_2 = 1.5$, and the velocity differentials across the interfaces are equal to 0.5. The odd shear layer stability criterion, which was presented earlier, can be cast into a criterion for the odd shear layer in Figure 9 by multiplying both sides of equation (262) by 1/4, so that the condition for instability is given by

$$\frac{R}{4} = R_1 = R_2 > \frac{k}{4}\left[\frac{e^{-2k} + \left(1 - e^{-2k}\right)^{1/2}}{1 + \left(1 - e^{-2k}\right)^{1/2}}\right] \quad . \tag{310}$$

If this condition is satisfied, then the odd shear layer is characterized by two unstable modes of disturbance and both modes have the same critical wave number. In Figure 9, the solid stability boundary is tangent to the lower dashed stability curve at $\lambda_2 = 1.5$, and thus the stability boundaries for both modes of disturbance lie on the dashed curve AB and $k^* = 1.54$. This value of the critical wave number can be calculated with equation (310) by making this expression an equality and setting $R_1 = R_2 = 0.2$.

The parameters of the odd shear layer can be related to the modified Goldstein-Taylor parameter equation (309), if we assume the velocity differential between the center of the middle layer and the upper or lower interface of the Goldstein-Taylor model corresponds to the velocity differential across the upper and lower interfaces in the Howard model. Thus, Goldstein's parameter in terms of three-layer model parameters is given by

$$J = \frac{R_1 + \beta_1^{-1} R_2}{4(1 - \lambda_1)^2} = \frac{R_1 + \beta_2^{-1} R_2}{4(1 - \lambda_2)^2} \quad . \tag{311}$$

If in this expression, we set $\lambda_2 = 1.5$, $R_1 = R_2 = 0.2$, and $\lambda_1 = 0.5$, which is the configuration of Howard's flow in Figure 9, then $J = 0.4$, where we have set $\beta_2 = 1$. Equation (307) predicts that for $J = 0.4$, the unstable perturbations of the Goldstein-Taylor model occur in the interval of wave numbers $0.77 < k < 1.66$. This interval of wave numbers is almost identical to the interval of wave numbers associated with the region within the dashed

curves in Figure 9 at $\lambda_2 = 1.5$. In other words, the three-layer odd shear flow predicts that neutral modes occur in the region that is predicted to be unstable according to the Goldstein-Taylor model. Thus, it would appear that the two models are inconsistent. Actually, the models are not inconsistent, because these models are not analogues of the same continuous flow configuration.

Miles [32] has examined the dynamic stability properties of the basic state flow given by

$$\bar{u}(z) = u_\infty \tanh\left(\frac{z}{\delta}\right) \tag{312}$$

$$\ln \frac{\bar{\rho}(0)}{\bar{\rho}(z)} = \left[1 - r \operatorname{sech}^2\left(\frac{z}{\delta}\right)\right] \tanh\left(\frac{z}{\delta}\right) \quad , \tag{313}$$

where δ is a characteristic length scale of the basic state flow, $u_\infty = -\bar{u}(-\infty) = \bar{u}(\infty)$, and r is a fixed parameter for any particular flow. In the context of Miles' analysis, the local Richardson number is given by

$$J_m(z) = \frac{-\frac{g}{\bar{\rho}}\frac{d\bar{\rho}}{dz}}{\left(\frac{d\bar{u}}{dz}\right)^2} = J\left[(1 - r)\cosh^2\left(\frac{z}{\delta}\right) + 3r \sinh^2\left(\frac{z}{\delta}\right)\right] , \tag{314}$$

where

$$J = \frac{g\delta}{2u_\infty^2} \ln\left[\frac{\bar{\rho}(-\infty)}{\bar{\rho}(\infty)}\right] \quad . \tag{315}$$

By varying r, one can simulate many flows; however, the local Richardson number and the velocity profile are even and odd functions of z for all values of r. If $r = 1$, then

$$J_m(z) = 3J \sinh^2\left(\frac{z}{\delta}\right) \quad . \tag{316}$$

This flow corresponds to the case examined by Garcia (cf. Miles [32]). If $r > 1$, then $J_m(z) < 0$ in a layer of fluid symmetrically disposed about the point $z = 0$. If $r < -1/2$, then $J_m(z) < 0$ for $|z| > |z^*|$, where z^* satisfies the equation

$$(1 - r)\cosh^2\left(\frac{z^*}{\delta}\right) + 3r\sinh^2\left(\frac{z^*}{\delta}\right) = 0 \quad . \tag{317}$$

The profiles associated with the values of r in the interval $-1/2 < r < 1$ have positive definite values of $J_m(z)$ for all values of z. As r increases away from $r = -1/2$, $J_m(0)$ decreases from a value of $3J/2$ at $r = -1/2$ to $J/4$ at $r = 3/4$. Miles restricted his analysis to values of r in the interval $-1/2 \leqq r < 1$.

$J_m(z)$ and $\bar{u}(z)$ are even and odd functions of z and, in this light, Miles' flow configurations are similar to the Howard and Goldstein-Taylor configurations. However, in the Howard and Goldstein-Taylor flows, the density or potential temperature distributions are identical and the wind profiles are different. In Miles' flow configuration, the velocity profiles are identical for all values of r, while the density profiles are different.

Miles found that the solutions to his problem are the Heun polynomials, and for each polynomial solution of degree n, he found that the critical value of J is functionally given by

$$J = J(k, n, r), \qquad n = 0, 2, 4, \ldots \quad . \tag{318}$$

For first mode ($n = 0$) solutions, Miles found that $J(k, 0, r)$ is a single-valued function of k if $r \leqq 0.895$, while $J(k, 0, r)$ can be a double-valued function of k for certain values of k if $r > 0.895$. These single- and double-valued functions qualitatively correspond to the stability boundaries of the Howard and Goldstein-Taylor shear layer flows, respectively.

Based upon the small-k approximate theory of Drazin and Howard [52], Miles found that for $n = 0$, the approximate expression

$$J = \frac{k}{2} - \left(1 - 2r + \frac{2}{3} r^2\right) \left(\frac{k}{2}\right)^2 + 0\left[\left(\frac{k}{2}\right)^3\right] \tag{319}$$

adequately describes the behavior of the single-valued stability boundaries for small k. Upon expressing equation (262) as an equality and expanding the right side of this equation in a Taylor series about the point $k = 0$, we find

$$R = k - 4k^2 + 0(k^3) \quad . \tag{320}$$

This expression is valid for those flows characterized by $\lambda_1 = 0$ and $\lambda_2 = 2.0$. If we make the following correspondences between Howard's shear layer and Miles' flow,

$$\left.\begin{array}{ccc} \delta & \longleftrightarrow & h \\ u_\infty & \longleftrightarrow & \bar{u}_2 \\ \ln \dfrac{\bar{\rho}(-\infty)}{\bar{\rho}(0)} & \longleftrightarrow & \dfrac{\bar{\theta}_2 - \bar{\theta}_1}{\bar{\theta}_2} \\ \ln \dfrac{\bar{\rho}(0)}{\bar{\rho}(\infty)} & \longleftrightarrow & \dfrac{\bar{\theta}_3 - \bar{\theta}_2}{\bar{\theta}_3} \end{array}\right\} , \tag{321}$$

then R/2 is the analogue of Miles' J. The first term in equation (319) is in agreement with first term in equation (320); however, for the second terms to agree we require

$$r = \frac{3 \pm \sqrt{51}}{2} \quad . \tag{322}$$

Miles restricted his analysis to values of r in the interval $-1/2 \leqq r < 1$, and the values of r given by equation (322) fall outside this interval. Thus, the models agree only to within the first terms of the series equations (319) and

(320). The important point here is that the three-layer model and Miles' flow are in agreement for sufficiently small k, so that the stability boundaries of the three-layer model have continuous counterparts.

Miles' results for the double-valued stability boundaries are extremely involved and too lengthy to present in this report. Nevertheless, some of the important results can be stated here. Miles' results seem to show that for $r > 0.895$ that $J(k, 0, r)$ is a single-valued function of k if $k < 1$, while $J(k, 0, r)$ is a double-valued function of k if $k \geqq 1$. The Goldstein-Taylor stability boundary is single-valued for $k < 1.35$ and double-valued for $k \geqq 1.35$; see equation (307). The approximate expression equation (319) is valid for the single-valued portion of the stability boundary for $r > 0.895$. The single-valued portion of the Goldstein-Taylor stability boundary is given by

$$J = \frac{k}{1 - e^{-k}} - 1 \quad . \tag{323}$$

If we make the following correspondences between the Goldstein-Taylor shear flow and Miles' flow,

$$\left.\begin{array}{ccc} \delta & \longleftrightarrow & h \\ u_\infty & \longleftrightarrow & \bar{u}(h) = -\bar{u}(-h) \\ \frac{1}{2} \ln \frac{\rho(-\infty)}{\rho(\infty)} & \longleftrightarrow & \sigma \end{array}\right\} \quad , \tag{324}$$

then the Goldstein-Taylor J is an analogue of Miles' J. Upon expanding the right side of equation (323) into a Taylor series about the point $k = 0$, we find that

$$J = \frac{k}{2} - \frac{10}{6}\left(\frac{k}{2}\right)^2 + 0(k^3) \quad . \tag{325}$$

The first-order terms in equations (325) and (319) are in agreement, and the second-order terms will agree if $r = 0.303$. However, this value of r is outside the interval $0.895 < r < 1$. Thus, the Goldstein-Taylor model and Miles' model are consistent only for sufficiently small k.

Based upon the above comparisons, we may conclude that both the Howard model and the Goldstein-Taylor model yield results that are consistent with continuous flows for sufficiently small k. Since Howard's model is a special case of the three-layer model and yields results consistent with Miles' continuous model, we might also infer that the stability boundaries of three-layer flows other than the odd shear layer correspond to the stability boundaries of continuous flows.

In the vicinity of the point of tangency ($\lambda_2 = 1.5$) of the solid and dashed stability curves in Figure 9, the shear flow is characterized by anomalous instability regions (shaded areas). The shear flows associated with these anomalous regions have mixed velocity profiles; i.e., they are neither odd nor even. However, the static stability distribution is even. Figures 10 and 11 are also characterized by anomalous instability regions, but the point of tangency in each figure occurs to the right of the point $\lambda_2 = 1.5$. This shift in the point of tangency probably results from the asymmetry in the distribution of static stability. In Figure 10, $R_1 = 0.2$ and $R_2 = 0.4$, and in Figure 11, $R_1 = 0.2$ and $R_2 = 0.6$. The anomalous regions in Figures 9 through 11 appear to be somewhat similar to the band of unstable solutions in the Goldstein-Taylor model. However, the similarity is only apparent. In the Goldstein-Taylor model, the instability zone in configuration space is characterized by two unstable modes of disturbance. Taylor explained that the unstable range of relative velocity, $\bar{u}(h) - \bar{u}(-h)$, is very narrow near that for which a backward-moving wave on the upper interface moves with the same speed as a forward-moving wave on the lower interface. Taylor explains further that these waves interact to produce a sort of resonance phenomenon, with the net result being dynamic instability. This instability mechanism is qualitatively the same as that of the odd shear layer. This mechanism requires two modes of instability; i.e, the eigenvalue equation possesses four complex roots, two of which have negative real parts, so that two modes of instability exist. The unstable shaded regions in Figures 9 through 11 are characterized by only one unstable mode of disturbance; thus, the instability mechanism is not a resonance phenomenon. An example of the eigenvalues associated with these anomalous regions is given in Figure 8. The segment of the real eigenvalue curve denoted by $-\nu_{r1,2}$ corresponds to the real part of the anomalous eigenvalues for the basic state flow configuration

given in the caption of that figure. We have not indicated the associated imaginary parts because they are less than 0.01. The important point here is that modes 3 and 4 in the anomalous range of wave numbers have pure real eigenvalues, so that the anomalous region is indeed characterized by only one mode of instability. The instabilities in these anomalous regions are the result of a type of Kelvin-Helmholtz instability produced by a global interaction of the shear flow as opposed to a local interaction. To clarify this point, let us examine the mathematical properties of the solid stability boundaries of these regions.

The eigenvalue equation (274) can be expressed in the form

$$\Omega_1^2 + \Omega_2^2 + \Omega_3^2 - kR_1 - kR_2 + \left(\Omega_1^2 - kR_1\right)\left(\Omega_3^2 - kR_2\right)\Omega_2^{-2}$$

$$-e^{-2k}\left(\Omega_2^2 - \Omega_1^2 + kR_1\right)\left(\Omega_2^2 - \Omega_3^2 + kR_2\right)\Omega_2^{-2} = 0 \quad . \tag{326}$$

Let us provisionally neglect the second and third terms on the left side of this equation, so that

$$\Omega_1^2 + \Omega_2^2 + \Omega_3^2 - kR_1 - kR_2 \simeq 0 \quad . \tag{327}$$

Upon solving this equation for ν, we find that

$$\nu \simeq -\frac{1 + \lambda_2 + \lambda_3}{3} \pm \left\{\frac{k(R_1 + R_2)}{3} - \frac{2}{9}\left[(\lambda_1 - \lambda_2)^2 + (\lambda_1 - 1)(\lambda_2 - 1)\right]\right\}^{1/2}$$

and the condition for instability is thus given by

$$k > \frac{3}{2}\,\frac{R_1 + R_2}{(\lambda_2 - \lambda_1)^2 + (\lambda_2 - 1)(\lambda_1 - 1)} = k^* \quad . \tag{329}$$

The critical state eigenvalues are given by

$$\nu_c = -\frac{(\lambda_1 + \lambda_2 + 1)}{3} k^* \quad . \tag{330}$$

Upon substituting ν_c and k^* as defined by equations (329) and (330) into equation (326), it is easily verified by a manual calculation that the second and third terms in equation (326) are an order of magnitude smaller than the first term in the same equation; thus, our initial assumption is valid a posteriori.

The values of the critical wave numbers given by equation (329) are within a few percent of the exact critical wave numbers associated with the solid stability curves that bound the anomalous instability regions in Figures 9 through 11. In addition, the approximate critical eigenfrequency given by equation (330) yields the exact value associated with the branch point of modes 1 and 2 in Figure 8 to within 1/2 of 1 percent. Thus, we can interpret k^*, as given by equation (329), as being the approximate form of the solid stability boundaries associated with the anomalous regions in Figures 9 through 11. However, the eigenvalues given by equation (328) are valid only in the immediate vicinity of the solid stability boundaries.

The approximate analytical form of the dashed stability boundaries associated with the anomalous regions in Figures 9 through 11 are elusive. An analysis of the eigenvalue equation (274) appears to show that an approximate form of this stability boundary cannot be obtained without including fourth-order terms in ν. Unfortunately, the author was not able to extract from equation (274) an approximate analytical expression for these stability boundaries.

The quantity on the left side of the equality in equation (329) can be interpreted as a gross Richardson number of the shear flow. The quantity $\lambda_2 - \lambda_1$ is the velocity differential between layers 1 and 2 of the three-layer model, and the quantities $\lambda_1 - 1$ and $\lambda_2 - 1$ are the velocity differentials across the lower and upper interfaces, respectively. Thus, we might think of the instabilities near the solid stability boundaries as being the result of both the gross velocity differential $\lambda_2 - \lambda_1$ and the interaction between the local velocity differentials at the lower and upper interfaces.

Let us now consider the order of events as we increase the wave number away from the point $k = 0$ for values of R_1, R_2, λ_1, and λ_2

associated with the anomalous instability regions. As k increases from $k = 0$ the first instability will occur for that wave number which satisfies equation (329). This instability is produced by the total shear layer configuration. As k increases, the wavelength becomes shorter until a critical value associated with the upper bound of the anomalous region is attained and the waves become neutral. This critical wave number is associated with a perturbation that is too short to accomplish the energy conversion from the mean flow to the perturbation, so that the stability properties tend to be controlled by the local conditions within the shear layer. As k increases, the waves tend toward instability, and instability will set in for that Fourier component that satisfies one of the approximate equations (237) and (238). If $R_1(1 - \lambda_1)^{-2} < R_2(1 - \lambda_2)^{-2}$, then the instability will set in via the Kelvin-Helmholtz instability at the lower interface, while the converse will be true if $R_1(1 - \lambda_1)^{-2} > R_2(1 - \lambda_2)^{-2}$.

As λ_2 approaches infinity, k^* is a single-valued function of λ_2 and approaches zero (Figs. 9 through 12) for $\lambda_2 > 0$ and fixed values of λ_1. This means that the spectrum of unstable Fourier components broadens as the strength of the vortex sheet at the upper interface intensifies, a result we should expect. However, it is noteworthy that as λ_2 approaches infinity the three-layer k^* curve lies below the Kelvin-Helmholtz curve based upon the local conditions at the upper interface. Thus, we do not obtain the Kelvin-Helmholtz instability criterion in a local context as λ_2 approaches infinity, because as k^* approaches zero, the wavelength of the critical perturbation becomes large, so that the critical perturbation is affected by the gross features rather than the local features of the shear layer flow, and thus, the instability is not controlled locally as for the short wave instabilities.

The jet flows appear to have a similar behavior as $-\lambda_2$ approaches infinity. As $-\lambda_2$ approaches infinity, the extensions of the dashed curves for $\lambda_2 < -3.0$ in Figures 13 through 16 intersect at finite values of $-\lambda_2$, and for larger values of $-\lambda_2$ past these intersection points, k^* is a single-valued function of $-\lambda_2$. This single-valued portion of the jet flow stability boundary qualitatively behaves like the associated shear layer stability boundary for sufficiently large $|\lambda_2|$.

We can think of the anomalous regions in Figures 13 through 16 (regions contained within dashed stability curves) as also being the result of a global interaction of the basic state flow. However, in this case, the interaction promotes stability in the region that is predicted to be unstable according to the Kelvin-Helmholtz theory. This result might be explained by examining the distribution of the basic state vorticity. For the jet flows

($\lambda_1 < 1$), the basic state vorticity vectors above and below the jet core have opposite signs, while in the shear layer flows ($\lambda_1 \geqq 1$), the basic state vorticity vectors at the interfaces have the same signs. Thus, in the case of the shear flows, the vorticity vectors enhance each other, while in the jet case, the vorticity vectors act in opposite directions and each tends to oppose the instability the other tends to promote.

Figures 9 through 11 and 13 through 15 show that as R_2 increases, the solid stability boundaries move toward larger values of k^* and the anomalous unstable and neutral zones shift toward larger values of λ_2. The percentage shift of the solid stability boundaries toward larger values of k^* is small in the vicinity of $\lambda_1 = 1$ and extremely large for large values of $|\lambda_2|$. Thus, for example, upon increasing R_2 from 0.2 to 0.4 for $R_1 = 0.2$ (Figs. 9, 10, 13, and 14), the values of k^* associated with the solid stability boundaries increase by a few percent near $\lambda_1 = 1$ and by approximately 100 percent at $|\lambda_2| = 3.0$. Figures 9, 12, 13, and 16 show that an increase in R_1 also tends to shift the solid stability boundaries toward larger values of k^*. However, the percentage shift is extremely large in the vicinity of $\lambda_1 = 1$ (on the order of 100 percent) and relatively small for $|\lambda_1| >> 1$ (a few percent near $|\lambda_1| = 3.0$). This means a local increase in the static stability in a shear layer or jet flow at the interface with the largest velocity differential promotes stability. However, an increase in the static stability at the interface with the smallest basic state velocity differential also has a stabilizing effect, but the magnitude of the effect is small compared to the former; this is a reasonable result.

Figures 9 through 11 and 13 through 15 show that for a given set of values R_1, R_2, $|1 - \lambda_1|$, and $|1 - \lambda_2|$, the shear layer flow configuration will have the smallest value of k^* associated with the solid stability boundaries. This means that the shear layer flows are more unstable to long-wave perturbations. The shear layer flows are more unstable because the basic state vorticity vectors have the same sign, and thus, the velocity differential at one interface reinforces the instability at the other interface and <u>vice versa</u>. For the jet flows, the velocity differential at one interface tends to cancel the instability at the other interface and <u>vice versa</u>.

Figures 19 through 22 are stability diagrams that depict the critical wave number as a function of R_2 for fixed values of R_1, λ_1, and λ_2. The three-layer stability boundaries are indicated by the solid curves. In Figures 19 through 21, the unstable region for a given value of R_1 is the entire region above the appropriate curve exclusive of the stability boundary; e.g., in Figure 19 at $R_1 = 0.2$ and $R_2 = 1.0$, all perturbations characterized by $k > 0.25$ are unstable and all perturbations characterized by $k \leqq 0.25$ are neutral. Figure 22 indicates the neutral and unstable regions.

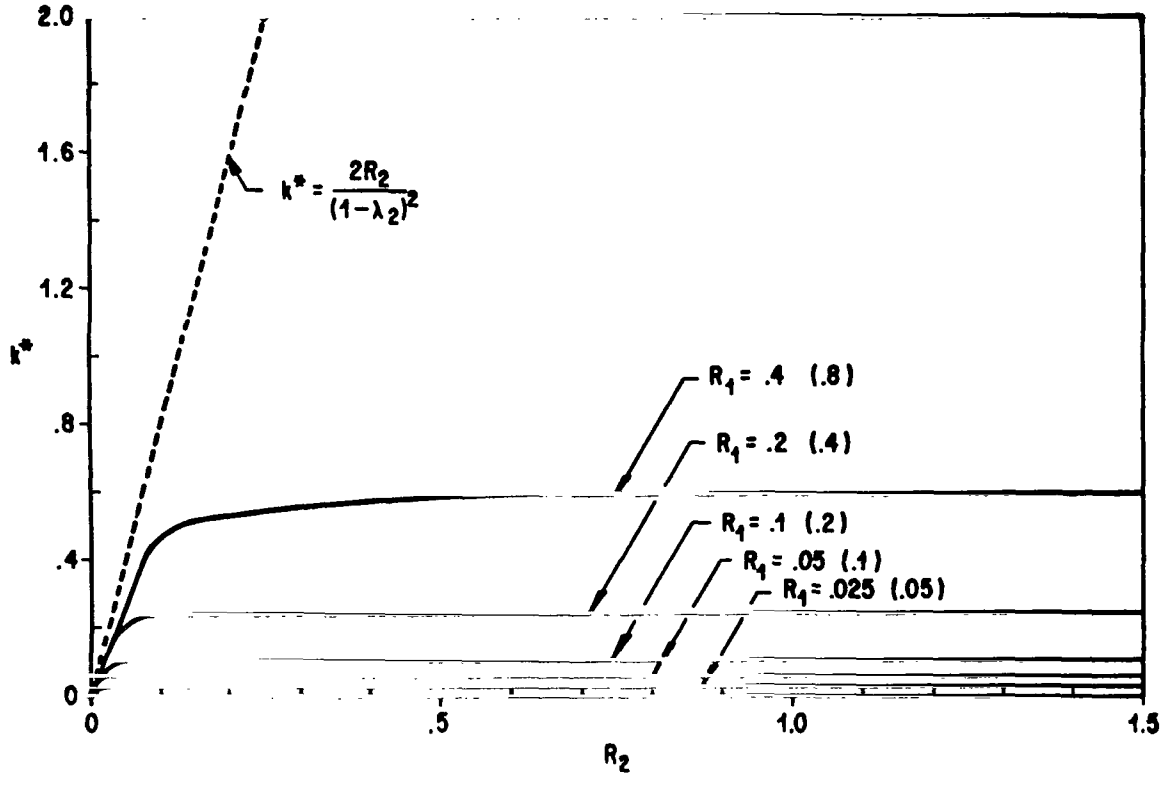

Note: The neutral solutions have wave numbers in the interval $0 \leqq k \leqq k^*$; otherwise, the solutions are unstable; e.g., at $R_2 = 1.0$ and $R_1 = 0.4$ the neutral solutions have wave numbers in the interval $0 \leqq k \leqq 0.6$. The critical wave numbers associated with a two-layer Kelvin-Helmholtz vortex sheet for conditions at the upper interface are indicated by the dashed line. The two-layer estimates of the critical wave numbers associated with conditions at the lower interface are given by the values within parentheses.

Figure 19. k^* versus R_2 for various values of R_1 and $\lambda_1 = 0$ and $\lambda_2 = 0.5$.

Figures 19 and 21 correspond to asymmetric velocity distributions characterized by the maximum shear being at the lower and upper interfaces, respectively, while Figure 20 corresponds to a symmetric velocity distribution. The diagrams show that for sufficiently small values of R_2, for fixed values of R_1, λ_1 and λ_2, k^* varies almost linearly with R_2. However, for

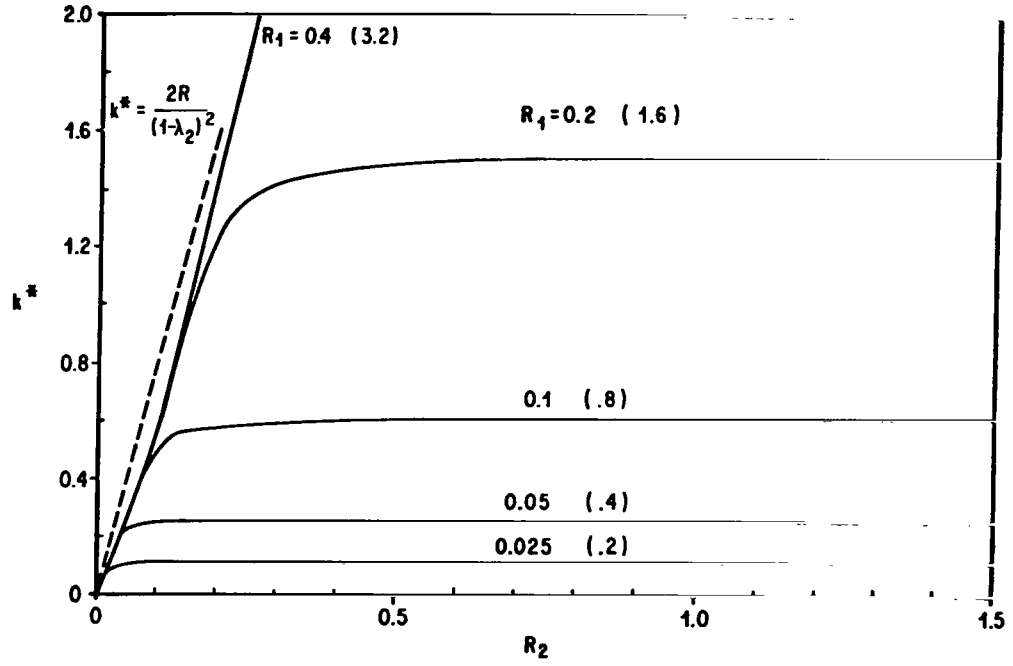

Figure 20. k^* versus R_2 for various values of R_1 and $\lambda_1 = 0.5$ and $\lambda_2 = 0.5$. (See Fig. 19 for an explanation of the curves.)

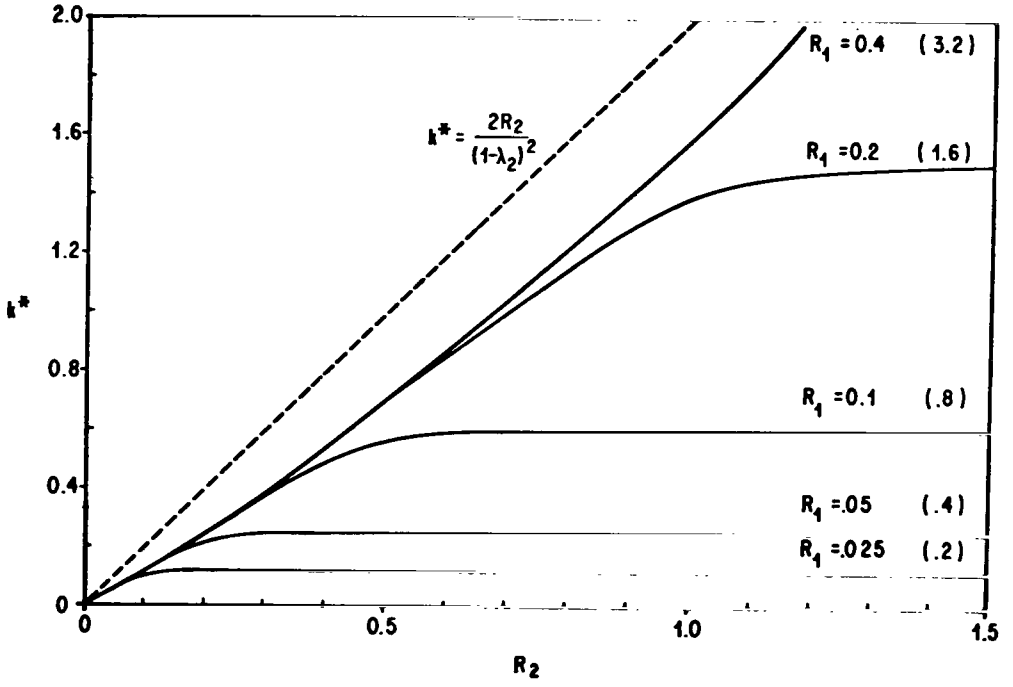

Figure 21. k^* versus R_2 for various values of R_1 and $\lambda_1 = 0.5$ and $\lambda_2 = 0$. (See Fig. 19 for an explanation of the curves.)

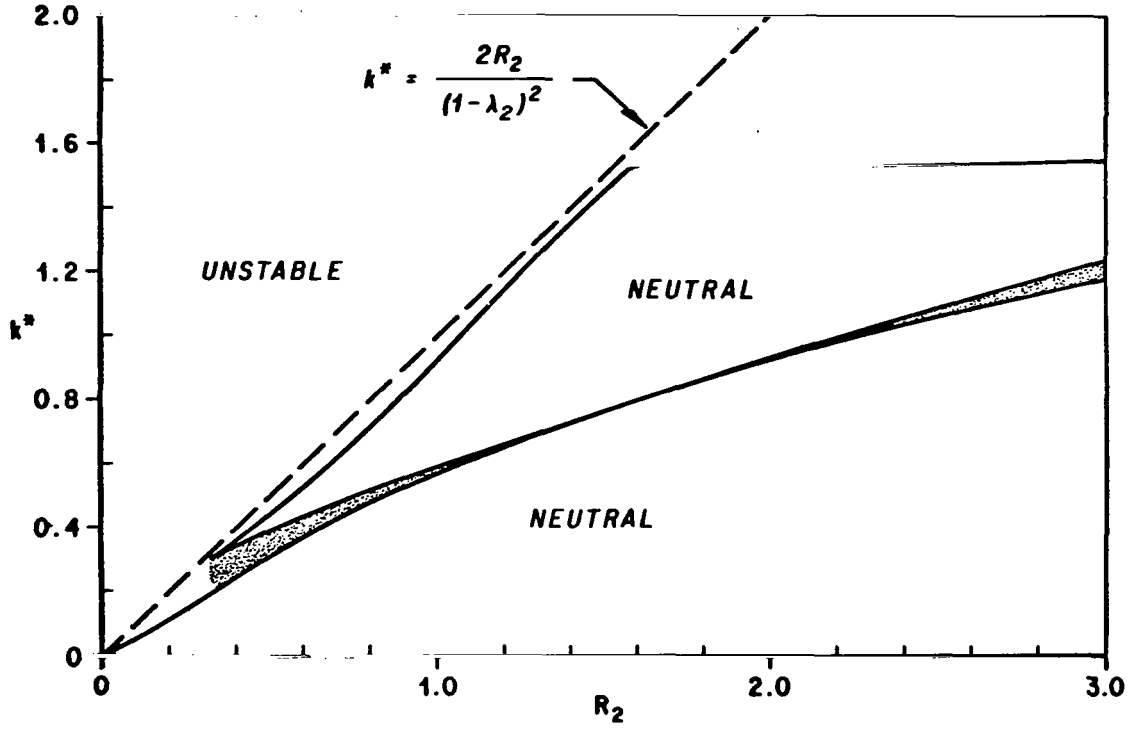

Note: The regions associated with unstable and neutral solutions are indicated in the figure. The critical wave numbers associated with the two-layer Kelvin-Helmholtz theory for conditions in the upper interface are indicated by the dashed line. The two-layer estimate of the critical wave number for conditions at the lower interface is 1.6.

Figure 22. k^* versus R_2 for $R_1 = 0.2$, $\lambda_1 = 1.5$, $\lambda_2 = 0$.

sufficiently large values of R_2, k^* approaches a constant value. The approximate linear dependence of k^* upon R_2 for sufficiently small values of R_2 means that the instability of the system is primarily controlled by the upper interface. However, by stabilizing the fluid from above, the instability, and thus k^*, tends to be controlled by the lower interface which corresponds to k^* tending toward a constant as R_2 approaches infinity.

The k^* curves that correspond to the Kelvin-Helmholtz criteria for conditions at the upper interface are indicated by the dashed lines in Figures 19 through 22, while the Kelvin-Helmholtz critical wave numbers for conditions

at the lower interface are indicated within parentheses for each (k^*, R_2)-curve. The Kelvin-Helmholtz estimate of the critical wave number for conditions at the lower interface in Figure 22 is equal to 1.6. These two-layer values of k^* can be used to construct an estimate of the k^* configuration associated with the three-layer flows. The procedure is similar to the one used previously with regard to the (k^*, λ_2) diagrams.

It is clear from Figures 19 through 21 that, for prescribed values of λ_1, λ_2, and R_1, k^* does not approach the Kelvin-Helmholtz result in the limit as R_2 approaches infinity, but rather approaches a value of k^* that is less than the Kelvin-Helmholtz result. In fact, the critical wave number is less than the Kelvin-Helmholtz result for all nonzero values of R_1 and R_2. In the event R_1 and/or R_2 vanish, k^* will vanish, which is identical to the Kelvin-Helmholtz result. This result appears to verify our earlier findings that homentropic flows are unstable to all perturbations. In addition, this result also shows that the static stability must be introduced into the system at both interfaces to promote dynamic stability at low wave numbers.

In Figures 19 through 21, the largest departures of k^* from the Kelvin-Helmholtz criteria occur in the vicinity of the bend of the (k^*, R_2)-curves. The departures are on the order of 60 percent for $R_1 = 0.025$ and 25 percent for $R_1 = 0.1$.

Figure 22 is a stability diagram of a shear layer flow $(\lambda_1 = 1.5, \lambda_2 = 0)$. The shaded areas in this diagram correspond to the anomalous unstable regions that can be found in a (k^*, λ_2) diagram (Figs. 9 through 11). The anomalous neutral and unstable regions in (k^*, R_2) diagrams occur for the same reasons they occur in the (k^*, λ_2) diagrams and thus require no further discussion.

Previously, we found that in a (k^*, λ_2) diagram, the jet flows are characterized by anomalous regions in which the solutions are predicted to be neutral in a three-layer context within a domain in configuration space that is predicted to be unstable according to the two-layer theory (Figs. 13 through 15). Similar regions also occur in certain (k^*, R_2) diagrams. Although an example of this type of diagram has not been presented in this report, preliminary calculations appear to indicate that these anomalous regions are closed areas above the Kelvin-Helmholtz curve, as in the (k^*, λ_2) diagrams.

JET STREAM INSTABILITIES

In this discussion, we analyze the generation of instabilities in the vicinity of the synoptic scale jet streams. The analysis is based on the three-layer model and an empirical model of the jet stream derived by Endlich and McLean [53]. In this analysis, we calculate the horizontal profiles of λ_1, λ_2, R_1, and R_2 associated with the Endlich and McLean jet stream, and determine the nature of the eigenvalues of the three-layer instabilities as a function of latitude across the jet stream. Based on these distributions, the horizontal distributions of the eigenvalues and the associated critical wave numbers are calculated and compared with those obtained from the two-layer Kelvin-Helmholtz model.

Basic State Parameters (λ_1, λ_2, R_1, and R_2)

The Endlich and McLean jet stream model is based upon data collected in middle latitude and subtropical jet streams. The average core velocity in their model is 73 m sec^{-1}, and occurs at an altitude of 10.3 km. Vertical cross sections that show the distributions of velocity and potential temperature can be found in their paper [53]. Now it is clear that broken-line profiles of potential temperature and horizontal wind speed do not occur in nature. However, it was shown previously that broken-line profiles behave like continuous profiles for sufficiently small wave numbers. To apply the three-layer model to the Endlich and McLean model, we must establish a procedure whereby we can "layer" continous profiles and specify their broken-line counterparts and thus calculate λ_1, λ_2, R_1, and R_2. This procedure will be established in this section by analyzing special cases.

Layering Approximation for $\bar{\theta}$. In examining the nature of the $\bar{\theta}$ layering approximation, we consider a quiescent layer of fluid of depth H characterized by S being a constant and bounded by rigid horizontal surfaces above and below. The solution of the governing differential equation (66) that satisfies the rigid boundary conditions of equation (68) is given by

$$\psi = A \sin \frac{n\pi z}{H} \qquad n = 1, 2, \ldots \quad , \tag{331}$$

provided ω satisfies the characteristic equation

$$\omega^2 = \frac{\kappa^2 gS}{\kappa^2 + n^2\pi^2 H^{-2}} \quad , \tag{332}$$

where A is a constant of integration.

If we approximate the $\bar{\theta}$ distribution with a two-layer model characterized by the lower and upper layers having depths h and H - h, respectively, with mean potential temperatures $\bar{\theta}_1$ and $\bar{\theta}_2$, then the solution to equation (66) that satisfies the boundary and interfacial conditions of equations (68), (87), and (89) is given by

$$\psi = A \sinh \kappa z \qquad (0 < z < h) \quad , \tag{333}$$

$$\psi = A\beta \frac{\sinh \kappa h \sinh \kappa (H - h)}{\sinh \kappa (H - h)} \qquad (h < z < H) \quad , \tag{334}$$

provided

$$\omega^2 = \frac{g\kappa (1 - \beta)}{\coth \kappa h + \beta \coth \kappa (H - h)} \quad , \tag{335}$$

where

$$\beta = \frac{\bar{\theta}_1}{\bar{\theta}_2} \quad . \tag{336}$$

Denoting the ω's for the constant S model and the two-layer model by ω_1 and ω_2, we find for the first mode (n = 1)

$$\left(\frac{\omega_2}{\omega_1}\right)^2 = \frac{S'}{Sk} \frac{k^2 + \pi^2}{\coth k\epsilon + \beta \coth k(1 - \epsilon)} \tag{337}$$

where

$$S' = \frac{1 - \beta}{H} \quad , \tag{338}$$

$$\epsilon = \frac{h}{H} \quad , \tag{339}$$

and

$$k = \kappa H \quad . \tag{340}$$

In the limit, as k approaches zero, we find that

$$\lim_{k \to 0} \left(\frac{\omega_2}{\omega_1} \right)^2 = \frac{\pi^2 \epsilon (1 - \epsilon)}{1 + \epsilon (\beta - 1)} \frac{S'}{S} \quad , \tag{341}$$

while the asymptotic behavior as k approaches infinity is given by

$$\left(\frac{\omega_2}{\omega_1} \right)^2 \sim \frac{S'}{S} \frac{k}{1 + \beta} \qquad (k \to \infty) \quad . \tag{342}$$

Thus, for sufficiently small k, ω_1 will differ from ω_2 by a constant and ω_2/ω_1 increases without bound as k becomes large.

If we are interested in layering the medium so that ω_2/ω_1 is unity for a particular wave number, then equation (337) serves as a basis for obtaining an estimate of ϵ and thus the appropriate layering of the zero-order state. The basic state potential temperature is given by

$$\theta(z) = \bar{\theta}(0) \, e^{Sz} \quad . \tag{343}$$

If we choose to represent $\bar{\theta}_1$ and $\bar{\theta}_2$ by vertical spatial averages, then

$$\bar{\theta}_1 = \frac{\bar{\theta}(0)}{SH\epsilon}\left(e^{SH\epsilon} - 1\right) \quad , \tag{344}$$

$$\bar{\theta}_2 = \frac{\bar{\theta}(0)}{SH(1-\epsilon)}\left(e^{SH} - e^{SH\epsilon}\right) \quad , \tag{345}$$

and thus

$$S' = \frac{\epsilon x + 1 - \epsilon - x^{\epsilon}}{\epsilon H\left(x - x^{\epsilon}\right)} \quad , \tag{346}$$

where

$$x = e^{SH} \quad . \tag{347}$$

Upon substituting equations (346) into (337), setting ω_2/ω_1 equal to unity, and utilizing the approximation $\beta \simeq 1$ except in the definition of S', we find

$$\frac{k^2 + \pi^2}{\coth \epsilon k + \coth k(1-\epsilon)} \cdot \frac{\epsilon x + 1 - \epsilon - x^{\epsilon}}{\epsilon\left(x - x^{\epsilon}\right)} - k \ln x = 0 \quad . \tag{348}$$

Upon selecting typical atmospheric values of SH ($0.02 \leqq SH \leqq 0.07$) and k ($0.025 \leqq k \leqq 2.0$), a numerical analysis revealed that equation (348) has two roots in the interval $0 < \epsilon < 1$. One root, denoted by ϵ_1, is in the interval $0.225 < \epsilon_1 < 0.285$, while the other, denoted by ϵ_2, is in the interval $0.715 < \epsilon_2 < 0.775$. Thus, for fluids characterized by S = constant, a reasonable approximation to the eigenvalues can be obtained by partitioning the layer of fluid into two layers having depths on the order of 0.75H and 0.25H and the thickest layer can be either above or below. Based upon this analysis, we might conclude that for large scale atmospheric jets characterized by constant, but different values of S above and below the jet maximum, that an appropriate layering scheme could be as follows:

1. Layer 1: $-0.5H < z < -0.125H$

2. Layer 2: $-0.125H < z < 0.125H$

3. Layer 3: $0.125H < z < 0.5H$

This is the layering scheme that was used to model the $\bar{\theta}$-field of the Endlich and McLean jet model.

To analyze the Endlich and McLean jet stream model, we selected $H = 4$ km, which implies $h = 0.5$ km. This selection of H has the feature that the lower and upper interfaces of the three-layer model are located in the regions where the jet stream model of the Endlich and McLean [53], the analysis of Sasaki [54], and the work of Clodman, Morgan, and Ball [55] show the majority of incidences of clear air turbulence to occur. The selection of H was also based upon a survey of jet profiles measured at Cape Kennedy, Florida, during the years of 1964 through 1967. This survey showed that many jet profiles are characterized by the wind shear being a minimum at approximately 2 km above and below the jet maximum. In fact, many profiles appear to have a shallow layer located at approximately 2 km above and below the jet maximum in which the speed was approximately constant.

Layering Approximation for $\bar{u}$. An estimate of how one should layer the $\bar{u}$ profiles can be obtained by examining the perturbations associated with the zero-order state given by

$$\bar{u} = u_\infty \tanh \frac{z}{\delta} \qquad (-\infty < z < \infty) \tag{349}$$

$$S = 0 \qquad (-\infty < z < \infty) \quad , \tag{350}$$

where u_∞ and δ are constants. Drazin and Howard [52] have solved equation (66) for this zero-order state for the case of longitudinal perturbations ($\kappa_1 = \kappa$). Based upon an approximation procedure, these authors find that for small values of κ

$$\omega = \pm \frac{u_\infty}{\delta} \left[\kappa\delta - 1.785(\kappa\delta)^2 + 1.526(\kappa\delta)^3 + \ldots \right] i \quad . \tag{351}$$

Let us now layer the velocity profile equation (349), so that

$$\bar{u} = \frac{z}{|z|} u_o \qquad (-\infty < z < \infty) \quad , \tag{352}$$

where u_o is a constant to be determined. This velocity profile is a Kelvin-Helmholtz vortex sheet and the eigenvalues are given by

$$\omega = \pm \kappa u_o i \quad , \tag{353}$$

[see equation (217)].

Equation (353), which will asymptotically tend toward equation (351) as κ approaches zero, implies that a velocity profile should be layered by selecting the velocities associated with the extremes of the continuous velocity profile. Thus, for a jet, one might select the core velocity and the minimum values of the velocity profile above and below the jet maximum to construct the broken-line counterpart for the three-layer model. This was the selection scheme used in the analysis of the Endlich and McLean [53] jet stream model. In the analysis, we selected the local maximum velocity, as well as the wind speed at 2 km above and below the jet maximum at intervals of 0.5 deg of latitude from 2 deg of latitude north to 3 deg of latitude south of the jet core. The selection of the winds at 2 km above and below the jet maximum was based on a survey of the jet profiles measured at Cape Kennedy, Florida, during the years 1964 through 1967.

The shear of the velocity profile [equation (349)] is given by

$$\frac{d\bar{u}}{dz} = \frac{u_\infty}{\delta} \operatorname{sech}^2 \frac{z}{\delta} \quad . \tag{354}$$

Evaluating this expression at $z = 0$ shows that $d\bar{u}/dz$ is proportional to δ^{-1}. This means that as δ tends to zero, the shear at the origin becomes large and the result given by equation (351) tends toward equation (353). This means the broken-line approximation improves as the shear of the zero-order state becomes large.

The validity of the layering approximation, for both the velocity and the potential temperature profiles, tends to improve as the wavelength of the disturbance tends toward infinity. This means that the larger disturbances with regard to the length scales of the zero-order flow are influenced less by the details of these profiles. These results are consistent with the analysis by Drazin [56] of discontinous velocity profiles for the Orr-Sommerfeld equation.

Distributions of λ_1, λ_2, R_1, and R_2. The horizontal profiles of λ_1, λ_2, R_1, and R_2, associated with the Endlich and McLean jet stream model and shown in Figures 23 and 24, were calculated with the layering procedures discussed above. In the calculations, $h = 0.5$ km. The horizontal profile of $\bar{u}_2$ that was used in the calculations is shown in Figure 25. In this figure, $\bar{u}_2$ is normalized with the Endlich and McLean jet core velocity ($\bar{u}_{core} = 73$ m sec^{-1}).

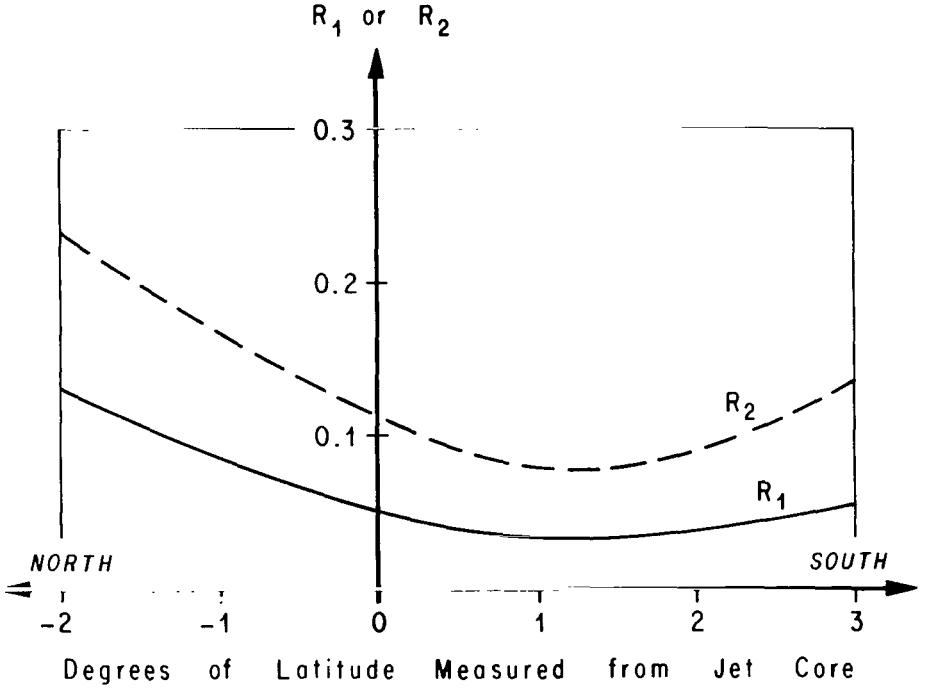

Note: These profiles were derived from the Endlich and McLean jet stream model.

Figure 23. Horizontal profiles of R_1 and R_2.

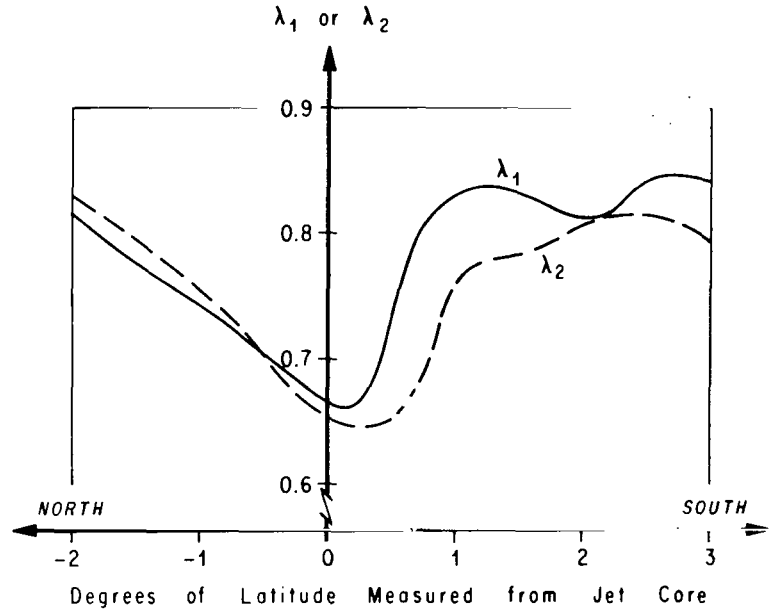

Note: These profiles were derived from the Endlich and McLean jet stream model.

Figure 24. Horizontal profiles of λ_1 and λ_2.

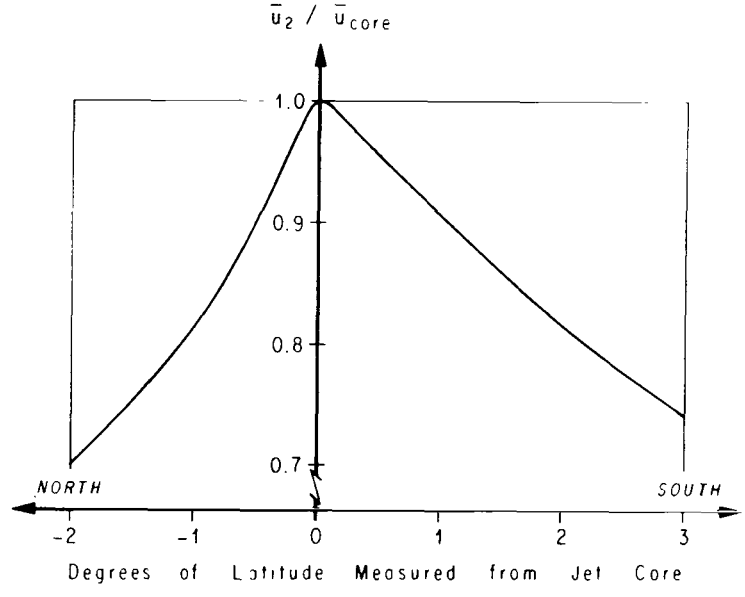

Note: $\bar{u}_{core}$ is the core velocity in the Endlich and McLean jet stream model ($\bar{u}_{core} = 73$ m sec^{-1}).

Figure 25. Horizontal profile of $\bar{u}_2/\bar{u}_{core}$.

Jet Stream Eigenvalues

The eigenvalues for the values of λ_1, λ_2, R_1, and R_2 in Figures 23 and 24 were calculated with equation (274). Figure 26, an eigenvalue diagram for the perturbations associated with the vertical core profiles of $\bar{\theta}$ and $\bar{u}$ of the Endlich and McLean jet model, is similar to the ones discussed previously (Figs. 3 through 7). The core eigenvalues possess only two branch points. Calculations with equation (274) and the profiles of λ_1, λ_2, R_1, and R_2 in Figures 23 and 24 showed that the eigenvalues for conditions away from the core also possess only two branch points. Thus, it appears that the synoptic scale jet streams are characterized by single-valued absolute stability boundaries; i.e., the absolute stability boundary for a particular location in the jet stream is characterized by only one critical wave number.

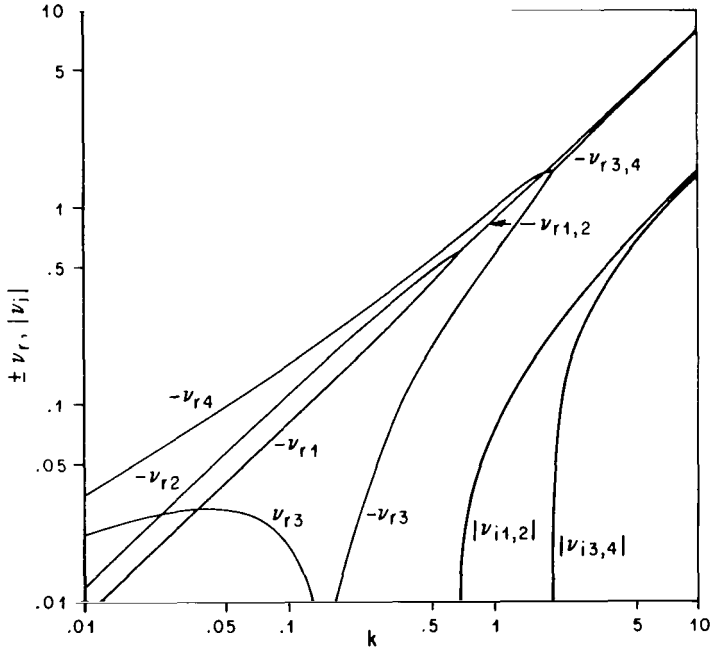

Note: An explanation of the notation in this figure is given in the caption of Fig. 3; these eigenvalues are associated with the vertical core profiles of $\bar{\theta}$ and $\bar{u}$ of the Endlich and McLean jet model.

Figure 26. Eigenvalue diagram for $\lambda_1 = 0.668$, $\lambda_2 = 0.658$, $R_1 = 0.048$, and $R_2 = 0.113$.

For sufficiently small k, the basic state flow is characterized by three neutral waves that propagate toward positive values of x and one neutral wave that propagates in the opposite direction (Fig. 26). As k increases, ν_{r3} becomes negative, and the flow for a given value of k is characterized by four neutral waves that propagate toward positive values of x; i.e., in the direction of the zero-order flow associated with the maximum wind level. The flow in the core becomes unstable at k = 0.66. The associated growth rates ν_i are indicated in Figure 26.

Figures 27 and 28 show the dependence of the eigenvalues upon the latitude with respect to the jet core for k = 0.1 and 1.0, respectively. Figure 27 shows that for k = 0.1, all perturbations are neutral. At 2 deg of latitude north of the jet core, for k = 0.1, the flow is characterized by three negative real eigenvalues, ν_{r1}, ν_{r2}, and ν_{r4}, and one positive real eigenvalue, ν_{r3}. As we approach the jet core from the north, ν_{r3} decreases, and upon traversing the core, ν_{r3} becomes negative at approximately 0.8 deg of latitude and experiences a minimum at 1.5 deg of latitude south of the core. The eigenvalue ν_{r3} then increases as we progress toward the south, and becomes positive at 2.3 deg of latitude south of the jet core. For sufficiently small k(~0.02), our calculations revealed that $\nu_{r3} > 0$ for the range of latitude being considered. Figure 28 shows that for k = 1.0, all the phase frequencies are negative. In the interval of latitude between 0.22 deg north and 0.58 deg south of the jet core, the real part of the eigenvalues ν_{r1} and ν_{r2} coalesce, and in this interval of latitude the flow is unstable for k = 1.0. This figure also indicates the growth rate ν_i of the perturbations, and in this case, ν_i is a maximum at approximately 0.2 deg of latitude south of the jet core. This result seems to imply that the south side of the jet stream is more unstable to shearing instabilities. For sufficiently large k (~1.7), it was found that ν_{r3} and ν_{r4} coalesce so that in the vicinity of the core the flow is characterized by two unstable modes and two damped modes. As k becomes large, the instability spreads to the north and south.

The values of k that correspond to the absolute stability boundaries and the unstable branch points (branch points that occur within an unstable domain), denoted by k_1^* and k_2^*, respectively, are represented by the solid curves given in Figure 29. The values of k_1^* and k_2^*, based upon conditions

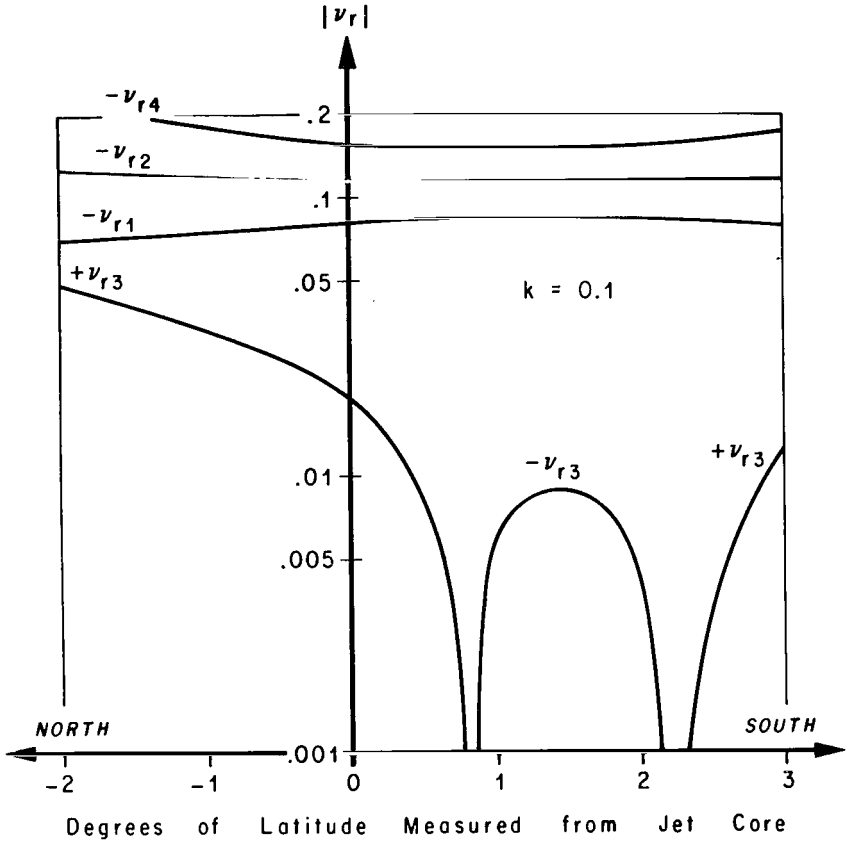

Note: The notation in this figure corresponds to that in Fig. 26. In this case the eigenvalues are real.

Figure 27. Horizontal profiles of eigenvalues for k = 0.1 based upon the Endlich and McLean jet model.

at the lower and upper interfaces, respectively, calculated with the two-layer Kelvin-Helmholtz model, are indicated by the dashed curves. This figure implies that the jet character of the wind profile, in the vertical, with regard to shearing instability calculations, is important only within approximately 1 deg of latitude north and south of the jet core. In the immediate vicinity of the jet core, the critical wave numbers associated with the three-layer model differ from those predicted by the Kelvin-Helmholtz model by approximately 35 percent. According to the Endlich and McLean model, λ_1 and λ_2 can vary by as much as 10 percent. A reduction of λ_1 and λ_2 by this percentage will reduce the critical wave numbers given in Figure 29, and the associated

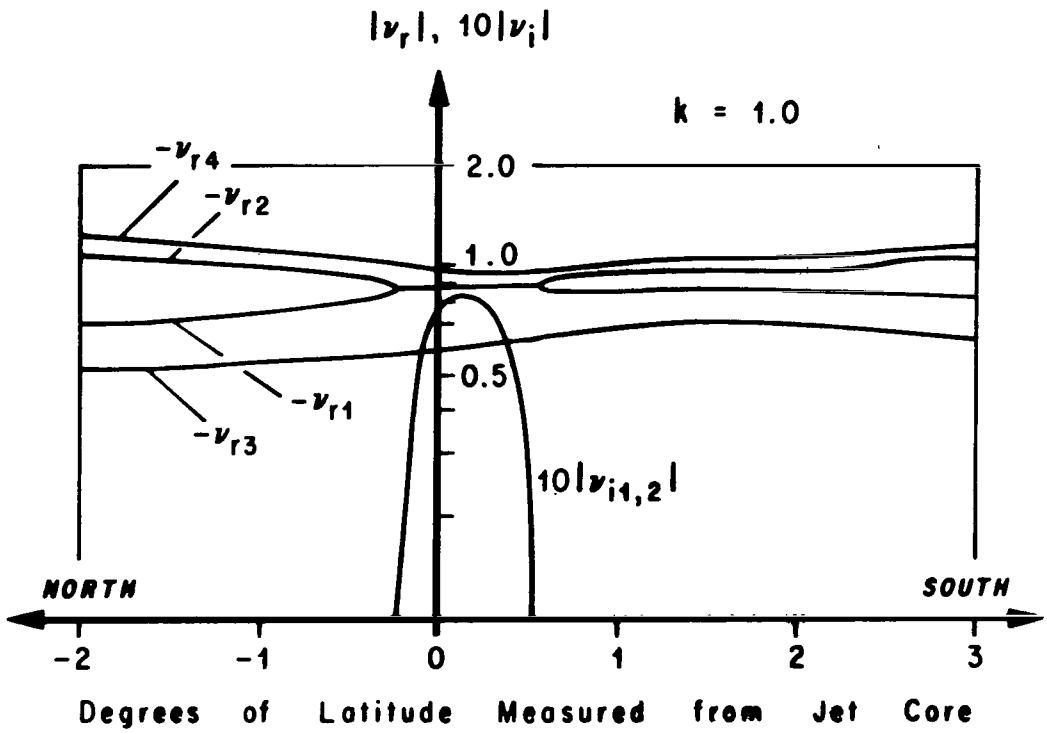

Note: The notation in this figure corresponds to that in Fig. 26. In this case the eigenvalues ν_1 and ν_2 are complex in the interval of latitude between 0.22 deg north and 0.58 deg south of the jet core.

Figure 28. Horizontal profiles of eigenvalues for k = 1.0 based upon the Endlich and McLean jet model.

departure of k^* predicted by the three-layer model from the Kelvin-Helmholtz model is on the order of 50 percent in the vicinity of the jet core.

The critical wavelength Λ_1^* associated with k_1^* can be calculated with the expression

$$\Lambda_1^* = \frac{6.28}{k_1^*} \quad , \tag{355}$$

where Λ_1^* is in units of kilometers and k_1^* is dimensionless. Thus, below the jet core, the three-layer model predicts $\Lambda_1^* = 10.45$ km, while at 1 deg of latitude removed from the core to the north and south, $\Lambda_1^* = 2.4$ km and $\Lambda_1^* = 2.72$, respectively.

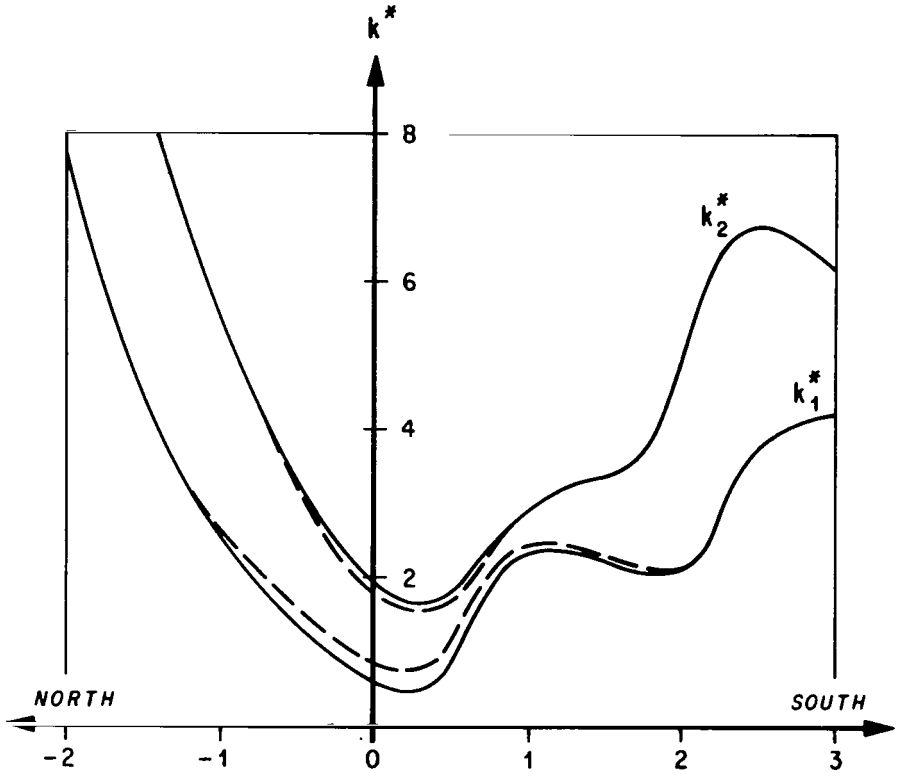

Note: The solid curves correspond to the three-layer results and the dashed curves are the values of k_1^* and k_2^* predicted by the two-layer theory.

Figure 29. Horizontal profiles of the critical wave numbers k_1^* and k_2^*.

Figure 30 shows the values of $\nu_{r1} = \nu_{r2} = \nu_{rc}$, ν_{r3}, and ν_{r4} associated with the absolute stability boundaries. One should remember that ν is scaled with the local value of $\bar{u}_2$. Figures 25 and 30 show that $\bar{u}_2/\bar{u}_{core}$ decreases more slowly than $-\nu_{rc}$ increases as we depart from the vicinity of the jet core to the north and south. This means that the frequency of the critical mode is lower in the vicinity of the core and is actually at a minimum at 0.5 deg of latitude south of the jet core. However, a calculation based upon the information in Figures 25, 29, and 30 revealed that the waves at critical conditions are characterized by the largest phase velocity occurring at the core with a slightly more rapid decrease in the phase velocity to the north as compared to the south. At 2 deg north and south of the core, the critical phase velocities normalized with $\bar{u}_{core}$ are 0.65 and 0.68, respectively.

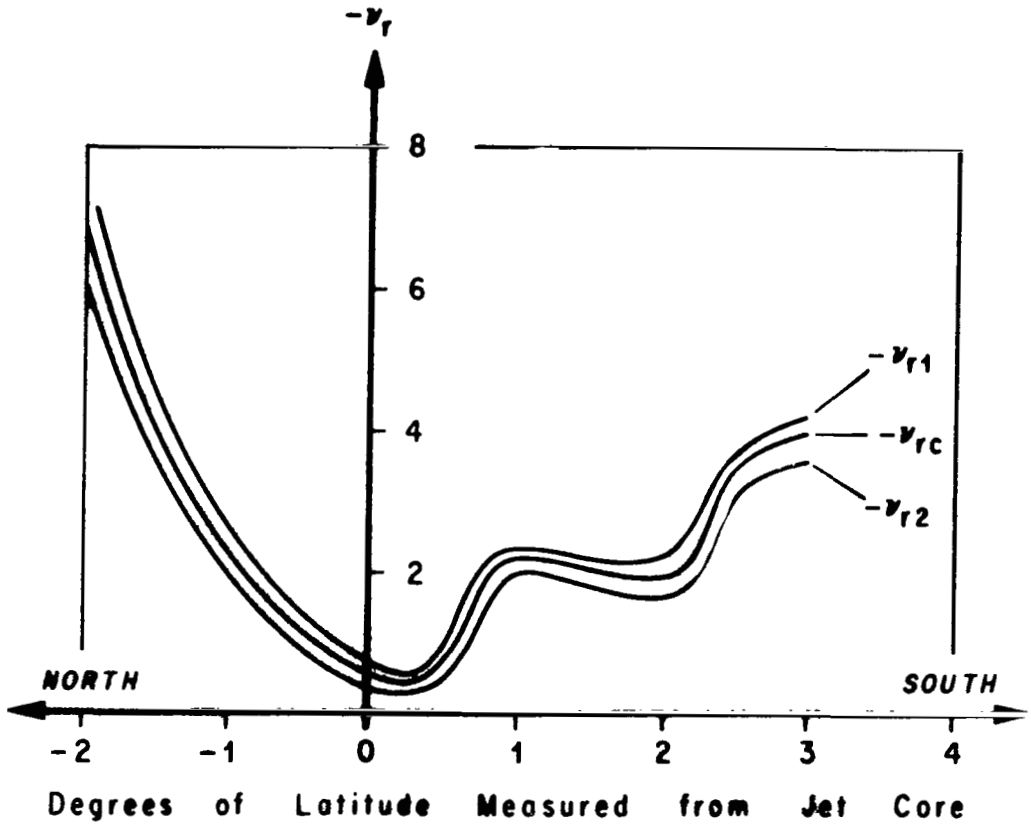

Note: In this figure, $\nu_{rc} = \nu_1 = \nu_2$. The notation in this figure corresponds to that in Fig. 26.

Figure 30. Horizontal profiles of the eigenvalues associated with the absolute stability boundary.

The vicinity of the synoptic scale jet stream has been found to be a preferred location of clear air turbulence. For example, Bannon [57, 58] reported 20 percent of all cases and two-thirds of severe turbulence associated with jet streams; Jones [59] found 71 percent of severe turbulence near the jet stream; Balzar and Harrison [60] reported 69 percent of 87 cases of severe turbulence near the jet stream; Estoque [61], Clem [62], and Lake [63] also found such relationships. Analyses of clear air turbulence case histories in the vicinity of the jet stream show that the quadrant below and on the cyclonic (cold air) side is a preferred area with a secondary maximum above the jet axis on the anticylconic side. However, this result was obtained by analyzing

case histories of clear air turbulence obtained primarily over land. Clodman et al. [55] have analyzed 62 cases of clear air turbulence in jet streams over the Atlantic Ocean and found that the maximum of turbulence occurrence is above the jet axis on the anticyclonic side, in contrast to findings over land.

In comparing clear air turbulence over land and water, Clodman et al. found that (a) the rate of occurrence of turbulence at high levels over the ocean is at least one order of magnitude lower than over land, (b) the percentage of turbulence reported over the ocean which is of light intensity is less over land, and (c) the horizontal dimensions of the turbulent patches over the ocean appear to be about twice as large as over land. These results imply that terrain features play a key role in the generation of clear air turbulence.

It is well known that mountains can induce lee waves which generate turbulence [64]. However, other authors find that ordinary rolling terrain with obstacles that are less than 300 to 700 m in height is important in the generation of clear air turbulence. Thus, for example, Jenkins [65] finds that the effect of obstacles can be felt to 25 times their height; Ludlum [66] suggests that cirrus cloud can be caused by hills 300 m high; Turner [67] found that high level turbulence over coastal areas in England was much more common than over the adjacent waters; and Clodman et al. [55] found that ordinary terrain with small obstacles is correlated with clear air turbulence and the effect of terrain is not simple since topographic features may be complex; however, the terrain effect appears stronger with a well-defined sharp ridge. The analysis in this report is most applicable to the generation of shear wave instability in jets over oceans because the lower boundary is a flat surface infinitely far removed from the jet core.

Reiter and Burns [68] have calculated spectra of clear air turbulence velocity components and find that the spectra of the horizontal components for wavelengths less than 3000 m behave like

$$E(\kappa) = E_o \kappa^q \quad , \tag{356}$$

where E_o and q are constants. The quantity q has values that range between -3 and -5/3. The spectra of the vertical velocity generally behave like equation (356) for wavelengths less than 200 m with $q = -5/3$. However, the w-spectra are characterized by a peak at wavelengths near 700 m. Several of the w-spectra have an energy minimum or "gap" at wavelengths on the order

of 1300 m. This behavior is only weakly or moderately expressed in the horizontal spectra. Reiter and Burns [68] concluded that the peaks in the w-spectra were manifestations of unstable shearing gravity waves because the degree to which the long-wave energy in the vertical component was less than the one observed in the horizontal components depended on the angle between the flight direction and the wind direction.

The peak of the w-spectrum will occur at a value of k that is greater than k^* if this peak is associated with breaking waves. The perturbation with the largest growth rate, $-\nu_i$, will grow faster than the other perturbations, and thus, this perturbation is the one which will ultimately break and result in clear air turbulence. However, the three-layer model predicts that the perturbations with infinitesimally small wavelengths have the largest growth rates (Fig. 26). If we would have included the effects of nonlinear interaction in the analysis, represented linearly with eddy coefficients, then the most preferred or unstable wave number, k_o, would have been finite [36]. However, the order of the governing differential equation (66) would have been of order six or greater, depending on the assumed forms of the eddy coefficients. For constant eddy coefficients, equation (66) becomes a sixth-order differential equation in ψ and the secular equation is a twelfth-degree polynomial in ν. Nevertheless, it is reasonable to suppose that the wavelength of the most unstable mode is positively correlated with the three-layer critical wave number. Thus, it might be concluded from Figure 29 that the wavelength associated with the peak of the w-spectrum is greatest below and slightly to the south of the core. As we proceed away from the core, the peak of the w-spectrum should shift toward smaller wavelengths. One should remember that not all w-spectra measured in jet streams are characterized by a shear gravity wave peak. Some observed spectra have a monotonic decrease of the spectral energy density from large scales to small scales located in the inertial subrange.

The root mean square response experienced by an aircraft that has response function $T(\omega)$ at frequency ω is given by

$$\sigma^2 = \int_0^\infty |T(\omega)|^2 E(\omega)\, d\omega \quad , \tag{357}$$

where $E(\omega)$ is the vertical velocity input turbulence spectrum and σ^2 is the variance of the gust loads. For most aircraft, the pitch-rate and acceleration

response transfer functions have a peak at frequency approximately equal to 0.5 cps with a secondary peak associated with the long-period Phugoid modes at a frequency on the order of 0.01 [69]. The Fourier components of the turbulence spectrum associated with high frequencies in the vicinity of the 0.5 cps peak of the aircraft transfer function give the major contribution to the response integral. Commercial aircraft which fly at jet stream altitude have true air speeds that are approximately equal to 250 m sec^{-1}. In terms of wavelength, the high frequency peak of the transfer function occurs at clear air turbulence wavelengths approximately equal to 500 m.

Upon breaking, the shear gravity waves supply energy to the clear air turbulence scales via a cascade of energy from the gravity wave scales to the turbulence scales. If the peak of the w-spectrum occurs at frequencies that are smaller than 0.5 cps, then σ^2 will be relatively large; however, if the peak occurs at frequencies greater than 0.5 cps the aircraft will not "feel" the full intensity of the turbulence.

An upper bound on the preferred wave number, k_o, is the critical wave number k^*. However, $k_o = k^*$ is a rather unlikely situation because this would mean that the generation of shear gravity waves is an extremely narrow band process. Reiter and Foltz [64] explain that the atmospheric microstructure, variable in space and time, prevents the formation of a "clean" wave of well-defined wavelength. Further, they note that it may be inferred from the appearance of stratus cloud decks viewed from an aircraft that "waves" forming on a stable interface may cover a relatively wide spectral band of wavelengths. For preferred wavelengths on the order of 500 m (aircraft turbulence scale) and $2h = 1$ km, we have $k_o = 12.6$. On the north side of the jet, the values of k^* increase rapidly from $k_1^* = 0.6$ at the jet axis to $k_1^* = 8.0$ at approximately 2 deg north (Fig. 29). It is possible to have $k_o > 12.6$ north of the core for latitudes greater than 2 deg north, so that from a shear wave instability viewpoint the occurrence of clear air turbulence that could affect aircraft is debatable. To the south of the jet axis, both k_1^* and k_2^* are less than 7.0. The overall lower values of k_1^* and k_2^* on the south side of the jet imply that k_{o1} and k_{o2} are usually less than the corresponding values associated with the north side. Thus, we might conclude from these arguments that the chance of finding turbulence is greater on the south side of the jet, other conditions being equal. The results of Clodman et al. [55] appear to confirm this result over the oceans. One should remember that we have only examined the effects of vertical shear on the generation of clear air turbulence. If we include the other factors that are

known to be correlated with clear air turbulence (curvature of the basic state flow, horizontal shear, vorticity advection, etc.) the picture becomes complicated, and thus, the above comments should be considered speculative. Thus, our conclusions fail if the energy gap is "filled-in" by energy releasing mechanisms other than vertical shear. In addition, we have applied the three-layer model to a mean jet stream model; it is possible to have a different picture emerge if we apply the theory to each individual jet stream in the sample.

Boundary Effects

To obtain the solutions to the three-layer model, we assumed that the lower rigid boundary was located at $z = -\infty$. In this section, we examine the effect this assumption has upon the solutions and the jet stream eigenvalues. To perform this task we will examine a Kelvin-Helmholtz shear layer with the origin of the coordinate system located at the vortex sheet. The solution of equation (66) that satisfies the boundary conditions of equations (68) and (71) and the interfacial condition of equation (87) is given by

$$\psi = A(\omega + \bar{u}_1\kappa)\,\frac{\bar{\theta}_2}{\bar{\theta}_1}\,\frac{\sinh \kappa(z + H)}{\sinh \kappa H} \qquad (-H < z < 0) \qquad (358)$$

$$\psi = A(\omega + \bar{u}_2\kappa)\, e^{-\kappa z} \quad , \qquad (0 < z < \infty) \qquad (359)$$

where H is the distance between the lower rigid surface, and the interface and the other symbols have their usual meaning. Upon substituting equations (358) and (359) into the interfacial condition equation (89), we find

$$\beta(\omega + \bar{u}_2\kappa)^2 + (\omega + \bar{u}_1\kappa)^2 \tanh \kappa H - g(1 - \beta)\kappa = 0 \quad , \qquad (360)$$

where $\beta = \bar{\theta}_1/\bar{\theta}_2$. The solution of equation (360) for ω is given by

$$\omega = -\kappa \left(\frac{\beta \bar{u}_2 + \bar{u}_1 \coth \kappa H}{\beta + \coth \kappa H} \right) \pm \left[g\kappa \frac{1 - \beta}{\beta + \coth \kappa H} \right.$$

$$\left. - \frac{\beta \coth \kappa H}{(\beta + \coth \kappa H)^2} (\bar{u}_2 - \bar{u}_1)^2 \kappa^2 \right]^{1/2} . \qquad (361)$$

The condition for the existence of complex eigenvalues and thus instability is given by

$$\frac{g(1 - \beta)(\beta + \coth \kappa H)}{\kappa (\bar{u}_2 - \bar{u}_1)^2 \beta \coth \kappa H} < 1 , \qquad (362)$$

or

$$R_\kappa = \frac{g(1 - \beta)}{\kappa (\bar{u}_2 - \bar{u}_1)^2} < \frac{\beta \coth \kappa H}{\beta + \coth \kappa H} , \qquad (363)$$

where R_κ is a Richardson number based upon the length scale being the disturbance size κ^{-1}. The critical conditions or the equation for the stability boundary is obtained by making equation (363) an equality, so that

$$R_\kappa^* = \frac{\beta \coth \kappa^* H}{\beta + \coth \kappa^* H} , \qquad (364)$$

where $*$ denotes a critical parameter. The asymptotic behavior of equation (364) as H approaches infinity is given by

$$R_\kappa^* \sim \frac{\beta}{1 + \beta} \quad (H \to \infty) . \qquad (365)$$

This is the result we would have obtained by placing the lower rigid boundary at $z = -\infty$ ab initio. If we hold H fixed and let κ^* approach infinity, we find

$$R_\kappa^* \sim \frac{\beta}{1 + \beta} \quad (\kappa^* \to \infty) . \qquad (366)$$

This means that the effect of the lower rigid boundary is negligible for sufficiently large κ^*. Upon letting $\kappa^* H$ approach zero, we find

$$R_\kappa^* \sim \beta \quad (\kappa^* H \rightarrow 0) \qquad . \tag{367}$$

This result implies that the effect of moving the lower boundary toward the Kelvin-Helmholtz sheet tends to destabilize the flow, since instability will set in for Richardson numbers greater than $\beta(1+\beta)^{-1}$ and the critical disturbance size will be increased. It was explained previously that $0.95 < \beta < 1.0$ for most statically stable stratifications in the atmosphere and that it is reasonable to approximate β as unity in those terms that do not contain the acceleration of gravity. It is clear that equations (365) and (367) do not suffer significant distortion with this approximation.

Equation (364) will yield the largest critical wavelength Λ^* that satisfies the limiting behavior in equation (365) to within a prescribed permissible error. If we select $R_\kappa^* = 0.55$ and approximate β as unity, then equation (364) predicts that those critical wavelengths that satisfy

$$\Lambda^* \leqq 5.4H \tag{368}$$

will also satisfy equation (365) to within 10 percent. If we use equation (368) to estimate an upper bound on the permissible critical wavelengths for the three-layer model and note that $\Lambda^* = 4\pi h k^{*-1}$, then those perturbations in jets and shear layers that satisfy

$$k^* \geqq 2.33 \frac{h}{H} \tag{369}$$

can be analyzed with the three-layer jet model, with the lower boundary displaced to $z = -\infty$. In the analysis of the Endlich and McLean jet model, $h = 0.5$ km; thus, according to equation (369) and $H = 10$ km, we must have $k^* \geqq 0.12$. Since the k^* configuration associated with the Endlich and McLean model satisfies this equation, the effect of the lower boundary can be neglected. However, this does not mean that all boundary effects can be neglected since this discussion is concerned only with horizontal boundaries. If the lower

boundary is characterized by hills, mountains, etc., then these results fail because the fluid will experience forced motions at the lower boundary. Finally, most meso- and micro-scale shear layers and jets above 4 km appear to satisfy equation (369).

Coriolis Effects

As discussed previously, to neglect Coriolis forces, we assumed as a working hypothesis that

$$\frac{L_1}{L_3} << 10^2 \quad , \tag{370}$$

where L_1 and L_3 are the longitudinal and vertical length scales; see equation (46). In the analysis of the stability properties of the Endlich and McLean jet model, we set $h = 0.5$ km, so that, in the middle layer of the three-layer model, L_3 is on the order of 1 km. To estimate the vertical length scale in the upper and lower layers, let us assume

$$L_3 \sim \frac{|\psi|}{\left|\frac{d\psi}{dz}\right|} \tag{371}$$

as we did previously. The solution in the upper and lower layers is proportional to $e^{-\kappa z}$ and $e^{\kappa z}$, respectively, so that

$$L_3 \sim \kappa^{-1} \quad . \tag{372}$$

We choose the horizontal length scale to be the wavelength of the perturbations, $2\pi\kappa^{-1}$. Thus, in the upper and lower layers, $L_1/L_3 \sim 2\pi$, so that equation (370) is satisfied. In the middle layer

$$\frac{L_1}{L_3} \sim \frac{2\pi}{\kappa} \quad , \tag{373}$$

where κ has the units of km^{-1}. In the Endlich and McLean model, the longest unstable perturbations have wavelengths approximately equal to 10 km so that in the middle layer $L_1/L_3 \sim 10$. Thus, the perturbations in the middle layer satisfy condition (370). We may conclude from this discussion that we can neglect Coriolis forces in the analysis of shear layer and jet instabilities.

SUMMARY AND RECOMMENDATIONS

The properties of shear layer and jet instabilities in stratified fluids have been examined. The first-order isentropic perturbation equations and the associated boundary and interfacial conditions suitable for analyzing shear layer and jet instabilities in heterogenous media were derived. The general properties of these equations and boundary and interfacial conditions for continuous and broken-line flows were examined. The dynamic stability properties of three-layer broken-line flows in which $\bar{u}$ and $\bar{\theta}$ had constant, but different, values in each layer were examined.

Summary

The main results in this report were obtained where the conclusions of the analyses were given in the course of the discussion. In this section, the conclusions are listed for convenience.

As discussed earlier, emphasis was on the solutions to the governing differential equation (66) and the associated boundary and interfacial conditions of equations (68), (71), (87), and (89). In the analysis, three types of broken-line flows were considered. In the analysis it was shown that the permissible number of modes associated with the types (1) and (3) broken-line flows, for specified values of κ_1 and κ_2, cannot exceed 2N, where N is the number of interfaces within the broken-line flow.

Also, the consequences of the transformation $\psi = \Omega F$ were examined in the context of continuous and discontinuous flows. In the case of continuous flows, a quadratic integral form was derived from which it was concluded that the eigenvalue equation for continuous flows has two and only two branches in the complex ω-plane. This quadratic form was also used to derive a necessary and sufficient condition for instability in continuous flows; however,

since the condition depended explicitly on the solution, its usefulness was limited. Nevertheless, the condition leads to the result that all continuous shear layer and jet flows that are statically unstable everywhere are dynamically unstable. The transformation $\psi = \Omega F$ leads to the result that for continuous flows $\kappa_1\bar{u} + \omega$ must vanish at least once in the interval $0 \leqq z \leqq \infty$ and the complex wave frequency for any unstable mode associated with $S > 0$ must lie inside the semicircle which has the range of $\kappa_1\bar{u}$ for diameter in the lower half of the complex ω-plane. These results were first obtained by Synge [37], Miles [31], and Howard [33]. For broken-line flows, it appears that it is possible only to derive a general necessary and sufficient condition for instability for the case in which θ is continuous across the interfacial surfaces; thus, a general necessary and sufficient condition for instability in broken-line flows has yet to be obtained. The theorems of Synge [37], Miles [31], and Howard [33] are valid for broken-line flows in which θ is continuous across interfacial surfaces. It remains to show that these theorems are universally valid for all broken-line flows.

For continuous flows, the transformation $\psi = \Omega^{1/2}H$ leads to a quadratic integral form from which it may be concluded that

$$gS - \frac{1}{4}\,\frac{\kappa_1^2}{\kappa^2}\,(D\bar{u})^2 \geqq 0 \quad ,$$

everywhere, is a sufficient condition for stability. This theorem was first derived by Miles [31]. In discontinuous flows, Miles' theorem is valid if $\bar{\theta}$, $\bar{u}$, and $D\bar{u}$ are continuous across the interfacial surfaces. A general discontinuous counterpart of Miles' theorem has yet to be obtained.

Later in the report, we analyzed the behavior of the eigenvalues of the three-layer model as the wave number of the disturbances approached infinity. Instability will set in for sufficiently large wave numbers and the limiting solutions represent localized Kelvin-Helmholtz instabilities at each interface.

Also, we analyzed two special cases: the symmetric jet and the odd shear layer. The absolute stability boundary of the symmetric jet is characterized by one critical mode of disturbance, and the interfacial Lagrangian displacements are out of phase by 180 deg (odd solutions). A second instability, characterized by even solutions in the vertical, sets in at somewhat larger wave numbers. The absolute stability boundary of the odd shear

layer is characterized by two critical modes, one even, the other odd. These modes propagate in opposite directions with the same phase speed, so that the interaction between these modes results in a standing wave instability in a frame of reference that is translating with the mean flow in the middle layer. In the symmetric jet, the Lagrangian displacements at the upper and lower interfaces for all modes of motion are either in phase or out of phase by 180 deg. In the odd shear layer, only the neutral modes of motion have these phase properties. As k increases past the critical value, in the odd shear layer, the phase of the interfacial Lagrangian displacements depart from 0 and 180 deg.

A general eigenvalue analysis of the three-layer model was presented. Based upon this analysis, we may make the general comment that no universal critical Richardson number exists for the onset of shearing instability. Of course, in continuous flows, the critical Richardson number has an upper bound of 1/4 for longitudinal disturbances, according to Miles' theorem. The three-layer flows are more unstable to long wave disturbances than the two-layer Kelvin-Helmholtz flows, and the absolute stability boundaries can be single-valued and multivalued functions of k^*. In the limit, as $|\lambda_1|$, $|\lambda_2|$, R_1, or R_2 approach infinity, the absolute stability boundaries become single-valued functions of k^*. For intermediate values of these parameters, the absolute stability boundaries are triple-valued functions of k^*. The multi-valued nature of these stability boundaries results from the global interaction of the shear layer or jet flow. For a given set of values for R_1, R_2, $|1 - \lambda_1|$ and $|1 - \lambda_2|$, the shear layer flow configuration will have the smallest value of k^* and thus are more unstable than jet flows to the long wave perturbations. This happens because the basic state vorticity vectors in the shear layer flows act in the same sense; i.e., the basic state vorticity has the same sign at the upper and lower interfaces, while in the jet flows the basic state vorticity at one interface tends to stabilize the instability at the other interface and vice versa.

The three-layer solutions are approximate long wave solutions for continuous flows. This is true because the long wave perturbations "feel" only the gross features of the basic state flow, while the short waves "feel" the details of the basic state flow. The broken-line solutions appear to obey Howard's [33] semicircle theorem and Synge's [37] result. In this sense, the three-layer flows behave like continuous ones.

The generation of shearing instabilities in synoptic scale jet streams were analyzed by applying the three-layer model to the jet stream model of Endlich and McLean [53]. The synoptic scale jet streams do not appear to be characterized by multivalued absolute stability boundaries; i.e., k^* is not a

multivalued function of the basic state parameters. The smallest critical wave numbers occur in the vicinity of the jet core. If k_1^* and k_2^* are identified with conditions, or rather the inflection points, above and below the jet maximum, then it can be concluded that, in the context of shearing instabilities, the most unstable region occurs below the jet core slightly to the south. However, it must be remembered that the Endlich and McLean jet model is an average of actual conditions, so that in actual flows it is possible that the most unstable region could occur to the north of the jet core. The important point here is that the most unstable region is below and in the vicinity of the jet core. The three-layer model and the two-layer Kelvin-Helmholtz model predict significantly different results within 1 deg of latitude north and south of the jet core. The predicted critical wave numbers differ by approximately 35 to 50 percent in this region. This means that the jet character of the wind profile is important in the vicinity of the jet core in the context of shearing instability. Outside of this region, the two models predict essentially the same results; therefore, it may be concluded that the instabilities in the regions outside of the jet core essentially occur as shear layer instabilities.

Recommendations for Future Work

The main purpose of this report is to extend the knowledge of the first-order instabilities in stratified shear layer and jet flows. In particular, we were interested in establishing the relationship between these instabilities and the symmetry properties of the flow. To do this, we used an inviscid broken-line three-layer model. Admittedly, the broken-line flows are artificial; however, they permit one to analyze many flows with relative ease, and in the context of the long wave instabilities, the broken-line flows yield qualitatively correct results. The approach taken in this report in regard to the problem of shear layer and jet instability in stratified media has been highly simplified. It is felt that if any further understanding of jet and shear layer instabilities is to be made, further theoretical advances must be made. The most logical approach that could be taken in the future would be to gradually increase the complexity of the problem.

The obvious next step would be to attempt the analysis of this report with continuous profiles of $\bar{\theta}$ and $\bar{u}$. This would be very difficult. Two approaches could be taken; an analytical or a numerical one. It would be desirable to perform analytical calculations whereby one could obtain an eigenvalue equation in which the parameters associated with the basic state flow could be varied. This would lead to a better insight into the problem.

However, to do this one must judiciously select basic state flows that permit one to obtain solutions to equation (66). It is well known that seemingly uncomplicated basic flows result in very complicated mathematical analyses in linear stability problems. The recent analytical work by Miles [32] could serve as a starting point in the area of analytical computations. If one is not so fortunate to develop a basic state flow that would permit one to obtain a solution to equation (66), then one might resort to numerical methods. The numerical methods that are used to solve the Orr-Sommerfeld equation could be used as a starting point [71]. In the event of either the numerical or the analytical solutions, the results of these calculations would yield valuable information about the intermediate and short wavelength instabilities.

At this point, one might complicate the problem by including the dissipative effects of eddy viscosity and heat conduction or molecular viscosity and heat conduction. These effects will introduce linear second-order terms in the momentum conservation and thermodynamic energy equations. For simplicity, it could be assumed that the eddy coefficients are constants. The molecular coefficients will be constants within the framework of the Boussinesq approximation. The dissipative eddy and molecular terms will have the same mathematical form. The addition of these terms results in a sixth-order governing differential equation in ψ. We have the added complication that this equation and the associated boundary conditions do not constitute a self-adjoint system, so that it might not be possible to use variational methods to solve this equation.

It is well known that the addition of resistance or dissipative effects to systems oftentimes results in instability. Examples in mechanics, electronics, and administration and economics can be cited. Betchov and Criminale [71] explain that resistive instability has been uncovered in magnetohydrodynamics and plasma physics, and that the destabilizing effect of resistance is oftentimes a matter of delay. They cite the case of the harmonic oscillator whose restoring force is simply retarded by the positive constant τ. In this case, the basic equation is

$$\ddot{x}(t) + x(t - \tau) = 0 \quad . \tag{374}$$

Upon expanding $x(t - \tau)$ in a power series in τ and retaining only the first two terms in the series, we obtain the equation of an oscillator with negative damping

$$\ddot{x}(t) - \tau\dot{x}(t) + x(t) = 0 \quad . \tag{375}$$

This equation has unstable solutions for all positive values of τ. Resistance instability has been discovered in the case of the Orr-Sommerfeld equation with the presence of rigid boundaries. In an investigation of the Orr-Sommerfeld equation, Heisenberg [72] demonstrated that the effect of viscosity is generally destabilizing at very large Reynolds numbers. According to Lin [42], Heisenberg's result states that, if a velocity profile has an inviscid neutral disturbance with nonvanishing wave number and phase velocity, the disturbance with the same wave number is unstable in a viscous fluid when the Reynolds number is sufficiently large. In view of the fact that the Orr-Sommerfeld equation possesses resistive instabilities, it is reasonable to assume that similar instabilities exist in stratified shear layer and jet flows. Our knowledge of these resistive instabilities in stratified flows is meager, and the subject offers considerable opportunity for the theoretician. The mathematical machinery of the Orr-Sommerfeld equation could serve as the starting point for this analysis. However, this equation is a fourth-order equation, while the corresponding equation for the stratified flows is a sixth-order differential equation.

Finally, the ultimate extension to this work can be made in the area of nonlinear fluid mechanics. The methods that can be used in this work could range from the direct finite difference methods that abound in the field of meteorology to the elegant energy integral methods of Stuart [2]. Additional contributions could be made by solving for the second- and higher-order instabilities mentioned initially in this report. These nonlinear calculations would yield information about how the instabilities modify the basic state flow.

George C. Marshall Space Flight Center
National Aeronautics and Space Administration
Marshall Space Flight Center, Alabama 35812, June 1969
933-50-02-00-62

REFERENCES

1. Pinus, N. Z., Reiter, E. R., Shur, G. N., and Vinnichenko, N. K.: Power Spectra of Turbulence in the Free Atmosphere. Tellus, 19, 1967, pp. 206-213.

2. Stuart, J. T.: On the Nonlinear Mechanics of Hydrodynamic Stability. J. Fluid Mech., 4, 1958, pp. 1-21.

3. Malkus, W. V. R., and Veronis, G.: Finite Amplitude Cellular Convection. J. Fluid Mech., 4, 1958, pp. 225-260.

4. Veronis, G.: Cellular Convection with Finite Amplitude in a Rotating Fluid. J. Fluid Mech., 5, 1959, pp. 401-435.

5. Helmholtz, H. von: Über discontinuirliche Flüssigkeitsbewegungen, Wissenschaftliche Abhandlungen. 146-157, J. A. Barth, Leipzig, 1882; translation by Guthrie in Phil. Mag., Ser. 4, 36, 1868, pp. 337-346.

6. Kelvin, Lord: Mathematical and Physical Papers, IV, Hydrodynamics and General Dynamics. Cambridge University Press, Cambridge, 1910.

7. Helmholtz, H. von: Über Atmosphärishe Bewegungen, II, zur Theorie Wind und Wellen. Nachr. Gesellsch. Wissensch. Göttingen, 3, 1889, pp. 309-332.

8. Wegener, A.: Studien Über Luftwogen. Beitr. Phys. Freien Atmos., 2 (2), 1906, pp. 55-72.

9. Wegener, A.: Nachtrag zu den "Studien Über Luftwogen." Beitr. Phys. Freien Atmos., 4 (1), 1912, pp. 23-25.

10. Haurwitz, B.: Zur Theorie der Wellenbewegung in Luft und Wasser. Veröff. Geophys. Inst. Univ. Leipzig, 5, 1931, pp. 1-106.

11. Sekera, Z.: Helmholtz Waves in a Linear Temperature Field with Vertical Wind Shear. J. Meteorology, 6, 1949, pp. 93-102.

12. Ludlum, F. F.: Characteristics of Billow Clouds and Their Relation to Clear-Air Turbulence. Quart. J. Roy. Soc., 93, 1967, pp. 419-435.

REFERENCES (Continued)

13. Bjerknes, V., Bjerknes, J., Solberg, H., and Bergeron, T.: Physikalische Hydrodynamik. Springer-Verlag, Berlin, 1933.

14. Godske, C. L., Bergeron, T., Bjerkens, J., and Bundgaard, R. C.: Dynamic Meteorology and Weather Forecasting. The Waverly Press, Inc., Baltimore, 1957.

15. Taylor, G. I.: Effect of Variation in Density on the Stability of Superposed Streams of Fluid. Proc. Roy. Soc., London, A, 132, 1931, pp. 499-523.

16. Goldstein, S.: On the Stability of Superposed Streams of Fluid of Different Densities. Proc. Roy. Soc., London, A, 1931, pp. 524-548.

17. Rosenhead, L.: Formation of Vortices From a Surface of Discontinuity. Proc. Roy. Soc., London, A, 134, 1932, pp. 170-190.

18. Thorpe, S. A.: A Method of Producing a Shear Flow in a Stratified Fluid. J. Fluid Mech., 32, 1968, pp. 693-704.

19. Kao, S. K., and Woods, H. D.: Energy Spectra of Meso-Scale Turbulence Along and Across the Jet Stream. J. Atmospheric Sci., 21, 1964, pp. 513-519.

20. Kao, S. K., and Sizoo, A. H.: Analysis of Clear Air Turbulence Near the Jet Stream. J. Geophys. Res., 71, 1966, pp. 3799-3805.

21. Reiter, E. R., and Burns, A.: The Structure of Clear-Air Turbulence Derived from "TOPCAT" Aircraft Measurements. J. Atmospheric Sci., 23, 1966, pp. 206-212.

22. Pinus, N. Z., and Shmeter, S. M.: Atmospheric Turbulence Affecting Aircraft Bumping. Gidromet, Moscow, 1962.

23. Pinus, N. Z.: Statistical Characteristics of the Horizontal Component of the Wind at Heights of 6-12 km. Bull. Academy of Sci., USSR, Geophys., Ser., 1963, pp. 105-107.

REFERENCES (Continued)

24. Shur, G. N.: Equipment for Atmospheric Turbulence Spectra Investigation by Means of Harmonic Analysis Using Magnetic Tape Records. Trudy TsAO, No. 31, 1959.

25. Shur, G. N.: Experimental Investigation of the Energy Spectrum of Atmospheric Turbulence. Trudy TsAO, No. 43, 1962.

26. Vinnichenko, N. K.: On Usage of Airborne Hot-Wire Anemometer. Trudy TsAO, No. 53, 1964.

27. Vinnichenko, N. K., Pinus, N. Z., and Shur, G. N.: Some Results of the Experimental Turbulence Investigations in the Troposphere. Paper Presented at the International Colloquium on the Fine-Scale Structure of the Atmosphere, Moscow, June 15-22, 1965.

28. Bolgiano, R., Jr.: Structure of Turbulence in Stratified Media. J. Geophys. Res., 67, 1962, pp. 3015-3023.

29. Lumley, J. L.: The Inertial Subrange in Non-Equilibrium Turbulence. Paper given at the International Colloquium on the Fine-Scale Structure of the Atmosphere, Moscow, June 15-22, 1965.

30. Panofsky, H. A., Dutton, J. A., Hemmerich, K. H., McCreary, G., and Loving, N. V.: Case Studies of Distribution of CAT in the Troposphere and Stratosphere. J. Appl. Met., 7, 1968, pp. 384-389.

31. Miles, J. W.: On the Stability of Heterogeneous Shear Flows. J. Fluid Mech., 10, 1961, pp. 496-508.

32. Miles, J. W.: On the Stability of Heterogeneous Shear Flows, II. J. Fluid Mech., 16, 1963, pp. 209-227.

33. Howard, L. N.: Note on a Paper of John W. Miles. J. Fluid Mech. 10, 1961, pp. 509-512.

34. Howard, L. N.: Neutral Curves and Stability Boundaries in Stratified Flow. J. Fluid Mech., 16, 1963, pp. 333-342.

REFERENCES (Continued)

35. Drazin, P. G.: The Stability of a Shear Layer in an Unbounded Heterogeneous Inviscid Fluid. J. Fluid Mech., 4, 1958, pp. 214-224.

36. Drazin, P. G.: On Stability of Parallel Flow of an Incompressible Fluid of Variable Density and Viscosity. Proc. Cambridge Phil. Soc., 58, 1962, pp. 646-711.

37. Synge, J. L.: The Stability of Heterogeneous Liquids. Trans. Roy. Soc. Can., 27, 1933, pp. 1-18.

38. Hines, C. O.: Internal Atmospheric Gravity Waves at Ionospheric Heights. Canadian J. Physics. 38, 1960, pp. 1441-1481.

39. Dutton, J. A., and Fichtl, G. H.: Approximate Equations of Motion for Gases and Liquids, J. Atmospheric Sci., 26, 1969, pp. 241-254.

40. Lin, C. C.: On the Stability of Two-Dimensional Parallel Flows, I, General Theory. Quart. Appl. Math., 3, 1945, pp. 117-142.

41. Lin, C. C.: On the Stability of Two-Dimensional Parallel Flows, II, Stability in an Inviscid Fluid. Quart. Appl. Math., 3, 1945, pp. 218-134.

42. Lin, C. C.: On the Stability of Two-Dimensional Parallel Flows, III, Stability in a Viscous Fluid. Quart. Appl. Math., 3, 1946, pp. 277-301.

43. Foote, J. R., and Lin, C. C.: Some Recent Investigations in the Theory of Hydrodynamic Stability. Quart. Appl. Math., 8, 1951, pp. 265-280.

44. Squire, H. B.: On the Stability of the Three-Dimensional Disturbances of Viscous Flow Between Parallel Walls. Proc. Roy. Soc., London, A, 142, 1933, pp. 621-628.

45. Lipps, F.: The Barotropic Stability of the Mean Westerly Winds in the Atmosphere. J. Fluid Mech., 12, 1962, pp. 397-407.

46. Lipps, F.: The Stability of an Asymmetrical Zonal Current in the Atmosphere. J. Fluid Mech., 21, 1965, pp. 225-239.

REFERENCES (Continued)

47. Ramm, D., and Warren, F. W. G.: Gravity-Wave Dispersion Under Wind Shear in Two Model Atmospheres. Quart. J. R. Met. Soc., 89, 1963, pp. 349-359.

48. Landau, L. D., and Lifshitz, E. M.: Fluid Mechanics. Pergamon Press, London, 1959.

49. Reiter, E. R.: Jet-Stream Meteorology. The University of Chicago Press, Chicago, 1963.

50. Chandrasekhar, S.: Hydrodynamic and Hydromagnetic Stability. Oxford University Press, London, 1961.

51. Hartree, D. R.: Numerical Analysis. Oxford University Press, London, 1958.

52. Drazin, P. G., and Howard, L. N.: Stability in a Continuously Stratified Fluid. J. Am. Soc., Civil. Eng., Eng. Mech. Div., 87, EM6, 1961, pp. 101-116.

53. Endlich, R. M., and McLean, G. S.: Jet-Stream Structure Over the Central United States Determined From Aircraft Observations. J. Applied Meteorology, 4, 1965, pp. 83-90.

54. Sasaki, Y.: A Theory and Analysis of Clear-Air Turbulence. A&M Scientific Report, Contract No. AF 19(604)-1565, 1958.

55. Clodman, J., Morgan, G. M., and Ball, J. T.: High Level Turbulence. NYU Research Division, Final Report Under Contract No. AF19(604)-5208, 1960.

56. Drazin, P. G.: Discontinuous Velocity Profiles for the Orr-Sommerfeld Equation. J. Fluid Mech., 10, 1961, pp. 571-583.

57. Bannon, J. K.: Meteorological Aspects of Turbulence Affecting Aircraft at High Altitudes. Great Britain Meteorological Office Professional Notes, No. 104, 1951.

REFERENCES (Continued)

58. Bannon, J. K.: Weather Systems Associated with Some Occasions of Severe Turbulence at High Altitude. Meteor. Magazine, London, 81, 1952, pp. 97-101.

59. Jones, D. C. E.: Further Investigations of High-Level Clear-Air Turbulence. Meteor. Magazine, London, 83, 1954, pp. 166-173.

60. Balzer, M. E., and Harrison, H. T.: The Nature of Clear Air Turbulence. United Air Lines Meteorology Circular No. 48, United Air Lines, Denver, 1959.

61. Estoque, M. A.: Some Characteristics of Turbulence at High Altitudes. Geophysics Research Directorate, GRD Research Notes, No. 4, AFCRC-TN-58-624, 1958.

62. Clem, L. H.: Clear-Air Turbulence From 25,000 to 45,000 Feet Over the United States. Air Weather Service Technical Report, AWS TR 105-47, 1954.

63. Lake, H.: A Meteorological Analysis of Clear Turbulence (A Report on the U. S. Synoptic High Altitude Gust Program). Geophysics Research Directorate, Geophysical Research Papers, No. 47, AFCRC-TR-56-201, 1956.

64. Reiter, E. R., and Foltz, H. P.: The Prediction of Clear-Air Turbulence Over Mountainous Terrain. J. Appl. Met., 6, 1967, pp. 549-556.

65. Jenkins, C. F.: Forecasting the Mountain Wave. Geophysics Research Directorate, Air Force Surveys in Geophysics, No. 15, 1952.

66. Ludlum, F. H.: Orographic Cirrus Clouds. Quart. J. R. Met. Soc., 78, 1952, pp. 554-562.

67. Turner, H. S.: The Geographicl Distribution of Clear-Air Turbulence. Meteor. Magazine, London, 88, 1959, pp. 33-38.

REFERENCES (Concluded)

68. Reiter, E. R., and Burns, A.: Atmospheric Structure and Clear-Air Turbulence. Paper Given at the International Colloquium on the Fine-Scale Structure of the Atmosphere, Moscow, June 15-22, 1965.

69. Etkin, B.: Dynamics of Flight. John Wiley and Sons, Inc., New York, 1959.

70. Betchov, R., and Criminale, W. O.: Stability of Parallel Flows. Academic Press, New York, 1967.

71. Heisenberg, W.: Über Stabilität und Turbulenz von Flüssigkeitsstromen. Ann. Physik, 74, 1924, pp. 577-627.

BIBLIOGRAPHY

Drazin, P. G., and Howard, L. N.: The Instability to Long Waves of Unbounded Parallel Inviscid Flow. J. Fluid Mech., 14, 1962, pp. 257-283.

Panofsky, H. A., and McLean, J. C., Jr.: Physical Mechanism of Clear Air Turbulence. Res. Report to U. S. Weather Bureau, Dept. of Meteorology, Pennsylvania State University, 1960.

Reiter, E. R., and Nania, A.: Jet-Stream Structure and Clear Air Turbulence (CAT). J. Appl. Met., 3, 1964, pp. 247-260.

Spiegel, E. A., and Veronis, G.: On the Boussinesq Approximation for a Compressible Fluid. Astrophys. J., 131, 1960, pp. 442-447.

NASA-Langley, 1970 —— 13 M147

"The aeronautical and space activities of the United States shall be conducted so as to contribute . . . to the expansion of human knowledge of phenomena in the atmosphere and space. The Administration shall provide for the widest practicable and appropriate dissemination of information concerning its activities and the results thereof."

—NATIONAL AERONAUTICS AND SPACE ACT OF 1958

NASA SCIENTIFIC AND TECHNICAL PUBLICATIONS

TECHNICAL REPORTS: Scientific and technical information considered important, complete, and a lasting contribution to existing knowledge.

TECHNICAL NOTES: Information less broad in scope but nevertheless of importance as a contribution to existing knowledge.

TECHNICAL MEMORANDUMS: Information receiving limited distribution because of preliminary data, security classification, or other reasons.

CONTRACTOR REPORTS: Scientific and technical information generated under a NASA contract or grant and considered an important contribution to existing knowledge.

TECHNICAL TRANSLATIONS: Information published in a foreign language considered to merit NASA distribution in English.

SPECIAL PUBLICATIONS: Information derived from or of value to NASA activities. Publications include conference proceedings, monographs, data compilations, handbooks, sourcebooks, and special bibliographies.

TECHNOLOGY UTILIZATION PUBLICATIONS: Information on technology used by NASA that may be of particular interest in commercial and other non-aerospace applications. Publications include Tech Briefs, Technology Utilization Reports and Technology Surveys.

Details on the availability of these publications may be obtained from:

SCIENTIFIC AND TECHNICAL INFORMATION DIVISION

NATIONAL AERONAUTICS AND SPACE ADMINISTRATION

Washington, D.C. 20546